Dissertation
submitted to the
Combined Faculties for the Natural Sciences and for Mathematics
of the Ruperto-Carola University of Heidelberg, Germany
for the degree of
Doctor of Natural Sciences

presented by

Anca Remes, M.Sc.
born in: Baia Mare, Romania
Oral-examination: 08.02.2018

Therapeutic transcription factor decoy oligodeoxynucleotides for Marfan syndrome and heart failure

Referees: Prof. Dr. Markus Hecker
Prof. Dr. Gert Fricker

Contents

List of abbrevations 1

1 Summary 6
1.1 English 6
1.2 German 8

2 Introduction 10
2.1 Therapeutic value of decoy oligonucleotides 10
2.2 Adeno-associated viruses as vectors for cardiovascular gene therapy 12
2.2.1 Life cycle of AAVs 12
2.2.2 AAV gene delivery for the therapy of cardiovascular disease 13
2.3 Marfan syndrome 15
2.3.1 General aspects 15
2.3.2 The importance of TGF-β and the AP-1 transcription factor family 16
2.3.3 Current treatment options 18
2.4 Heart hypertrophy and heart failure 19
2.4.1 General aspects 19
2.4.2 The role of NFAT in the development of heart hypertrophy 20
2.4.3 Current treatment options 21
2.5 Aims of the projects 22
2.5.1 Aims of Marfan syndrome project 23
2.5.2 Aims of heart hypertrophy project 23

3 Materials 24
3.1 Chemicals 24
3.1.1 Stimulants, inhibitors and substrates 24
3.1.2 Antibodies 24

3.1.3 Cloning enzymes 25
3.2 Oligonucleotides 26
3.2.1 Primers 26
3.2.2 Decoy ODNs 26
3.2.3 Molecular beacons 27
3.3 Plasmids and AAVs 27
3.4 Growth media and buffers 29
3.5 Kits 32

4 Methods 33
4.1 Cell culture 33
4.1.1 Isolation and culture of primary SMCs 33
4.1.2 Isolation and culture of primary neonatal cardiomyocytes 33
4.1.3 Isolation of adult cardiomyocytes 34
4.1.4 Culturing of HL-1 cells 34
4.1.5 *In vitro* hp decoy ODN treatment and AAV transduction 35
4.1.6 Cell stimulation 35
4.1.7 Functional *in vitro* assays 36
4.2 AAV production 37
4.3 Molecular biology 37
4.3.1 Hairpin decoy ODNs 37
4.3.2 Cloning of hpRNA decoy ODNs expressing plasmids 37
4.3.3 Quantitative real time PCR 39
4.3.4 *In situ* hybridization 40
4.4 Protein methods 41
4.4.1 Protein extraction and Western blot analysis 41
4.4.2 ELISA 42
4.4.3 Immunocytochemistry 42
4.4.4 Immunohistochemistry 43
4.4.5 Zymography 43
4.4.6 SUnSET assay 44
4.5 ROS measurement 44
4.5.1 *In vitro* 44
4.5.2 In tissue cryosections 45
4.6 Other tissue based methods 45
4.6.1 Cell size measurement 45

4.6.2 T-tubule analysis 45
4.6.3 Heart histology 46
4.7 Mouse models and techniques 48
4.7.1 Animal models 48
4.7.2 Aortic grafts transplantation 48
4.7.3 Transverse aortic constriction and echocardiography 49
4.8 Statistical data analysis 49

5 Results 51
5.1 Cloning of the AAV vectors 51
5.1.1 Digestion of the vectors 51
5.1.2 Analysis of cloned plasmids 51
5.2 Marfan syndrome project 53
5.2.1 ”Naked” hpAP-1 decoy ODNs uptake by SMCs 53
5.2.2 ”Naked” hpAP-1 consensus decoy ODN effects on mgR/mgR SMCs 53
5.2.3 Transduction efficiency of SMCs with AAV9 modified with targeting capsid peptides 58
5.2.4 Effect of AAV9SLR-mediated hpAP-1 RNA decoy ODNs generation in primary mgR/mgR SMCs 61
5.2.5 *Ex vivo* transduction of murine mgR/mgR aortic grafts with AAV9SLR 65
5.2.6 Effect of *ex vivo* transduction with AAV9SLR expressing hpAP-1 consensus RNA decoy ODNs 67
5.3 Heart hypertrophy project 77
5.3.1 ”Naked” hpNFAT decoy ODNs uptake by cardiomyocytes 77
5.3.2 ”Naked” hpNFAT decoy ODNs effect on cardiomyocyte hypertrophy 78
5.3.3 AAV6 effect on cardiomyocyte hypertrophy 81
5.3.4 NFAT5 activation in the presence of hp decoy ODNs 83
5.3.5 *In vivo* hpNFAT RNA decoy ODNs effect 86
5.3.6 Effect of AAV9 injection on phospholamban phosphorylation status 90
5.3.7 Effect of AAV9 injection on protein translation rate 94
5.3.8 Effect of AAV9 injection on cardiomyocyte size 95
5.3.9 Effect of AAV9 injection on T-tubule organization 96

6 Disussion 100
6.1 Marfan syndrome 100
6.1.1 Clinical importance 100
6.1.2 The role of AP-1 in aortic aneurysm dissection 101
6.1.3 Novelty of the study 102
6.1.4 Hairpin AP-1 decoy ODNs delivery 103
6.1.5 The importance of inflamation in aortic aneurysm development . . . 104
6.1.6 Endothelial permeability in Marfan syndrome 106
6.1.7 Targeting other transcription factors for treatment of Marfan syndrome 106
6.1.8 Limitations and perpectives 107
6.2 Heart hypertrophy 108
6.2.1 Clinical importance 108
6.2.2 Novelty of the study 109
6.2.3 Regulation of fetal gene program in heart hypertrophy 110
6.2.4 Cardiomyocyte architecture in heart failure 112
6.2.5 Remodeling of extracelular matrix in heart failure 113
6.2.6 NFAT transcription factors involved in heart hypertrophy 114
6.2.7 Limitations and perspectives 114
6.3 Conclusions 116

7 Acknowledgements 118

8 References 119

List of abbrevations

Units

°C	centigrade Celsius
bp	base pairs
g	gram(s)
h	hour(s)
Hz	hertz
IU	international units
kDa	kiloDalton
kbp	kilo base pair(s)
L	liter(s)
min	minute(s)
mL	milliliter, 10^{-3} L
mmol	millimole(s), 10^{-3} mole(s)
mm	millimeter, 10^{-3} m
ng	nanogram(s), 10^{-9} g
rpm	rotations per minute
s	second(s)
U/mL	Units/milliliter
μ	microgram, 10^{-6} g
μm	micrometer, 10^{-6} m
μmol	micromole(s), 10^{-6} mole(s)

Materials

AAV	Adeno-associated virus
AC	Adult cardiomyocytes
ATP	Adenosine triphosphate
BHQ	Black Hole Quencher
BSA	Bovine serum albumine
cons	Consensus
DAPI	4',6-Diamidino-2-phenylindole
DCFDA	2,7-Dichlorofluorescin diacetate
DEPC	Diethyl pyrocarbonate
DHE	Dihydroethidium
DNA	Deoxyribonucleic acid
DMEM	Dulbecco's Modified Eagle Medium
DMSO	Dimethyl sulfoxide
DTT	Dithiothreitol
EDTA	Ethylenediaminetetraacetic acid
ET-1	Endothelin-1
FBS	Fetal bovine serum
HBSS	Hank's Balanced Salt solution
HEPES	4-(2-Hydroxyethyl)-1-piperazineethanesulfonic acid
HRP	Immunoglobulin G
IgG	Horseradish peroxidase
IL1-β	Interleukin1-β
LB	Luria-Bertani
mut	Mutated
NCM	Neonatal cardiomyocytes
ODN	Oligodeoxynucleotide
PBS	Phosphate-buffered saline
PFA	Paraformaldehyde
PVDF	Polyvinylidene difluoride
RNA	Ribonucleic acid
SDS	Sodium dodecyl sulfate
SSC	Saline-sodium citrate
SMCs	Smooth muscle cells
SURE2	Stop Unwanted Rearrangement Events 2

TBS	Tris-buffered saline
TBS-T	TBS + Triton X-100
Tris	Tris(hydroxymethyl)aminomethane
TEMED	Tetramethylethylenediamine
WGA	Wheat germ agglutinin

Methods

ANOVA	Analysis of variance
ELISA	Enzyme-linked immunosorbent assay
FACS	Fluorescence-activated cell sorting
F.I.S.H.	Fluorescent *in situ* hybridization
ICC	Immunocytochemistry
IHC	Immunohistochemistry
SD	Standard deviation
SUnSET	Surface sensing of translation
TAC	Transverse aortic constriction
WB	Western Blot

Genes and proteins

ACE	Angiotensin converting enzyme
AP-1	Activator protein-1
AngII	Angiotensin-II
ANP	Atrial natriuretic peptide
BNP	Brain natriuretic peptide
CaMKII	Ca^{2+} calmodulin-dependent protein kinase II
CCL12	Chemokine (C-C motif) ligand 12
CD31	Cluster of differentiation 31
CT-1	Cardiotrophin-1
CTGF	Connective tissue growth factor
EGFP	Enhanced green fluorescent protein
eIF4E	Eukaryotic initiation factor 4E
FBN1	Fibrillin-1

FOXP3	Forkhead box P3
HSP70	Heat shock protein 70
IFN-γ	Interferon-γ
IP3R	Inositol 1,4,5-trisphosphate receptor
JNK	c-Jun N-terminal kinase
KLF4	Kruppel like factor 4
LDLR	Low density lipoprotein receptor
MCP-1	Monocyte chemoattractant protein-1
M-CSF	Macrophage colony stimulating factor
MHC	Matrix metalloproteinase
MMP	Myocyte enhancer factor-2
MEF2	Myocyte enhancer factor-2
NADPH	Nicotinamide adenine dinucleotide phosphate
NOX4	NADPH Oxidase 4
NFAT	Nuclear factor of activated T cells
NF-κB	Nuclear factor kappa-light-chain-enhancer of activated B cells
RCAN1	Regulator of calcineurin
RPL32	Ribosomal protein L32
RyR	Regulator of calcineurin
SERCA2a	Sarcoplasmic/ endoplasmic reticulum Ca^{2+} ATPase 2a
SMA	Smooth muscle actin
SMIT	Sodium/myo-inositol cotransporter
STAT-1	Signal transducer and activator of transcription 1
RCAN1	Regulator of calcineurin
TGF-β	Transforming growth factor-β
TIMP	Tissue inhibitors of matrix metalloproteinases
UBF	Upstream binding factor
VEGF	Vascular endothelial growth factor
ZO-1	Zona occludens-1

Other abbreviations

$<$	Smaller than
%	Percentage

BW	Body weight
cDNA	Complementary DNA
CMV	Cytomegalovirus
ds	Double stranded
EC coupling	Excitation-contraction coupling
EF	Ejection fraction
Em	Maximal emission
Ex	Maximal excitation
FRET	Frster resonance energy transfer
FS	Fractional shortening
HW	Heart weight
LV	Left ventricle
MOI	Multiplicity of infection
mRNA	Messenger RNA
OMIM	Online Mendelian Inheritance in Man
PEX	Hemopexin
ROS	Reactive oxygen species
shRNA	Short hairpin RNA
TF	Transcription factor
tRNA	Transfer RNA
TL	Tibia length
UV	Ultraviolet
WT	Wild type

1

Summary

1.1 English

The inhibition of transcription factor activation can be translated into a novel therapeutic strategy for a wide range of disease models. Decoy oligodeoxynucleotides (ODNs) containing the consensus binding site of a target transcription factor (TF) subsequently prevent binding of the TF to the promoter regions of its target genes associated with certain disorders. Decoy ODNs were shown to be safe and effective, but until now the main delivery route consisted of local application. However, depending on the target organ, this approach is not always feasible. Therefore, the main aim of this study is the establishment of an adeno-associated virus (AAV)-based method of decoy ODNs delivery, which allows continous generation of the therapeutic nucleic acid compound as a short hairpin RNA (shRNA) in AAV-transduced cells.

In Marfan syndrome, increased Transforming growth factor-β (TGF-β) bioavailability induces enhanced activity of activator protein-1 (AP-1), which in turn upregulates expression of matrix metalloproteinases (MMPs). These endopeptidases were proven to be involved in the elastin degradation and aortic fragility which causes aortic aneurysm formation and dissection. The effect of ”naked” hpAP-1 decoy ODNs application and AAV9SLR transduction was analysed using primary mgR/mgR SMCs as an *in vitro* model and AP-1 activation was induced by interleukin-1 β (IL-1β) treatment. Both treatments led to decreased mRNA level of AP-1 target genes MMP9 and monocyte chemotactic protein-1 (MCP-1), as well as decreased MMP activity and smooth muscle cells (SMCs) migration capacity. Moreover, IL-1β-induced reactive oxygen species (ROS) production was reduced.

In vivo experiments were performed using mgR/mgR mice. By F.I.S.H. experiments, the expression of the hpAP-1 RNA decoy ODNs in endothelial cells and SMCs was demonstrated, 4 weeks after *ex vivo* tissue transduction and reimplantation into mgR/mgR

mice. Furthermore, AP-1 target genes MMP9 and MCP-1 were downregulated and MMP protein level and activity was significantly reduced. Additionally, AAV9SLR transduction caused a remarkable decrease in the number of infiltrating macrophages and improved endothelial tight junction integrity. Importantly, AP-1 inhibition significantly decreased the level of elastin degradation, as shown by a reduction in the number of islands of damage.

The second aim of this study was the preclinical validation of AAV9 vector expressing hpNFAT decoy ODNs as a therapeutic approach in an experimental model of left ventricular hypertrophy and heart failure in mice (transverse aortic constriction, TAC). The effect of hpNFAT decoy ODNs and AAV9 transduction was first assessed *in vitro* by employing the cardiomyocyte cell line HL-1, as well as primary neonatal cardiomyocytes, which were treated with the pro-hypertrophic stimulus endothelin-1 (ET-1). The results revealed a significant downregulation of the fetal gene programme, represented by atrial natriuretic peptide (ANP) and brain natriuretic peptide (BNP) as well as decreased myosin heavy chain-β (β-MHC) protein expression. Moreover, hpNFAT decoy ODNs and AAV9 expressing hpNFAT RNA decoy ODNs reduced ET-1 induced protein synthesis rate.

Two weeks prior to inducing myocardial hypertrophy through aortic stenosis by TAC surgery, AAV9 was injected systemically. The vector led to the intracellular synthesis of the active RNA decoy ODNs in cardiomyocytes and decreased expression of fetal gene programme. In addition, markers of myocardial hypertrophy heart weight/tibia length (HW/TL) and heart failure lung weight/tibia length (LW/TL) were significantly reduced in treated mice. At the same time, heart function was markedly improved and fibrosis markers were reduced by NFAT neutralization through AAV9 injection.

In conclusion, AAV-mediated decoy ODN delivery to the target organ may be a powerful tool to regulate the expression of genes involved in the progression of certain diseases. The present study showed the therapeutic efficacy of this concept by investigating two cardiovascular disease models.

1.2 German

Herz-Kreislauf-Erkrankungen stellen in der westlichen Welt die häufigste Todesursache dar. Eine neuartige therapeutische Strategie zum Einsatz für ein breites Spektrum dieser Erkrankungsarten ist es, die Transkriptionsfaktor-Aktivierung zu hemmen. In dieser Studie werden zwei Erkrankungen betrachtet, zum einen die Aortenaneurysma-Dissektion bei Patienten mit Marfan-Syndrom und zum anderen die Herzinsuffizienz. Die molekularen Mechanismen und beteiligten Transkriptionsfaktoren dieser kardiovaskulären Komplikationen wurden bereits in anderen Arbeiten intensiv untersucht.
Decoy Oligodeoxynucleotide (ODNs) enthalten die Konsensbindungsstelle eines Ziel-Transkriptionsfaktors und verhindern so eine Bindung an die Promotorregion der Gene, die mit bestimmten Erkrankungen assoziiert sind. Decoy ODNs erweisen sich als effektiv und sicher. Jedoch bestand der Applikationsweg bisher hauptsächlich in der lokalen Anwendung, was je nach Zielorgan allerdings nicht immer möglich ist. Daher ist das Hauptziel dieser Studie die Etablierung einer AAV-basierten Methode, um die kontinuierliche Bildung von Decoy ODNs als shRNA in den transduzierten Zellen zu ermöglichen.
Die gesteigerte TGF-β Bioverfügbarkeit ist für das Marfan-Syndrom kennzeichnend. Sie induziert die Aktivierung des Transkriptionsfaktors AP-1, was eine gesteigerte Expression von MMPs zur Folge hat. Diese Endopeptidasen sind ursächlich am Elastinabbau und der Fragilität der Aorta beteiligt, welches zur Bildung bzw. Dissektion eines Aortenaneurysmas führen kann. Der Effekt der nackten hpAP-1 Decoy ODNs und der AAV9SLR Transduktion wurde zunächst in primären kultivierten mgR/mgR SMCs *in vitro* analysiert, bei denen IL-1β-vermittelt AP-1 aktiviert wurde. Beide Ansätze führten zu einer Reduktion der mRNA-Expression der AP-1 Zielgene MMP9 und MCP-1. Ebenso konnten verminderte MMP Aktivität und Migrationskapazität der SMCs beobachtet werden. Darüber hinaus wurde die durch IL-1β-induzierte ROS-Produktion gehemmt.
In vivo Experimente wurden mit Fibrillin-1-defizienten mgR/mgR Mäusen durchgeführt. 4 Wochen nach *ex vivo* Transduktion und Reimplantation in den mgR/mgR Mäusen wurde mittels der F. I. S. H. Methode die Bildung der hpAP-1 RNA Decoy ODNs in den Endothelzellen und SMCs der aortalen Transplantate erfolgreich nachgewiesen. Darüber hinaus konnte die Expression der AP-1 Zielgene MMP9 und MCP-1 und auch die MMP-Aktivität signifikant gehemmt werden. Zusätzlich bewirkte die AAV9SLR Transduktion eine Abnahme der infiltrierenden Makrophagen in der Aorta und verbesserte die Integrität der endothelialen Zellkontakte. Insbesondere verhinderte die

Hemmung der AP-1-Aktivität das Fortschreiten der aortalen Elastolyse und somit die Schädigung der Gefäßwand.
Das zweite Studienziel war die präklinische Validierung des AAV9-Vektors, der neutralisierende hpNFAT Decoy ODNs als therapeutischer Ansatz in einem experimentellen Modell der linksventrikulären Hypertrophie und Herzinsuffizienz bei Mäusen (TAC) exprimiert. Die Wirkung der hpNFAT decoy ODNs nach der AAV9 Transduktion wurde zunächst wiederum *in vitro* mit kultivierten Zellen der HL-1 Kardiomyozytenzellinie sowie primären neonatalen Kardiomyozyten untersucht, die mit dem pro-hypertrophen Stimulus ET-1 behandelt wurden. Die Ergebnisse zeigten eine signifikante Hemmung der Aktivierung des pro-hypertrophen fetalen Genprogramms für ANP und BNP sowie eine verminderte β-MHC Proteinexpression. Darüber hinaus wurde die ET-1-induzierte und für die Hyprophie-Entstehung charakteristische Steigerung der Proteinsynthese durch die AAV9-meditierte Bildung von hpNFAT RNA Decoy ODNs gehemmt.
Zwei Wochen vor der durch die operative Aortenkonstriktion (TAC) induzierte Myokardhypertrophie wurde der AAV9-Vektor systemisch injiziert. Die intrazelluläre Synthese der hpNFAT Decoy ODN in den Kardiomyozyten hatte eine verminderte Expression von fetalen Genen in den transduzierten Zellen zur Folge. Zusätzlich waren die Marker der Myokardhypertrophie (Herzgewicht/Tibialänge) und der Herzinsuffizienz (Lungengewicht/Tibialänge) bei den behandelten Mäusen signifikant reduziert. Gleichzeitig konnte durch NFAT-Neutralisation mittels AAV9-Injektion bei den behandelten Tieren die Herzfunktion deutlich verbessert und die Fibrosemarker reduziert werden.
Zusammenfassend ist festzustellen, dass die AAV-vermittelte kontinuierlich längerfristige Decoy ODN-Bildung in Zellen des Zielorgans eine therapeutische Möglichkeit eröffnet, die Expression von Genprodukten zu hemmen, welche an der Pathogenese und Progression bestimmter Krankheiten beteiligt sind. Die vorliegende Studie hat in zwei Tiermodellen für kardiovaskuläre Erkrankungen erfolgreich den Nachweis der therapeutischen Wirksamkeit dieses Konzepts erbracht.

2

Introduction

2.1 Therapeutic value of decoy oligonucleotides

Transcription factors (TF) are proteins that play a crucial role in gene regulation by binding to the promoter region of target genes and initiating transcription. One approach of controlling abnormal gene expression in a pathological context is to target the process of transcription. Decoy oligodeoxynucleotides (decoy ODNs) are short double stranded DNA molecules that harbour the sequence of the TF binding site in the promoter region of the target gene [85]. After cellular uptake, decoy ODNs bind to the TF therefore inhibiting transcription. Hence, this approach can be translated into therapeutic strategies to inhibit genes involved in disease initiation or development by neutralizing specific TFs. The main advantage of the decoy ODNs technology is that gene transcription is not totally abolished, which is beneficial for physiological processes.

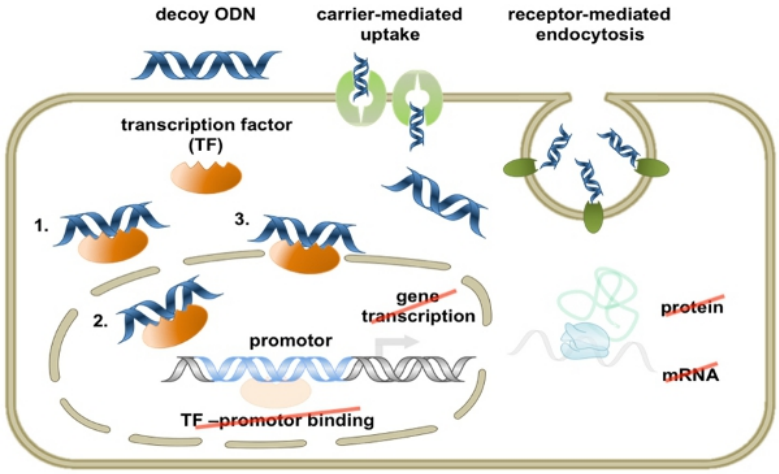

Fig. 1: The mechanism of action of TF decoy ODNs. Decoy ODNs are taken up by cells either through a carrier-mediated mechanism or receptor-mediated endocytosis. Afterwards, they bind to the target TF and gene transcription is inhibited. (Reproduced from [191].)

The therapeutic effect of decoy ODNs was proven in various preclinical disease models. Strategies of blocking nuclear factor kappa-light-chain-enhancer of activated B cells (NF-κB) through decoy ODNs were shown to be effective in attenuating respiratory disease [118], rheumatoid arthritis [202], myocardial infarction [139], abdominal aortic aneurysm [135], atopic dermatitis [144] and some types of cancer [161] in animal models. In addition, activator protein-1 (AP-1) and signal transducer and activator of transcription 1 decoy ODNs were shown efficient in reducing transplant vasculopathy [189] and a dual AP-1 and SMAD decoy ODNs injection reduced fibrosis in an acute dermal wound repair mouse model [232].

Clinical trials making use of the decoy ODNs technology are summarized in Table 2. These studies suggest the potential of decoy ODNs to be translated into therapeutic approaches for diverse disease models. Moreover, the low toxicity of the compounds, suggested in clinical trials, attests for the safety of these nucleic acid drugs. More transcription factors targets and delivery options have to be investigated in order to turn decoy ODNs into effective therapies.

TF target	Disease	Clinical Phase	Key outcome	Year
E2F	Venous bypass graft vasculopathy	3	Failed to demonstrate clinical efficacy, but demonstrated clinical safety (ClinicalTrials.gov Identifier: NCT00041925, ClinicalTrials.gov Identifier: NCT00042081)	2005–2013
NF-κB	Restenosis after percutaneous coronary intervention	Open-label 1/2a	Stent-based local delivery of NF-κB decoy ODN reduced in-stent neointima formation; no adverse drug reactions; only small patient cohort (17 cases); further placebo controls necessary	2008
NF-κB	Mild-to-moderate atopic dermatitis	1/2	Topical application of three concentrations of a NF-κB decoy ODN; no study results published so far	2005–2008
NF-κB	Moderate-to-severe facial atopic dermatitis	3	Efficacy and safety of the drug in 221 atopic dermatitis patients (aged 16 and over); no statistically significant difference between the NF-κB decoy ODN treated group and the placebo group in the primary endpoint (improvement in the dermatological condition scores at week 4); no serious adverse events related to treatment with the NF-κB decoy ODN	2015–
NF-κB	Discogenic lower back pain (DLBP)		FDA clearance of investigational new drug (IND) application for NF-κB decoy ODN for DLBP treatment	2017–
STAT6/NF-κB chimera	Asthma, rheumatoid arthritis, osteoarthritis, and chronic inflammatory bowel disease		product development including optimization in drug formulation and safety studies	2016–
STAT3	Head and neck squamous cell carcinoma	1	Single intravenous injection inhibited xenograft growth and downregulated STAT3 target genes in tumours (ClinicalTrials.gov identifier: NCT00696176)	2008–2015

Fig. 2: Main clinical trials employing decoy ODNs for various disease models. Reproduced from [85].

2.2 Adeno-associated viruses as vectors for cardiovascular gene therapy

First isolated as a contaminant during adenovirus production in HEK-293 (human embryonic kidney-293) cells [5], adeno-associated viruses (AAVs) soon became feasible and attractive tools for gene therapy. The main advantages are the non-pathogenic nature and low immunogenicity of the AAVs. One of the most successful clinical trials involving AAV-mediated gene transfer was designed to treat hemophilia B, which showed that a single AAV injection led to a stable expression of the transgene and induced no immunogenic response or toxicity in hepatocytes [147]. Moreover, an AAV-based drug was approved for use in Europe and in the United States in 2012 for the treatment of lipoprotein lipase deficiency [218].

2.2.1 Life cycle of AAVs

AAVs belong to the family of *Parvoviridae* and require the presence of other viruses, mostly adenoviruses to replicate [145]. Other virus types such as Herpes simplex virus type 1, human Cytomegalovirus, Vaccinia virus and human Papilloma virus type 16 were shown to assist in promoting the life cycle of AAVs. The single-stranded genome of about 4.8 kbp contains three genes: *Rep* (Replication), *Cap* (Capsid) and *aap* (Assembly). Palindromic inverted terminal repeats (ITRs) flank the *Rep* and *Cap* regions and play an important role in AAV packaging and replication. In addition to *Rep* and *Cap*, AAV production requires a helper plasmid which provides adenoviral genes [43]. One of the disadvantages of AAV design is the limited capacity of packaging. The first step required for AAV infection is represented by binding of the capsid to cell membrane receptors. Several receptors have been identified, depending on the AAV serotype investigated. AAV2 and AAV3 anchor to heparan sulfate proteoglycan, while AAV9 employs O-linked galactose [6]. Several integrin types and laminin receptor were described as coreceptors [133]. Recently, a previously uncharacterised transmembrane protein was shown to be an essential AAV receptor [160]. Afterwards, cell entry is carried out through clathrin-coated endosomes. The endosomal release of AAVs occurs after acidification of the vesicles which precedes cytoplasmatic release. Subsequent to nuclear translocation, the ds DNA is released from the capsid and emphRep genes are expressed. Next, the genes required for capsid assembly are synthetized inside the nucleus. Subsequently, the release of the newly produced AAV particles is mediated by the helper virus (Fig. 3) [107].

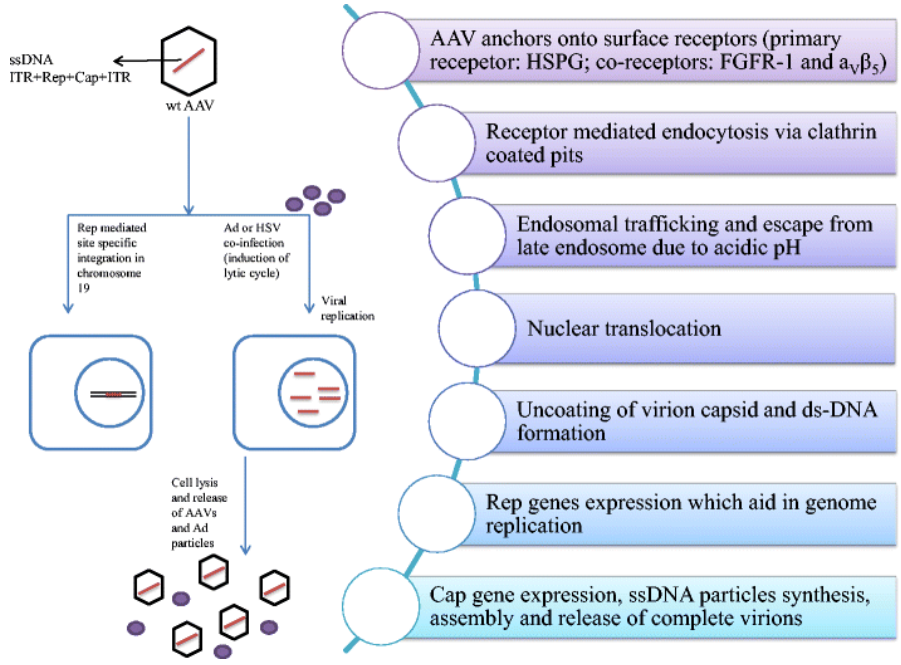

Fig. 3: The steps of AAV infection. AAV requires co-infection with a helper virus for production of the viral genes and generation of the progeny AAVs. Reproduced from [10].

2.2.2 AAV gene delivery for the therapy of cardiovascular disease

Cardiovascular disease represents the main cause of mortality worldwide (World Health Organization).The understanding of molecular mechanisms leading to various types of cardiovascular complications enabled development of new therapeutic strategies. Surgery or pharmacological treatment offer solely temporary beneficial effects and symptom relief but in most of the cases do not provide a long-term solution [210]. Gene therapy using AAV as gene delivery systems was shown to be a feasible approach by allowing the modulation of pathogenic gene levels.

Until now, 12 AAV serotypes have been characterized, each with distinctive tissue tropism. AAV9 was shown to have elevated heart specificity, as well as high transgene expression in cardiomyocytes, being a valuable tool for myocardial gene delivery [239]. AAV8 also led to cardiomyocyte transduction, while AAV1 and AAV6 efficiently transduce neonatal mouse myocytes *in vivo* [214]. The performance of each AAV serotype is highly dependent on the delivery route. Although systemic intravenous injection was demonstrated to lead to cardiomyocyte transduction in mice, large animals require more advanced delivery systems for successful infection. Retrograde injection through the coronary veins was proven to be a feasible approach of gene delivery in pigs [162]. Directed injection into the myocardium was also shown to lead to transgene expression in large animals [153]. Moreover, ultrasound-directed microbubbles improved the

directed myocardial delivery of the AAVs and increased significantly cardiomyocyte transduction efficiency. In addition, substances that induce capillary permeability, such as vascular endothelial growth factor (VEGF), serotonin or histamine were employed to allow higher contact of AAVs and cardiomycytes by allowing the vector to pass the endothelial barrier [168].
Recent advances in AAV research has made it possible to obtain highly specific vectors which transduce the target organ. For example, small ligands or peptides have been introduced in capsid structure in order to direct AAV to endothelial cells [188, 217, 208]. Another approach which was proven to be successful in improving the organ specificity is the use of bispecific antibodies or biotin, that interacts with receptors on the cell membrane [43].
In addition, the use of AAV vectors with cardiac-specific promoters have been developed, highly improving transduction specificity. These include α-myosin heavy chain, cardiac troponin and myosin light chain 2 promoters [234].

Depending on the disease model, different AAV-based strategies have been employed:

Stimulation of therapeutic angiogenesis

Pro-angiogenic factors VEGF-165 and angiopoietin-1 overexpression through AAV9 injection was shown to lead to increased endothelial cell proliferation and therefore to the formation of new blood vessels in a murine model of myocardium infarction [194]. Moreover, cardiomyocyte apoptosis was dramatically reduced. In order to minimize the possible side effects that could occur after the overexpression of the pro-anigiogenic factors, a hypoxia-responsive element was introduced, to induce transgene expression only in hypoxic conditions [194]. Another approach consisted of AAV9-mediated delivery of angiogenin and human growth hormone, which significantly attenuated infarction size [10].

Gene therapy of heart failure

The promising results obtained by SERCA2a (Sarcoplasmic/endoplasmic reticulum Ca^{2+} ATPase 2a) overexpression in pre-clinical animal models [23] was followed by CUPID phase 2b clinical trial [240]. However, the trial failed to reach its end point and no significant differences were noted between treated and placebo groups (clinical trial number NCT02346422). In another study, AAV9-mediated downregulation of phospholamban, a SERCA2a inhibitor, inhibited heart failure in mice [195].

AAV-targeting of the β-adrenergic receptor was also shown to be a novel approach for the treatment of heart failure. The protein level of GRK2 (G protein-coupled receptor kinase 2) in cardiomyocytes was shown to be upregulated under stress conditions and desensitizes β-adrenergic pathway, leading to decompensated cardiomyopathy [166]. Downregulation of GRK2 through AAV9 transduction was shown to inhibit myocardium hypertrophy transition into decompensated heart failure [185].

Correction of genetic cardiomyopathies

Several types of genetic cardiomyopathies have been described [24]. For these types of disease, AAV9-mediated gene transfer is advantageous due to long-term correction of the genetic defect. Through this method, the attenuation of Duchenne muscular dystrophy related cardiomyopathy was demonstrated in large animals [15]. Silencing of mutant MHC transcripts which lead to heart failure by using RNA interference was also proven successful in mediating gene expression in cardiomyocytes and exerting a positive effect on cardiac function [97].

Gene therapy for aortic diseases

Targeting inflammation was shown to reduce the size of atherosclerotic plaques. For example, AAV2/8-mediated gene transfer of forkhead box P3, a marker of regulatory T cells, decreased aortic wall thickness and lowered systolic blood velocity as compared to control animals [28]. Additionally, overexpression of interleukin-10 and STAT-3 by AAV8 transduction of the aorta decreased atherogenesis in low density lipoprotein receptor-knockout mice [27].

2.3 Marfan syndrome

2.3.1 General aspects

Marfan syndrome, first described in 1896 by Dr. Antoine Marfan, is a rare genetic disorder (2 individuals in 10,000, according to OMIM), caused by a loss-of-function mutations in the fibrillin-1 gene (*FBN1*). This disease affects the skeletal, ocular and most importantly, the cardiovascular systems. Cardiac complications observed in Marfan syndrome patients include aortic dilatation, thickening and prolapse of the aortic valves, as well as dilated cardiomyopathy [101], [192], while the main mortality cause constitutes

aortic aneurysm dissection [101].
More than 600 types of *FBN1* mutations have been described, with 25 % of the cases occuring *de novo* [169]. Fibrillin-1 is a 350 kDa glycoprotein and has been shown to be one of the main components of the elastic fibers in blood vessels [212]. Moreover, it was proven to be a structural substrate for elastin deposition and assembly during development [42]. The internal elastic fibers anchor endothelial cells through integrins [222], providing integrity to the endothelial monolayer (Fig. 4).

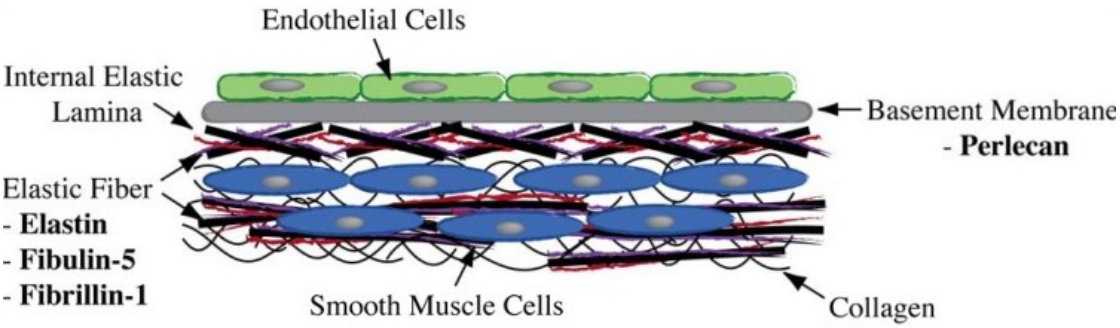

Fig. 4: The interaction between vascular cells and elastic fibers. The close proximity of endothelial cells, SMCs and fibers shows the structural role of fibrillin-1 in the vessel. Reproduced from [223].

2.3.2 The importance of TGF-β and the AP-1 transcription factor family

Apart from its structural role, fibrillin-1 has a major effect on transforming growth factor β (TGF-β) bioavailability, as depicted in Fig. 5. TGF-β factors are synthesized as precursor proteins, consisting of the latency associated peptide (LAP) in the N-terminal domain, and the growth factor in the C-terminal domain. Two precursor proteins dimerize through disulfide bonds and are afterwards cleaved in the Golgi apparatus leading to the formation of the small latex complex (SLC). Under these conditions, the mature TGF-β is non-covalently bound to the LAP. The SLC is bound to latent TGF-β binding protein (LTGBP), constituting the complex called large latent complex (LLC). The LLC can bind to extracellular matrix through the C-terminal domain of the LTGP. Through this mechanism, the inactive TGF-β is localized close to the microfibrils and interacts with fibrillin, which in turn can affect its activation status [99], [9], [236].
Functional fibrillin can bind TGF-β into an inactive form, whereas mutant fibrillin, characteristic for Marfan syndrome, causes an increase in its bioavailability and hence activity. Dysfunctional TGF-β signalling was shown to be the cause for the phenotype

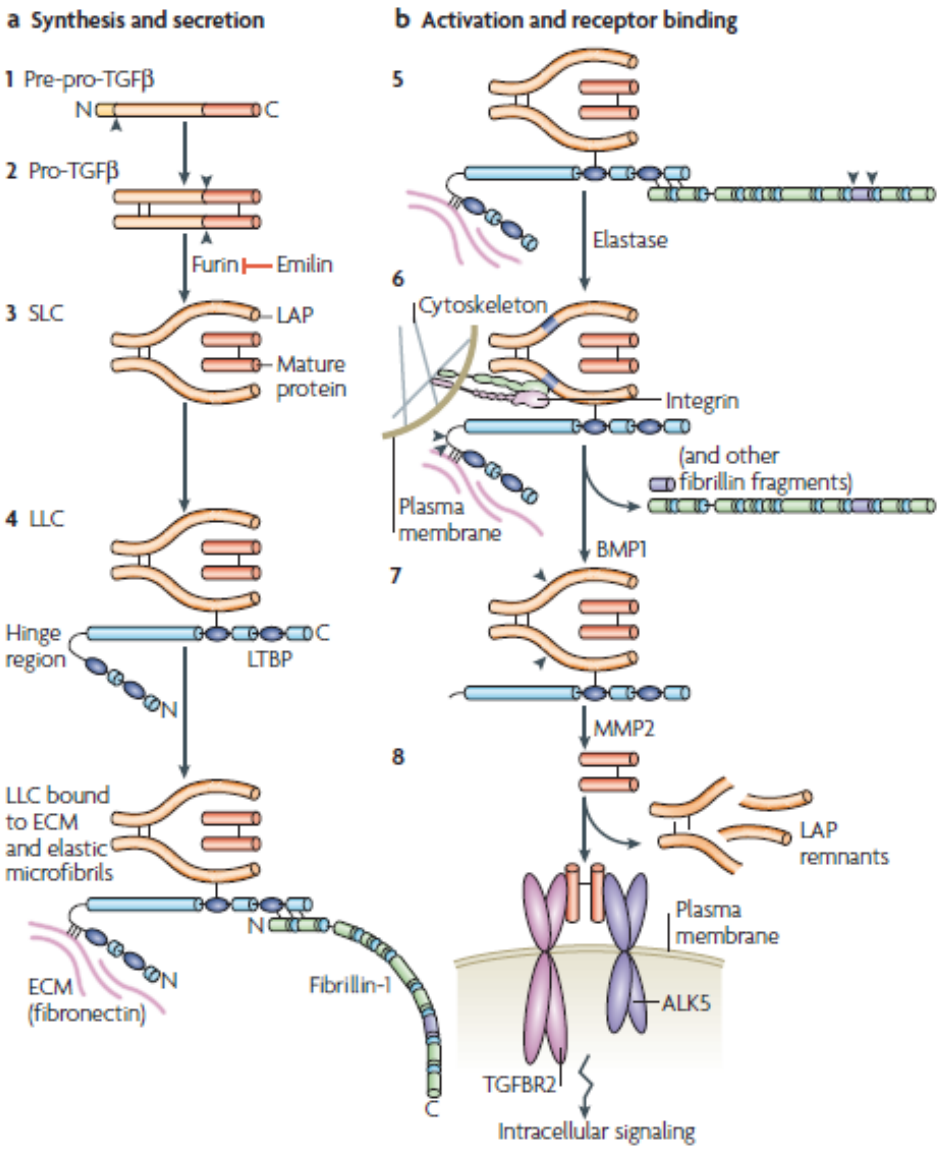

Fig. 5: The mechanism of TGF-β processing and the role of microfibrils in TGF-β inactivation. Reproduced from [200].

observed in the mgR/mgR mouse model, including aortic aneurysm formation, skeletal defects, mitral valve prolapse and pulmonary complications [150, 37, 149]. These studies suggest that Marfan syndrome is not only a structural defect of the connective tissue caused by mutant fibrillin-1 protein and disorganized microfibrils, but is caused by elevated TGF-β activity.

Consistently, an increased TGF-β protein level in plasma isolated from mgR/mgR mice was measured in comparison to wild type littermate controls [130]. Moreover, TGF-β

concentration correlated with the size of the aortic diameter. The same trend was observed in human samples isolated from Marfan patients, who had significantly higher amounts of circulating TGF-β related to healthy donors [130].
The importance of TGF-β in the pathogenesis of Marfan syndrome was confirmed by administration of a TGF-β neutralizing antibody to young (4 weeks old) mgR/mgR mice before aortic aneurysm formation was apparent. The treated mice presented with a significant decrease in the aortic root diameter, as compared to the placebo-treated group. Moreover, the aortic wall architecture was significantly improved, as suggested by the decrease in the number of elastin breaks in aortic cryosections. [80].
The non-canonical TGF-β signalling pathway was shown to be critical for the aortic aneurysm progression in the context of Marfan syndrome [88]. Fibrillin-1 deficient mice were confirmed to have increased JNK (c-Jun N-terminal kinase) activity, which phosphorylates Jun proteins [88]. As a consequence, AP-1 (activator protein-1) target genes are activated. Other studies confirm this hypothesis, showing that AP-1 transcription factor family is activated by TGF-β [211].
AP-1 induces the expression of matrix metalloproteinases (MMPs), as well as pro-inflammatory cytokines, which were demonstrated to be increased in the context of Marfan syndrome [94]. Significantly higher protein levels of gelatinases MMP2 and MMP9 were shown to be present in the plasma and aortic tissue isolated from mgR/mgR mice, as compared to wild type controls [35]. Moreover, mgR/mgR mice treatment with doxycycline, a non-specific MMP inhibitor, led to a significant increase in the mean survival rate of the Marfan mice by decreasing the elastin fibers degradation through diminishing MMP activity [228].

2.3.3 Current treatment options

Before the implementation of open-heart surgery, life expectancy of Marfan syndrome patients was 45 years [141], with the leading cause of death being represented by aortic aneurysm rupture. Recently, due to advances in the surgical management of patients, the life span of Marfan patients was significantly increased to over 60 years [59]. The 1-year mortality rate of prophylactic surgery in case of extreme dilatation of the aorta (larger than 50 mm) is under 2% [38].
Pharmaceutic therapy for Marfan patients involves β-adrenergic blockade through propanolol administration. The treated group showed decreased rate of aortic root dilatation in comparison to controls by negative chronotropic and inotropic effects of the drug and therefore reducing the stress on aortic wall.

Losartan, an angiotensin type II receptor antagonist, was previously proven to reduce TGF-β plasma levels in a mouse model of hypertrophic cardiomyopathy [119] and allograft nephropathy [26]. The efficiency of this drug was therefore studied in the context of Marfan syndrome. Losartan solution was injected either pre- or post-natally, leading to the normalization of aortic wall structure, which was undistinguishable to the wild type control [80].

2.4 Heart hypertrophy and heart failure

2.4.1 General aspects

Heart failure is defined as a syndrome in which heart function cannot support the metabolic requirements of the tissues. Common factors that trigger heart failure are hypertension, myocardial infarction, coronary heart disease, inflammation and genetic predisposition. Other conditions that increase the risk of heart failure are diabetes, thyroid disorders and the use of cardiotoxic substances [125]. Heart failure affects 3-4 % of the people over 45 years of age in the Western world. With increasing rates of diabetes and obesitiy, as well as with an aging population, the rates of this disease are expected to grow [13]. Currently, no cure can reverse heart failure, and the prognosis of the patients remains extremely poor, with a mortality of 1 in 3 patients one year after diagnosis [13]. In the presence of biomechanical stress, the myocardium undergoes the process of hypertrophy which is an adaptive response to the increase in wall tension. This first step consists of increase in myocyte dimensions, elevated protein translation rate and reactivation of fetal gene program [64]. Cardiomyocytes are terminally differentiated cells and stop dividing soon after birth. Therefore, stress stimuli cause growth in cardiomyocyte size, without increase in cell number and re-activation of the fetal gene program, atrial natriuretic peptide (ANP), brain natriuretic peptide (BNP) and MHC-β which are considered markers of hypertrophic response. Moreover, altered protein translation rate is observed, caused by increase in the ribosome biogenesis, as well elevated translation capacity [83]. On the functional level, reduced cardiomyocyte contractility and slow relaxation is observed. [84]. On the other hand, cardiomyocyte loss following myocardial infarction leads to inflammatory cell infiltration and alteration in the extracellular matrix, processes that contribute to infarct healing.

Other cell types participate in the development of heart disease. Fibroblast proliferation increase the extracellular matrix production, SMCs promote vascular stiffness and endothelial cells become dysfunctional [22]. In turn, heart function rapidly deteriorates

and the risk of sudden death increases [48].
In contrast, physiological hypertrophic response manifests through distinct mechanisms and is a reversible process [7]. Stress induced by exercise or pregnancy preserves or even enhances contractility. Additionally, a normal sarcomere organization is observed [84]. Physiological hypertrophy does not involve fibrosis or cardiomyocyte apoptosis.
Pathological heart hypertrophy is a progressive disease. As it advances, myocardium function decreases and the patient symptoms worsen. As cardiac hypertrophy becomes maladaptive, cardiomyocyte death is observed, through apoptosis and necrosis. Autophagy is also noted, accompanying cell death [216]. Pathological extracellular matrix accumulation is another hallmark of heart failure. This process is driven by cardiac fibroblasts, which proliferate in response to the stress stimuli and differentiate into myofibroblasts. Collagen1, collagen3 and fibronectin are the main constituents of the extracellular matrix observed in heart failure. Fibrosis can be detected in between cells (interstitial fibrosis), in the perivascular areas or replacing lost cardiomyocytes. Extensive fibrosis explains the arrhythmias that occur in heart failure patients [180].
Some studies showed that hypertrophy development in a pressure-overload mouse model does not improve cardiac function, concluding that targeting hypertrophy can be relevant in heart failure prevention [58]. Moreover, increased left ventricular mass was proven to correlate with worse prognosis in patients at risk of developing heart failure [116]. Therefore, the mechanisms leading to myocardial hypertrophy have been intensively studied in order to advance new therapeutic strategies.

2.4.2 The role of NFAT in the development of heart hypertrophy

A number of transcription factors have been proven to play a central role in the development of maladaptive cardiac hypertrophy. An enhanced activity of nuclear factor of activated T cells (NFAT), myocyte enhancer factor-2 (MEF-2), GATA and HAND transcription factor families was observed during pathological remodelling in heart failure [3].
Chronic stress on the myocardium leads to increased cytosolic Ca^{2+} concentration, which is a key molecule that induces pro-hypertrophic signalling pathways [235] and regulates physiological processes such as EC-coupling, metabolism and cell death [52]. Reduced SERCA activity and increased Ca^{2+} leak through ryanodine receptor 2 (RyR2) are the main causes of elevated Ca^{2+} concentration in the cytoplasm. Moreover, myocyte hypertrophy causes an influx of Ca^{2+} through voltage-gated L-type Ca^{2+} channel or IP3 (inositol 1,4,5-trisphosphate) receptor. Continuous increase in cytosolic Ca^{2+} amount leads to the activation of calcineurin/NFAT and Ca^{2+} calmodulin-dependent protein ki-

nase II (CaMKII) pathways [52], as depicted in Fig. 6.
The role of calcineurin signalling was first characterized in the immune system. This pathway is activated by elevations in Ca^{2+} concentrations [60]. Calcineurin dephosphorylates NFAT isoforms 1-4, enabling their translocation to the nucleus in the non-phosphorylated form and therefore inducing the transcriptional activity of these proteins [209].
The importance of calcineurin-NFAT pathway in the development of heart hypertrophy was previously demonstrated in transgenic mice by using gain and loss of function studies. Cardiac-specific overexpression of the catalytic subunit of calcineurin under control of the α-MHC promoter induced an elargement of myocardium size, reactivation of fetal gene program and developement of heart failure[137]. In addition, transgenic mice expressing only the active form of NFAT3, located constitutively in the nucleus, exhibit a similar phenotype including cardiac fibrosis, cardiomyocyte hypertrophy and dilated cardiomyopathy [137]. Administration of the immunosuppressant drug cyclosporin A could reduce the severity of heart failure in these mice, further proving the importance of this pathway. Moreover, NFATc2 deletion in mice caused resistance to TAC (transverse aortic constriction)-induced heart hypertrophy and reduction in heart failure parameters [16].
Calcineurin-NFAT pathway was shown to play a major role in pathological, but not physiological cardiac hypertrophy. Pathological stimulation through myocardium infarction caused a significant increase in nuclear translocation of NFAT, while exercise-induced hypertrophy did not [220]. In addition, VIVIT, a specific NFAT inhibitory peptide, was proven to be effective in preventing heart hypertrophy in a pressure-overload rat model. The systemic application of the compound led to downregulation of fetal gene program and to a significant improvement in heart function parameters [112].

2.4.3 Current treatment options

Treatment strategies for heart failure include pharmacological drug treatments, implantation of devices that improve heart contractility and surgery [110].
Angiotensin converting enzyme (ACE) inhibitors were first proven effective in treating hypertensive disease, but their therapeutic effect was later shown in slowing the maladaptive remodelling process in heart failure. This class of compounds could decrease the hospitalization due to congestive heart failure and decreased the mortality rate [233]. Ramipril, an ACE inhibitor drug, was shown to decrease the cardiovascular events in the case of diabetic patients with high risk of myocardial infarction and heart failure (HOPE

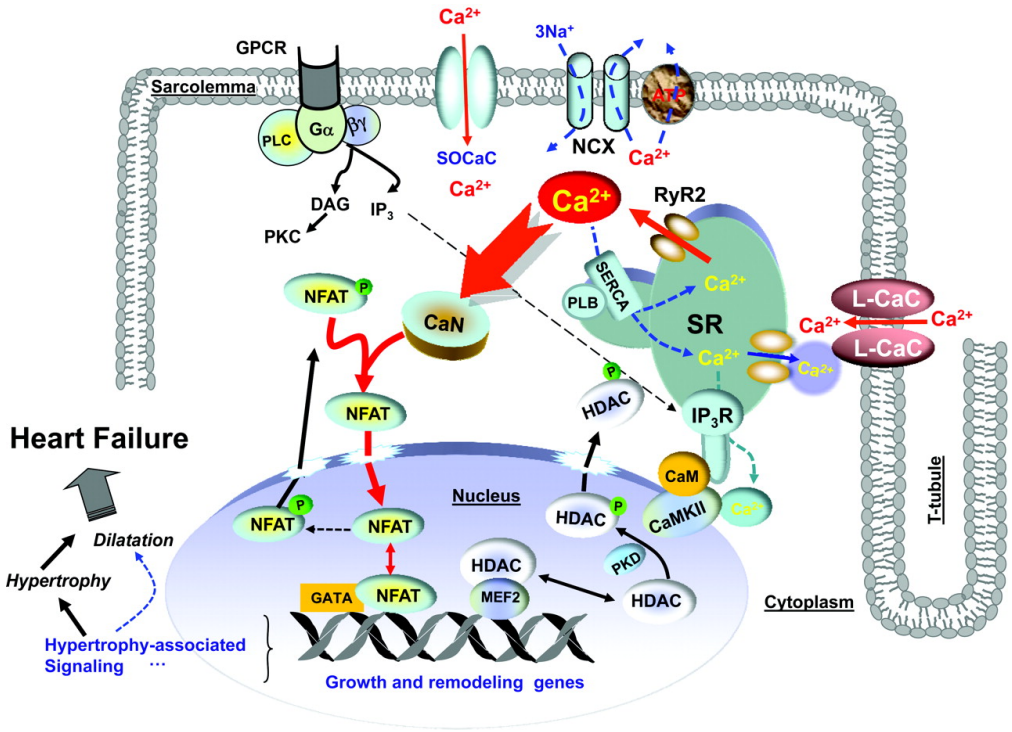

Fig. 6: Calcium-dependent signalling during cardiomyocyte hypertrophic response. CaN: calcineurin, HDAC: histone deacetylase, GPCR: G proteincoupled receptor, L-CaC: voltage-gated L-type Ca^{2+} channel, NCX: sodium-calcium exchanger, PKC: protein kinase C, PKD: protein kinase D, PLC: phospholipase C, SOCaC: store-operated Ca^{2+} channel, SR: sarcoplasmic reticulum. Reproduced from [52].

clinical trial) [41].

Inhibitory drugs that act on β-adrenergic signalling are currently used to treat hypertension, arrhythmias and patients presenting signs of heart failure [227]. β-Blockers reduce the severity of symptoms, improve heart function and were shown to increase the survival rate of patients [227]. With progression of heart failure, diuretics are used to diminish the symptoms associated with fluid retention [227].

Induction of signalling pathways associated with physiological hypertrophy through exercise was proven to be a safe and beneficial modality of improving maladaptive heart hypertrophy and failure [148].

2.5 Aims of the projects

The main goal of the projects is the development of new therapeutic strategies for inhibiting aortic aneurysm formation in Marfan syndrome (first project) and heart hypertrophy and heart failure (second project), by means of decoy ODNs that neutralize the main transcription factors involved in the progression of the two diseases.

Previous studies showed the efficiency of decoy ODNs for therapeutic purposes in various disease models. However, the application of nucleic drugs was made locally, which requires continous administration of the compund to inhibit the disease progression. In terms of further clinical treatments, this approach is not always feasible. Therefore, the establisment of a long-term AAV-mediated delivery of the decoy ODNs into the target tissue is more relevant in a medical context.

2.5.1 Aims of Marfan syndrome project

(1) Design of a hp (hairpin) AP-1 decoy ODN and its *in vitro* validation in isolated primary aortic mgR/mgR SMCs.
(2) Development of a long-term expression system of the hpAP-1 decoy ODNs in target SMCs by means of AAV transduction.
(3) *Ex vivo* transduction of mgR/mgR thoracic aortic grafts with AAV9SLR
(4) Analysis of the effects of aortic grafts transduction with AAV9SLR expressing hpAP-1 decoy ODNs on AP-1 target genes, inflammatory cells infiltration, tight junctions integrity in endothelial cell layer and most importantly, on elastin architecture.

2.5.2 Aims of heart hypertrophy project

(1) Establishment of an *in vitro* hypertrophy model using HL-1 cells and primary neonatal cardiomyocytes.
(2) Design of a hpNFAT decoy ODN and evaluation of its *in vitro* effects on cardiomyocyte hypertrophy.
(3) Development of a long-term expression system of the hpNFAT decoy ODNs in cardiomyocytes by AAV6 transduction *in vitro*, and AAV9 tail vein injection *in vivo*.
(4) Assessment of the *in vivo* effects of systemic injection of AAV9 expressing hpNFAT decoy ODNs on TAC-induced myocardial hypertrophy and heart failure.

3

Materials

3.1 Chemicals

3.1.1 Stimulants, inhibitors and substrates

Stimulants, inhibitors and substrates used in the present study are listed in Tab. 1.

Tab. 1: List of cell culture stimulants and inhibitors

Reagent	Provider	Concentration
IL1-β	R&D Systems, Wiesbaden, Germany	20 ng/mL
ET-1	Sigma-Aldrich, Munich, Germany	100 nM
MLS000048818	Mcule, Budapest, Hungary	10 μmol/L
520 MMP FRET Substrate XIV	Anaspec, Göttingen, Germany	0.1 μg/mL
Dihydroethidium	Sigma-Aldrich, Munich, Germany	0.1 μmol/L
2,7-Dichlorofluorescin diacetate	Sigma-Aldrich, Munich, Germany	5 μmol/L
Alamar Blue	Sigma-Aldrich, Munich, Germany	10 %

3.1.2 Antibodies

A list of primary and secondary antibodies are given in Tab. 2 and Tab. 3 respectively. The corresponding working dilutions and providers are also included. (ICC: immunocytochemistry, IHC: immunohistochemistry, WB: Western Blot).

Tab. 2: List of primary antibodies

Reactivity	Provider/Catalogue Number	Dilution	Application
EGFP	Abcam, Cambridge, UK ab111258	1:1000	ICC, IHC
F4/80	Dianova, Hamburg, Germany MOF4PU	1:500	IHC
CD31	Santa Cruz, Heidelberg, Germany sc-18916	1:500	IHC
MMP2	Abcam, Cambridge, UK ab37150	1:1000	IHC
MMP9	Abcam, Cambridge, UK ab38898	1:1000	WB, ICC, IHC
MMP12	Abcam, Cambridge, UK ab137444	1:1000	IHC
MyHC-β	Santa Cruz, Heidelberg, Germany sc-20641	1:300	ICC, IHC
NFAT5	Abcam, Cambridge, UK ab105886	1:500	ICC
SMA	Abcam, Cambridge, UK ab5694	1:1000	IHC
ZO-1	Thermo Fischer Scientific, Darmstadt, Germany 61-7300	1:500	IHC
Phospholamban	Badrilla, Leeds, UK A010-12	1:1000	WB
Puromycin	Merck Millipore, Darmstadt, Germany MABE343	1:1000	ICC, IHC

Tab. 3: List of secondary antibodies

Secondary antibody	Provider	Reactivity	Dilution	Application
Donkey IgG - Cy2	Dianova, Hamburg, Germany	Mouse	1:300	ICC, IHC
Donkey IgG - Cy5	Dianovag, Hamburg, Germany	Mouse	1:300	ICC, IHC
Goat IgG - Cy3	Dianova, Hamburg, Germany	Rat	1:300	IHC
Goat IgG - Cy5	Dianova, Hamburg, Germany	Rabbit	1:300	ICC, IHC
Goat IgG - HRP	Sigma-Aldrich, Munich, Germany	Rabbit	1:5000	WB
Goat IgG - HRP	Sigma-Aldrich, Munich, Germany	Mouse	1:5000	WB

3.1.3 Cloning enzymes

All enzymes used in cloning experiments were purchased from New England Biolabs (Frankfurt am Main, Germany).

Tab. 4: List of enzyme used in cloning experiments

Enzyme	Catalogue number	Recognised DNA sequence
KasI	R0544S	5′-G**GCGCC**-3′ 3′-**CCGCG**G-5′
XhoI	R0146S5	5′-C**TCGAC**-3′ 3′-**GAGCT**C-5′
Antarctic Phosphatase	M0289S	-
T4 DNA Ligase	M0202S	-

3.2 Oligonucleotides

3.2.1 Primers

Primers were purchased from Biomers (Ulm, Germany) or as a mix of forward and reverse primer mix (QuantiTect Primer Assays, Qiagen, Hilden, Germany), as shown in Tab. 5.

Tab. 5: List of primer sequences used in the present study.

Gene	Primer sequence/Catalogue Number	Annealing
ANP	Qiagen (QT00250922)	55 °C
BNP	Qiagen (QT00107541)	55 °C
CTGF	Qiagen (QT00096131)	55 °C
EGFP	*forward*: 5′-AAGCAGCACGACTTCTTCAAGTC-3′ *reverse*: 5′-TCGCCCTCGAACTTCACCTC-3′	60 °C
H1 *forward*	TCGCTATGTGTTCTGGGAAA	(Sequencing primer)
HSP70	*forward*: 5′-CCCGGTGTGGTCTAGAAAACA-3′ *reverse*: 5′-CCATGAAGAAGACTTTAAATAACCTTGAC-3′	57 °C
MCP-1	*forward*: 5′-TTCCTCCACCACCATGCAG-3′ *reverse*: 5′-CCAGCCGGCAACTGTGA-3′	60 °C
MMP9	Qiagen (QT00108815)	55 °C
RCAN1	Qiagen (QT01053430)	55 °C
RPL32	*forward*: 5′-GGGAGCAACAAGAAAACCAA-3′ *reverse*: 5′-ATTGTGGACCAGGAACTTGC-3	55 °C
SMIT	Qiagen (QT00341355)	55 °C
TGF-β	Qiagen (QT00145250)	55 °C

3.2.2 Decoy ODNs

Decoy ODNs were purchased from Biomers (Ulm, Germany). For decoy ODNs uptake experiments, the DNA was labelled with Atto590 at 5′ end position.

Tab. 6: Sequence of hp decoy ODNs used in the present study

Decoy ODN	Sequence
hpAP-1 cons	5′-CTGCGGTGCTGACTCAGCACGAAACGTGCTGAGTCAGCACCGCAG-3′
hpAP-1 mut	5′-CTGCGGTGCTTACTTAGCACGAAACGTGCTAAGTAAGCACCGCAG-3′
hpNFAT cons	5′-GAGTGGAAACATACAGCCACTGAAACAGTGGCTGTATGTTTCCACTC-3′
hpNFAT mut	5′-GAGCTTAAACATACAGCCACTGAAACAGTGGCTGTATGTTTAAGCTC-3′

3.2.3 Molecular beacons

Molecular beacons (purchased from Biomers, Ulm, Germany) were used in F.I.S.H. (fluorescent *in situ* hybridization) experiments and the sequences were designed as complementary to the decoy ODNs. BHQ: black hole quencher.

Tab. 7: Sequence of molecular beacons used in F.I.S.H. experiments

Beacon	Sequence
hpAP-1 cons	5′-CTGCGGTGCTGACTCAGCACGAAACGTGCTGAGTCAGCACCGCAG-3′ Modifications: 5′ - Cy5; 3′ - BHQ
hpNFAT cons	5′-GAGTGGAAACATACAGCCACTGAAACAGTGGCTGTATGTTTCCACTC-3′ Modifications: 5′ - Cy5; 3′ - BHQ

3.3 Plasmids and AAVs

A list of plasmids used for AAV production is shown in Tab. 8. Individual sequences of

Tab. 8: List of plasmids used in the present study

Plasmid	Description	Ref.
pDP9rs	Derivate from pDP2rs, containing AAV9 capsid gene. Used as a helper plasmid for AAV9 production.	[73]
p5E18-VD9-SfiI1959-SLR	Capsid plasmid used for AAV9SLR production	[208]
pDS1-H1-AP1cons-EGFP	hpAP-1 cons RNA decoy ODNs generating vector	This study
pDS1-H1-AP1mut-EGFP	hpAP-1 mut RNA decoy ODNs generating vector	This study
pDS1-H1-NFATcons-EGFP	hpNFAT cons RNA decoy ODNs generating vector	This study
pDS1-H1-NFATmut-EGFP	hpNFAT mut RNA decoy ODNs generating vector	This study

decoy ODNs for cloning into pDS1-H1-AP1cons-EGFP plasmid were ordered as gene synthesis (GeneArt Gene synthesis, Thermo Fischer Scientific, Darmstadt, Germany). For insert isolation, the restriction sites for KasI (5′) and XhoI (3′) enzymes were added to flank the designed sequence as shown in Tab. 9.

Tab. 9: List of gene synthesis sequences. Sequences recognised by restriction enzymes are presented in italic and decoy ODN sequences are shown in bold.

Plasmid	**Sequence**
P-AP1 cons	5′-A*GGCGCC*CTGCAATATTTGCATGTCGCTATGTGTTCTG GGAAATCACCATAAACGTGAAATGTCTTTGGATTTGGGA ATCTTATAAGTTCTGTATGAGACCACAGTCGAC **CTGCGGTGCTGACTCAGCACGAAACGTGCTGAGTCAGCACCGCAG** CACCGCAGTTTCGAC*CTCGAG*A-3′
P-AP1 mut	5′-A*GGCGCC*CTGCAATATTTGCATGTCGCTATGTGTTCTG GGAAATCACCATAAACGTGAAATGTCTTTGGATTTGGGA ATCTTATAAGTTCTGTATGAGACCACAGTCGAC **CTGCGGTGCTTACTTAGCACGAAACGTGCTAAGTAAGCACCGCAG** CACCGCAGTTTCGAC*CTCGAG*A-3′
P-NFAT cons	5′-A*GGCGCC*CTGCAATATTTGCATGTCGCTATGTGTTCTG GGAAATCACCATAAACGTGAAATGTCTTTGGATTTGGGA ATCTTATAAGTTCTGTATGAGACCACAGTCGAC **GAGTGGAAACATACAGCCACTGAAACAGTGGCTGTATGTTTCCACTC** CACCGCAGTTTCGAC*CTCGAG*A-3′
P-NFAT mut	5′-A*GGCGCC*CTGCAATATTTGCATGTCGCTATGTGTTCTG GGAAATCACCATAAACGTGAAATGTCTTTGGATTTGGGA ATCTTATAAGTTCTGTATGAGACCACAGTCGAC **GAGCTTAAACATACAGCCACTGAAACAGTGGCTGTATGTTTCCACTC** CACCGCAGTTTCGAC*CTCGAG*A-3′

AAV serotypes were chosen according to the transduction specificity for particular cell types. A summary of AAVs used in the study is shown in Tab. 10.

Tab. 10: List of AAV serotypes used in the present study

AAV serotype	**Target cells**	**MOI**	**Type of transduction**
AAV9SLR	SMCs, ECs	10^5 vp/cell	*In vitro*
		10^{12} vp/mouse	*Ex vivo*
AAV2RGD, AAV2APV AAV2NDV, AAV2DLG	SMCs	10^5 vp/cell	*In vitro*
AAV9NDV, AAV9RGD	SMCs	10^5 vp/cell	*In vitro*
AAV6	HL-1 cells	10^5 vp/cell	*In vitro*
AAV9	Adult cardiomyocytes	10^{12} vp/mouse	*In vivo*

3.4 Growth media and buffers

All cell culture reagents were purchased from Thermo-Fischer Scientific (Darmstadt, Germany) unless otherwise noted.

Tab. 11: List of growth media

Growth medium/Cell type	**Composition**
Complete Claycomb medium	Claycomb medium (Sigma-Aldrich)
(HL-1 cells)	5 % FBS (Sigma-Aldrich)
	2 μ/L L-Glutamine
	100 U/mL Penicillin
	100 μg/mL Streptomycin
	100 μmol/L Norepinephrine (Sigma-Aldrich)
Complete DMEM medium	Low glucose DMEM
(Primary aortic SMCs)	15% FBS
	2 mmol/L L-Glutamine
	100 U/mL Penicillin
	100 μg/mL Streptomycin
Complete M199 medium	M199 medium
(Neonatal cardiomyocytes)	10% FBS
	10 μmol/L Norepinephrine
	100 U/mL Penicillin
	100 μg/mL Streptomycin
LB medium (liquid)	10% bacto-tryptone
(Competent bacteria)	5% yeast extract
	10% NaCl
	(For selection: 100 μg/mL Ampicillin, Sigma-Aldrich)
LB medium (agar)	10% bacto-tryptone
(Competent bacteria)	5% yeast extract
	10% NaCl
	10 % agar
	100 μg/mL Ampicillin, (Sigma-Aldrich)

Tab. 12: List of buffers used in our study

Buffer/Purpose	**Composition**
Heart buffer	Ca^{2+}/Mg^{2+} free HBSS, pH=7.4
(Neonatal cardiomyocytes isolation)	10 mmol/L HEPES
	100 U/mL Penicillin
	100 μg/mL Streptomycin
NCM digestion buffer	Ca^{2+}/Mg^{2+} free HBSS, pH=7.4
(Neonatal cardiomyocytes isolation)	10 mmol/L HEPES
	0.5 μg/mL Trypsin (Sigma-Aldrich)
	0.3 mg/mL Collagenase II (Worthington)
	100 U/mL Penicillin
	100 μg/mL Streptomycin
Digestion inhibition solution	Ca^{2+}/Mg^{2+} free HBSS, pH=7.4
(Neonatal cardiomyocytes isolation)	10 mmol/L HEPES
	10 % FBS
	100 U/mL Penicillin
	100 μg/mL Streptomycin
Ca^{2+}-free Tyrode solution	140 mmol/L NaCl
(Adult cardiomyocytes isolation)	5.4 mmol/L KCl
	1.1 g $MgCl_2$
	5 mmol/L HEPES
	1 mmol/L Na_2HPO_4
	10 mmol/L Glucose
ACM digestion buffer	Ca^{2+}-free Tyrode solution
(Adult cardiomyocytes isolation)	50 μmol/L Ca^{2+}
	1 mg/mL Collagenase II
	2 mg/mL Protease (Sigma-Aldrich)
TEN buffer	40 mmol/L Tris-HCl pH 7.5
(Decoy ODNs solubilization)	1mmol/L EDTA pH 8.0
	150 mmol/L NaCl
Zinc fixative	0.1 M Tris-HCl pH=7.4
(Tissue fixation)	3.2 M Ca^{2+} acetate
	35.9 $ZnCl_2$
	22.8 M Zn^{2+} acetate
Blocking and permeabilization buffer	PBS pH=7.4
(ICC, IHC)	3 % BSA
	0.05% Triton-X100
Complete RIPA buffer	RIPA buffer (Sigma-Aldrich)
(Total Protein extraction)	50 M Pefabloc SC (Sigma-Aldrich)
	25 mol/L Protease inhibitors
	0.1 M DTT
12 % Running acrylamide gel	1.2 mL H_2O
(Western Blot)	2 mL Tris-HCl pH=8.8
	1.7 mL Acrylamide
	50 μL SDS 20 %

Continued on next page

Tab. 12 – continued from previous page

Buffer/Purpose	Composition
	50 μL 10 % APS
	3 μL TEMED
Stacking gel	1.1 mL H_2O
(Western Blot)	188 μL Tris-HCl pH=6.8
	200 μL Acrylamide
	15 μL SDS 20 %
	15 μL APS
Running buffer	25 mmol/L Tris HCl, pH 8.3
(Western Blot)	192 mmol/L Glycine
	0.1 % SDS
	15 μL 10 % APS
	1.5 mL TEMED
Transfer buffer	25 mmol/L Tris HCl, pH=8.3
(Western Blot)	192 mmol/L Glycine
Tris-buffered Saline (TBS)	0.5 M Tris-HCl
(Western Blot)	1.5 M NaCl
Blocking buffer	TBS
(Western Blot)	0.05 % Tween 20
	5 % Non-fat dry milk (Roth)
Gelatin running gel	Acrylamide 1 mL
(Getalin zymography)	1.25 mL Tris-HCl pH=8.8
	50 μL SDS 1%
	2 mL Gelatin 5 mg/mL
	0.65 mL H_2O
	5 0μL APS 10 %
	5 μL TEMED
Non-reducing sample buffer	5 mL Tris-HCl pH=6.8
(Gelatine zymography)	5 mL Glycerol
	1g SDS
	0.35 g Bromphenol blue
Wash buffer	0.1 M NaCl
(Gelatine zymography)	50 mmol/L Tris-HCl pH=7
	0.025 % Triton X-100
Incubation buffer	10 mmol/L $CaCl_2$
(Gelatine zymography)	Tris-HCl pH=7
Staining buffer	50% Methanol
(Gelatine zymography)	7% Acetic acid
	43 % H_2O
	0.001 % Comassie Brilliant Blue
Saline-sodium citrate buffer 20x	4 M NaCl
(F.I.S.H.)	100 mmol/L EDTA
	200 mmol/L Tris-HCl pH 7.5
	100 mmol/L NaH_2PO4

Continued on next page

Tab. 12 – continued from previous page

Buffer/Purpose	Composition
Denhardt's solution 100x (F.I.S.H.)	10 g ficoll 10 g polyvinylpyrrolidine 10 g BSA 500 mL sterile RNase free H_2O
Hybridization buffer (F.I.S.H.)	50% deionized formamide (Sigma-Aldrich) 4x SSC 5x Denhardt's solution 2.5 mg/mL Salmon DNA (Thermo Fischer Scientific) 0.5 mg/mL Yeast tRNA (Sigma-Aldrich)
TBE buffer (Agarose gel electrophoresis)	90 mmol/L Tris-HCl pH=7.5 90 mmol/L Boric acid 4 mmol/L EDTA, pH=8

3.5 Kits

A list of kits used in the present study is shown in Tab. 13.

Tab. 13: List of kits used in our study

Product	Supplier/Catalogue number
QIAprep spin miniprep kit	Qiagen, Hilden, Germany (27104)
Maxiprep kit	Qiagen, Hilden, Germany (740424.10)
ZymoPURE Plasmid Gigaprep Kit	Zymo Research, Freiburg, Germany (D4204)
QIAquick Gel Extraction Kit	Qiagen, Hilden, Germany (28704)
DNeasy Blood & Tissue Kits	Qiagen, Hilden, Germany (69504)
RNAeasy mini kit	Qiagen, Hilden, Germany (74104)
Sensiscript RT kit	Qiagen, Hilden, Germany (205211)
QuantiTect SYBR Green kit	Qiagen, Hilden, Germany (204243)
Brain Natriuretic Peptide EIA Kit	Sigma-Aldrich, Munich, Germany (RAB0386-1KT)
Elastic Stain Kit	Sigma-Aldrich, Munich, Germany (HT25A-1KT)
DC^{TM} Protein Assay	Bio Rad, Munich, Germany (5000111)

4

Methods

4.1 Cell culture

4.1.1 Isolation and culture of primary SMCs

For the isolation of primary aortic SMCs, thoracic aorta of fibrillin-1 deficient mice (mgR/mgR) was used (reference number T-17/14, animal experiments number 35-9185.81/G-52/17). Mice were sacrificed by CO_2 inhalation, the chest was cleaned with 70 % ethanol before opening and the heart was exposed. Next, 5 mL of cold sterile NaCl solution (Braun, Melsungen, Germany) was perfused through the left ventricle using a 23 gauge needle syringe in order to remove the blood present in the aorta. The thoracic aorta was isolated, cleared from fat and connective tissue and cut into small pieces under sterile conditions in complete DMEM medium (Tab. 11, page 29). The tissue pieces were incubated at 37 °C, 5% CO_2 for 24 h in the presence of 100 μmol/L Collagenase I (Worthington Biochemical Corporation, Lakewood, USA). Afterwards, medium was replaced and explants were further cultured until cells reached 80% confluency. Lastly, cells were passaged and either propagated, frozen in liquid nitrogen or used for experiments up to passage 5, in order to avoid the phenotypical changes that occur with long-term subculture of SMCs. Cells were cultured either on plastic, for RNA and Western Blot experiments, or on gelatine-coated glass coverslips, when the assays demanded the use of confocal microscopy.

4.1.2 Isolation and culture of primary neonatal cardiomyocytes

Neonatal cardiomyocytes were isolated as previously described [201]. For each cell isolation, 8-9 neonatal mice (1-2 days old) were used (T-47/14, notification to sacrifice animals for scientific purposes). In brief, mice were sacrificed by decapitation, hearts were removed and placed in ice-cold sterile Ca^{2+}/Mg^{2+}-free heart buffer (composition given in Tab. 12, page 30). Ventricles were separated, minced and incubated in NCM

(neonatal cardiomyocyte) digestion solution at 37 °C under continuous shaking, in order to induce cell dissociation. Every 5 min, dissociation solution was replaced and isolated cells were collected and placed in digestion inhibition solution to inactivate the enzymes. These steps were repeated until no tissue pieces were visible. Finally, cells were centrifuged at 1000 rpm for 5 min and the pellet was resuspended in complete M199 growth medium. The purification of the resulting cell suspension was achieved by differential attachment technique. Therefore, the cells were plated in a cell culture flask for 90 min at 37 °C in a cell culture incubator to allow fibroblast attachement, while cardiomyocytes remained in culture medium. Neonatal cardiomyocytes were grown on collagen (Biochrom, Berlin, Germany) pre-coated plates in complete M199 medium. For immunofluorescence analysis, cells were cultured on glass coverslips. Primary neonatal cardiomyocytes were used within 3 days after isolation.

4.1.3 Isolation of adult cardiomyocytes

100 IU (international units) heparin (Ratiopharm, Ulm, Germany) were injected by intraperitoneal injection 10 min prior to mouse sacrifice to prevent blood cloths formation (reference number T-16/15 notification to sacrifice animals for scientific purposes). The chest was wiped with 70% ethanol, opened and the heart was isolated together with the aorta and immediately placed in ice-cold Ca^{2+}-free Tyrode solution. The thymus, fat and lungs were trimmed and aorta was clamped to the cannula using surgical silk. The heart was suspended on the Langendorf system (Schmizo, Oftringen, Switzerland) and perfused with Ca^{2+}-free Tyrode solution for less than 5 min. Afterwards, the perfusion solution was changed to warm ACM (adult cardiomyocytes) digestion buffer (composition in Tab. 12, page 30). After 7-9 min, isolated adult cardiomyocytes were transferred to Tyrode solution containing 100 μmol/L $CaCl_2$, the ventricles were cut and Ca^{2+} concentration was slowly increased. Adult cardiomyocytes were then transferred in growth medium and plated on laminin (10 μg/mL) coated glass coverslips with a seeding density of 10^4 rod-shaped cells/cm^2. After one hour, medium was gently changed to remove non-adherent cells. Isolated cells were used for hpNFAT decoy ODNs uptake experiments the same day.

4.1.4 Culturing of HL-1 cells

HL-1 cells (Dr. William Claycomb, Louisiana State University School of Medicine, New Orleans, USA, [36]) were cultured on gelatine-fibronectin coated dishes and maintained in complete Claycomb medium (Tab. 11, page 29). Cultures were grown in 37

°C, 5% CO_2 until high confluency was observed and then passaged 1:4. Stimulations, transfections and transductions were carried out when HL-1 cells reached 90 % confluency.

4.1.5 *In vitro* hp decoy ODN treatment and AAV transduction

SMCs and cardiomyocytes were seeded in culture dishes the day before treatment and allowed to adhere overnight. Hairpin decoy ODNs (sequences given in Tab. 6, page 27) were added in cell culture medium to a final concentration of 10 μmol/L and incubated for 2 h before stimulation with transcription factors activators. For Lipofectamine mediated hp decoy ODN uptake experiments, the DNA was incubated with 5μL Lipofectamine 3000 (Thermo Fischer Scientific, Darmstadt, Germany) in OptiMEM medium (Thermo Fischer Scientific, Darmstadt, Germany) in the absence of antibiotics for 15 min prior to addition to the cells.
AAV transduction was conducted at MOI=10^5 vp (virus particles)/cell in serum-free medium. After the infection period (12-16 h), culture medium was replaced. Cells were observed under fluorescence microscope (Zeiss, Oberkochen, Germany) for EGFP expression 3 days after vector application.
SMCs were treated with a series of virus serotypes with targeting capsides (AAV2NDV, AAV2APV, AAV2DLG, AAV9RGDLLLG, AAV9SLR, AAV9WT, provided by Dr. Karl Varadi, Prof. Oliver Müller, Clinic for Cardiology, Angiology and Pneumology, University Clinic Heidelberg) expressing EGFP in order to detect the viral construct which leads to the highest transduction efficiency. Fluorescence was visualized after 3 days using a fluorescence microscope.
HL-1 cells were transduced with AAV serotype 6.

4.1.6 Cell stimulation

In order to activate AP-1, SMCs were serum depleted overnight and IL1-β (R&D Systems, Wiesbaden, Germany) was supplemented to a final concentration of 20 ng/mL for 24 h for protein expression experiments or 8 h for examination of mRNA levels of target genes.
Cardiomyocytes, both HL-1 cell line and primary neonatal cells were stimulated with ET-1 100 nM (Sigma-Aldrich, Munich, Germany) after serum deprivation, for 24 h. Transduced cells were stimulated 3 days after infection.

4.1.7 Functional *in vitro* assays

SMCs migration assay

SMCs were cultured to a confluent layer in migration inserts (Ibidi, Munich, Germany) and treated with hpAP-1 decoy ODN or transduced with AAV9SLR expressing hpAP-1 RNA decoy ODNs. Afterwards, IL1-β 20 ng/mL was added to the medium and inserts were removed to allow the formation of free space in between cells, as shown in Fig. 7. Pictures were taken at various time points between 0-24 h with a brightfield microscope

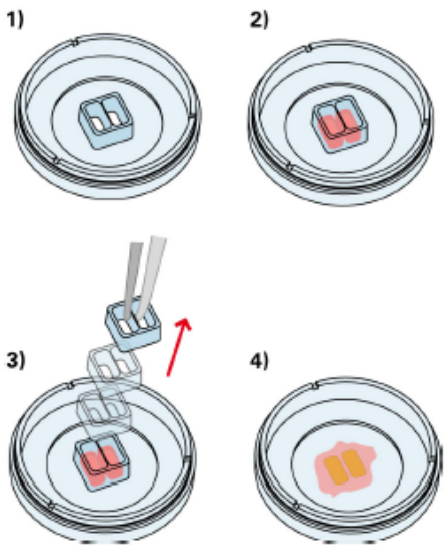

Fig. 7: Principle of Ibidi migration chambers (adapted from Ibidi website). 1: Silicone inserts are applied on cell culture dishes. 2: Cells are seeded in the empty spaces of the chambers and allowed to adhere. 3: After cell treatments, chambers are removed to allow empty space formation in between SMCs. 4: The area between cells is analysed at different time points. Image adapted from ibidi website.

(4x magnification) and the area between cells was analysed using ImageJ (FiJi version 1.51p, National Institute of Health, USA). Relative migration capacity was calculated as follows:

$$Percent\ Migration = \frac{(Initial\ wound\ area - Final\ wound\ area)}{Initial\ wound\ area} \cdot 100 \quad (4.1)$$

Viability assay

Cell viability was measured by using AlamarBlue assay (Thermo Fischer Scientific, Darmstadt, Germany). Resazurin, the active ingredient of the reagent, is taken up by viable cells and reduced to resorufin, a highly fluorescent compound. The cells, cultured in 96-well plates, were treated with AlamarBlue (1:10 dilution, in serum-free medium) and incubated at 37 °C, 5% CO_2, for 30 min. Afterwards, fluorescence intensity was measured using a fluorescent reader (Fluoroskan Ascent, Thermo Fischer Scientific, Munich, Germany).

4.2 AAV production

AAV production was performed in collaboration with Prof. Oliver Müller, Dr. Andreas Jungmann, Clinic for Cardiology, Angiology and Pneumology, University Clinic Heidelberg according to standard protocols [208]. The full list of plasmids used for AAV synthesis are recorded in Tab. 8, page 27.

4.3 Molecular biology

4.3.1 Hairpin decoy ODNs

The sequences of the designed decoy ODNs used in this study are summarized in Tab. 6, page 27. The decoy ODNs were solubilized in sterile TEN buffer to a final concentration of 500 μmol/L (stock solution) and incubated at 95°C for 7 min. Afterwards, they were gradually cooled down at room temperature and transferred on ice in order to allow the hybridization to a hairpin structure, which was confirmed by electrophoresis on 2.5% agarose gels. Ethidium bromide (4 μL/gel) was added to visualize the DNA bands under a UV light source illumination. In parallel with the samples, an ultra-low range ladder (GeneRuler, Thermo Fischer Scientific, Darmstadt, Germany) was loaded to monitor the DNA molecular weight. For decoy ODNs uptake experiments, a 5′-Atto-590 labelled hp decoy ODN was used.

4.3.2 Cloning of hpRNA decoy ODNs expressing plasmids

The hpRNA decoy ODNs were generated as shRNAs under the H1 promoter (plasmid backbone provided by Prof. Oliver Müller, Dr. Andreas Jungmann, Clinic for Cardiology, Angiology and Pneumology, University Clinic Heidelberg). The plasmid contains

EGFP as an expression marker, initiated by CMV promoter. The vector also includes inverted terminal repeats (ITR) sequences, which are crucial for AAV production. The individual sequences for each shRNA subcloning were ordered as gene synthesis (9, page 28). The synthetized gene sequence contains a part of the H1 promoter (5′ end) and the shRNA (3′ end), flanked by KasI and XhoI restriction sites.

Maintainence of bacterial cells

For AAV plasmid cloning, recombination-deficient SURE2 (Stop Unwanted Rearrangement Events 2) bacterial cells (Agilent Genomics, Waldbronn, Germany) were used, in order to prevent the deletion of ITR sequences. Liquid cultures, grown in sterile LB medium (composition given in 11, page 29) were expanded at 37 °C under continuous agitation (150-200 rpm) in a bacterial incubator. Bacteria stocks for transformation were stored as 50 μL aliquotes at -80 °C.

Digestion of plasmid DNA

Plasmid digestion with KasI and XhoI restriction enzymes was performed in the corresponding buffers for 2 h for each μg plasmid DNA, at 37 °C. Reaction efficiency was analysed by agarose gel electrophoresis (100V for approximately 70 min). A molecular weight ladder was used to determine band size (GeneRuler 1kb DNA Ladder, Thermo Fischer Scientific, Munich, Germany). The DNA was imaged by using GelDoc XR unit and analysed with Quantity One software package version 4.06 (Bio Rad, Munich, Germany). The DNA bands corresponding to the backbone and the insert were cut and DNA was purified from the gel using QIAquick Gel Extraction Kit (Qiagen, Hilden, Germany) according to manufacturer's instructions. Eluted DNA concentration was measured using NanoDrop Spectrophotometer (PeQlab Biotechnologie, Erlangen, Germany).

Modification of DNA ends

In order to reduce the process of backbone religation, 5′ phosphate ends were removed by using Antarctic phosphatase (New England Biolabs, Frankfurt am Main, Germany). The gel-purified vector backbone was incubated with the enzyme in the specific buffer for 30 min at 37 °C. Phosphatase heat-inactivation was afterwards performed at 65 °C for 30 min on a thermoblock (Eppendorf, Hamburg, Germany).

Ligation of plasmid DNA

Ligation of DNA fragments was performed in a ratio 1:4 backbone:insert ration by using T4 DNA ligase in the specific ATP-containing buffer provided by the producer. For each ligation reaction, 50 μg backbone was used. The dephosphorylated backbone was incubated with the insert in the presence of ligase for 16 h at 16 °C using a thermoblock. The reaction mixture was further used for bacteria transformation.

Bacteria transformation

50 μL of bacteria were allowed to thaw on ice and then incubated with the ligation mixture for 30 min at 4 °C. Heat-shock was performed at 42 °C for 45 s, on a thermoblock. Afterwards, bacteria were transferred on ice for 10 min and then cultured for 30 min at 37 °C in 300 μL LB medium without antibiotics. Next, the suspension was spread on sterile LB-plates with 15% agar and 100 μg/mL ampicillin (Sigma-Aldrich, Munich, Germany). Plates were incubated overnight at 37 °C to allow colony formation. Individual bacterial colonies were randomly picked and further cultured in 5 mL LB medium with ampicillin for 16 h. Plasmid DNA was isolated QIAprep Spin Miniprep Kit (Qiagen, Hilden, Germany) according to manufacturer's instructions.
The presence of the insert was confirmed by KasI and XhoI digestion as well as DNA sequencing (Eurofins Genomic, Luxembourg). Positive colonies were expanded in 1 L of ampicillin containing LB medium overnight and DNA was isolated using ZymoPURE Plasmid Gigaprep Kit (Zymo Research, Freiburg, Germany) according to manufacturer's instructions. Each preparation yielded at least 1.5 g plasmid DNA, which was further used for AAV preparation.

4.3.3 Quantitative real time PCR

Total RNA was extracted from adherent cells or tissue using RNeasy Mini Kit (Qiagen, Hilden, Germany) following the manufacturer's instructions and the concentration was measured using NanoDrop Spectrophotometer (PeQlab Biotechnologie, Erlangen, Germany). First strand synthesis of cDNA was completed using Omniscript Reverse Transcriptase kit (Qiagen, Hilden, Germany) and OligodT primers (Promega, Mannheim, Germany), starting from equal amount of RNA for each sample. SYBR Green (Qiagen, Hilden, Germany) qRT-PCR was performed using Qiagen Rotor-Gene machine, in reactions of 20 μL (10 μL SYBR Green, 2 μL primer mix, 3 μL RNase free water, 5 μL cDNA). cDNA was amplified using specific primers for the investigated genes, as shown in Table 5, page 26.

The qPCR program consisted of an initial denaturation step of at 95 °C for 5 min, followed by 40 cycles of denaturation (95 °C for 60 s), annealing (primer dependent temperature, 25 s) and elongation (72 °C, 60 s), followed by melting curve. The presence of a single amplicon was determined by the existence of a single peak in the melting curve graph. Data was analysed by relative quantification method, double delta Ct (cycle threshold) method, using RPL32 as a housekeeping gene [158]. The Ct was defined as the cycle number at which the fluorescence signal crosses the fluorescence threshold, considered as background. Corresponding controls (non stimulated cells or samples isolated from control mice) were used for relative gene expression calculation. In order to quantify the change in gene expression levels, the following equation was used [158]:

$$Ratio = \frac{2^{Ct_{target,untreated} - Ct_{reference,untreated}}}{2^{Ct_{target,treated} - Ct_{reference,treated}}} \tag{4.2}$$

4.3.4 *In situ* hybridization

For the detection of RNA decoy ODNs both *in vitro* and *in vivo*, samples (tissue sections or cells) were subjected to RNA *in situ* hybridization. In brief, cells cultured on gelatin coated glass coverslips or 5μm tissue cryosections were fixed with DEPC (diethyl dicarbonate)-treated 4 % PFA (Sigma-Aldrich, Munich, Germany) for 10 min followed by incubation with 20 μg/mL Proteinase K (Sigma-Aldrich, Munich, Germany) at 37 °C for 15 min in order to induce tissue permeabilization and antigen retrieval. As a probe we used a molecular beacon (Biomers, Ulm) with complementary sequence to the hp decoy ODNs (Tab. 7, page 27), with 5'-Cy5 labeling and 3'-BHQ-2 (Black Hole Quencher) as a quencher. In a hybridized state the molecular beacon itself does not emit fluorescence signal due to the dye and the quencher being located proximally. After hybridization to the target sequence, red fluorescence can be detected, as shown in Fig. 8. Prior to hybridization, the molecular beacon was heated at 95 °C and gradually cooled down to room temperature to allow the hairpin structure formation; afterwards it was kept on ice until use.

Samples were incubated overnight at 55 °C with the probe dissolved in hybridization buffer in a humidified atmosphere. As blocking reagents we used salmon DNA and yeast tRNA (complete hybridization buffer composition is listed in Tab. 12, page 30) which were added in the mixture. After extensive washes (3x20 min) in hybridization buffer and DEPC-treated PBS (1x15 min) in order to remove non-hybridized molecular beacon, EGFP immunofluorescence staining was performed. Finally, DAPI staining was performed (Ex/Em=358/461) for nuclei visualization using Fluoroshield with DAPI mounting medium (Sigma-Aldrich, Munich, Germany).

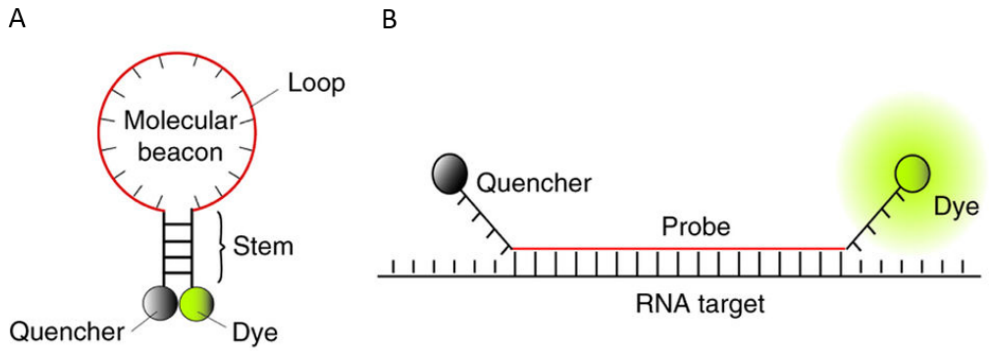

Fig. 8: The use of molecular beacons for RNA sequences detection. A. The hybridized molecular beacon, as a hairpin form, does not emit fluorescence. B. As soon as the probe binds to the target RNA, fluorescence can be detected. Scheme was adapted from [219].

4.4 Protein methods

4.4.1 Protein extraction and Western blot analysis

Total protein was extracted from SMCs using complete RIPA buffer and quantified using Bradford method (Bio Rad, Munich, Germany). The lysate was snap-frozen and stored at -80 °C until further use.

In order to isolate total protein extract from heart tissue, a piece of the left ventricle was cut, briefly washed with NaCl to remove blood residuals, and treated with 300 μL of ice-cold complete RIPA buffer. Afterwards, a Dounce homogenizer was used to disrupt the tissue. Protein lysates were snap frozen and maintained at -80 °C before completing downstream measurements.

30 μg of protein were denatured by incubation at 95 °C for 10 min with 4x sample buffer (Roth, Karlsrue, Germany) and loaded into SDS-12% acrylamide gels (composition is given in Tab. 12). A pre-stained protein standard (Bio Rad, Munich, Germany) was used for molecular weight estimation. Separated proteins were transferred on a methanol pre-activated PVDF (polyvinylidene difluoride) membrane (Merck Millipore, Darmstadt, Germany) with pore size 0.45 μm. Ponceau staining was used to prove equal loading of protein samples. For this purpose, membranes were incubated with the dye (Roth, Karlsrue, Germany) for 5 min, until red lines were visible, representing the transferred proteins. Afterwards, extensive washing in H_2O was carried out until red, clearly defined bands were observed on white, destained background. The membranes were then digitized using a Lexmark scanner. Prior to further processing, the membranes were completely destained by TBS washing.

Blocking was made using 5% non fat dry milk diluted in TBS-T for one hour, followed by overnight incubation at 4 °C, under continuous shaking with primary antibodies (listed in Tab. 2, 25). β-actin was used as a loading control. After washing, membranes were incubated with corresponding horseradish-peroxidase labelled secondary antibodies (summarized in Tab. 3, page 25) for one hour at room temperature. Membranes were developed with the chemoluminescent substrates Luminata Classico for β-actin and Luminata Forte for MMP9 and phospholamban detection (Merck, Darmstadt) for 3 min. Afterwards, membranes were imaged using ImageQuant LAS 4000 mini system (GE Healthcare Life Sciences, Munich, Germany). The band intensities were analysed and related to β-actin using ImageJ software.

4.4.2 ELISA

ELISA (Enzyme-linked immunosorbent assay) was used for the assessment of *in vitro* BNP protein level secreted in cardiomyocyte supernatant and total cell lysate. In addition, BNP concentration in left ventricular protein extracts and in plasma were measured. For this purpose, a Brain Natriuretic Peptide EIA Kit (Sigma-Aldrich, Munich, Germany) was used, following the instructions provided by the producer. The absorbance were read using a colorimetric plate (BioTek, Bad Friedrichshall, Germany). The absorbance of samples and standards were measured in duplicates. A standard curve for the target protein (provided by the producer) was plotted in each experiment. The amount of BNP protein was normalised to the total protein content of the samples, determined by Bradford method.

4.4.3 Immunocytochemistry

For immunocytochemistry experiments, SMCs or HL-1 cardiomyocytes were plated on glass coverslips pre-coated with gelatine. After treatments, cells were washed with PBS and fixed with 4% PFA for 5 min. Subsequently, the glass slides were washed and blocked in 3% BSA (Sigma-Aldrich) and 0.05% Triton-X100 as a permeabilization reagent, dissolved in PBS. Primary antibodies (summarized in Table 2, page 25) were diluted in blocking buffer and incubated overnight at 4°C. Next, a set of 3 washing steps with PBS were performed, followed by fluorescently labelled secondary antibody incubation (listed in Tab. 3, page 25) for one hour at room temperature and DAPI nuclear staining. Images were taken using confocal microscopy (Leica TCS SP8, Leica Microsystems, Mannheim) and mean fluorescence intensity was calculated using ImageJ.

4.4.4 Immunohistochemistry

Aortic and heart tissues were collected and washed in NaCl in order to remove blood residuals. Next, tissue was embedded into optimal cutting temperature medium TissueTek (Leica Biosystems, Wetzlar, Germany) and snap-frozen by immersion into liquid nitrogen. A cryotome (Leica, Mannheim, Germany) was used to section the frozen tissue (cryosectioning temperature: -21°C). 5μm thick cryosections were fixed with Zinc fixative (composition provided in Tab. 12, page 30) and blocked with PBS containing 3% BSA and 0.05% Triton-X100 for one hour. Primary antibodies against the proteins of interest were diluted in blocking buffer and incubated overnight at 4°C in a humidified athmosphere. A list of primary antibodies and the working dilution are provided in Table 2, page 25. As secondary antibodies, compatible Cy3 or Cy5 labelled IgG were used, diluted in blocking buffer. Nuclei were visualised by DAPI counterstaining and images were recorded by confocal microscopy. Relative mean fluorescence intensity was measured using ImageJ as previously described [96] and related to corresponding controls.

4.4.5 Zymography

Gel zymography

Gel zymography was used for the detection of MMP activity secreted by SMCs. Cell culture supernatant was incubated for 24h on a rotor at 4 °C with gelatin- coated beads (Sepharose 4B Beads, Sigma Aldrich, Munich, Germany) in order to concentrate the MMPs present in the medium. Afterwards, MMPs were eluted using non-reducing sample buffer followed by electrophoretic separation on 5 mg/mL gelatine-containing acrylamide gels. A standard ladder was used to identify the molecular weights of the bands. Following electrophoresis, gels were incubated for 2 h in wash buffer containing Triton X-100 in order to remove the SDS and renature the enzymes. Afterwards, gels were placed in a 37 °C incubator overnight, in incubation buffer (composition is presented in 12), which contains $CaCl_2$, essential for enzymatic activity of MMPs. Gels were then transferred to Coomassie Brilliant Blue staining solution for one hour at room temperature under shaking and afterwards incubated in destaining buffer until clear bands were visible on the blue background. The bands correspond to the level of gelatinase activity, and were further quantified. For this purpose, gels were scanned and the relative band intensity was measured using ImageJ.

In situ zymography

In situ zymography was performed using a broad spectrum MMP substrate (520 MMP FRET Substrate XIV, Anaspec, Göttingen, Germany), which detects the activity of MMP-1, 2, 3, 7, 8, 9, 12, and 13 present in the sample. For *in vitro* measurement of MMP activity, SMCs were treated with the substrate to a final concentration of 0.1 μg/mL in serum-free medium for 1 hour at 37 °C. After cell fixation with PFA 4% and DAPI staining, the cells were visualised using a confocal microscope and red fluorescence (Ex/Em=494/521 nm) was analysed as a measure of MMP activity.
Similarly, MMP activity was analysed in 5 μm aortic cryosections. The tissue was fixed with Zinc fixative and incubated with the substrate at 37 °C for 4 h in a humidified atmosphere to avoid the evaporation of the substrate solution. The sections were then extensively washed to remove the non-bound substrate. Red fluorescence intensity was measured and reported to the wild type control aorta values.

4.4.6 SUnSET assay

SUnSET (Surface sensing of translation) assay was used for measurement of total protein translation rate as previously described [181]. For *in vitro* protein translation measurements in HL-1 cells, a viability curve was performed to determine the suitable concentration of the compound to be used in further experiments. For this purpose, HL-1 cells, cultured in 96-well plates were treated with increasing concentration of puromycin (0.1, 0.5, 1, 5, 10, 50, 100 μmol/L) for 30 min, followed by Alamar Blue viability test (described in detail in section 4.1.7, page 36).
Afterwards, either cardiomyocytes or 5 μm heart cryosections were incubated with puromycin 10 μmol/L for 30 min, followed by PFA fixation. Then, anti-puromycin antibody was diluted in blocking buffer, added to samples and incubated overnight at 4 °C. After 3 steps of PBS washing, a Cy5-labelled secondary antibody was used. Red fluorescence signal was recorded using a confocal microscope and relative means were analysed using ImageJ.

4.5 ROS measurement

4.5.1 *In vitro*

The level of oxidative stress *in vitro* was measured using 2′,7′-Dichlorofluorescin diacetate (DCFDA, Sigma Aldrich, Munich, Germany) or, when SMCs were transduced

with EGFP expressing AAV, with Dihydroethidium (DHE, Sigma Aldrich, Munich, Germany). For this purpose, cells were cultured on gelatine-coated glass coverslips and subjected to hp decoy ODNs treatement or AAV transduction. Afterwards, cells were incubated with DCFDA (5 μmol/L) or DHE (0.1 μmol/L) for 30 min at 37 °C in serum-free medium. The dye was then removed by PBS washing and cells were stimulated with IL1-β for 6 h. Non-stimulated cells were used as control. Next, coverslips were washed again with PBS and fixation was performed using methanol. After DAPI nuclear staining, cells were visualised using a confocal microscope (DCFDA:Ex/Em=485/535nm; DHE:Ex/Em=518/605) and the fluorescence intensity was measured using ImageJ.

4.5.2 In tissue cryosections

Aortic cryosections were fixed with 4% PFA for 5 min and rinsed in PBS. DHE was applied to the tissue to a final concentration of 10 μmol/L and incubated at 37°C for 30 min in a humidified atmosphere. The sections were then briefly washed with PBS and visualised by confocal microscopy. Mean fluorescence intensity was measured using ImageJ.

4.6 Other tissue based methods

4.6.1 Cell size measurement

WGA (Wheat Germ Agglutinin) staining is an already established method for analysis of cell size in cardiac tissue [82]. Left ventricles embedded in TissueTek medium were sectioned (5 μm) and the cell orientation was observed. The analysis was made on both short and long axis. Cryosections were fixed with PFA 4% for 5 min and stained with WGA-Alexa Fluor 594 (Thermo Fischer Scientific, Darmstadt, Germany, 1:400 diluted in PBS). The incubation with the dye was performed at room temperature, for 10 min. Afterwards, tissues were briefly washed with PBS and mounted. Images were taken using confocal microscopy and cell diameter was analysed using ImageJ.

4.6.2 T-tubule analysis

After WGA staining, T-tubule organization was assessed using ImageJ, as previously described [215]. In brief, cells were analysed individually, by application of Fast fourier transformation (FFT), as described in Fig. 9. This method allowed the identification of

repeating patterns and the frequency with which they appear (T-power). The peak corresponding to the 2 μm distance was further analysed. In addition, the percentage of cell area occupied by T-tubules (T-index) was calculated by using threshold method determined in ImageJ. This parameter was defined as the area above-threshold divided by cell cross-sectional area. Cardiomyocytes presenting a T-index above 2 % were considered to be tubulated, in a similar manner as other studies [65]. The level of tubularization was defined as the percentage of tubulated cells in each treatment group.

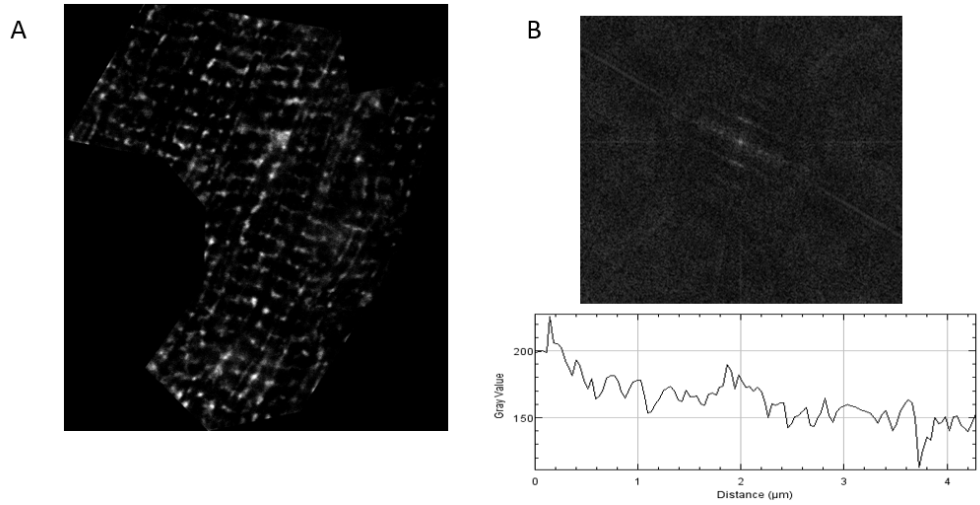

Fig. 9: Image analysis of T tubule organization. (A) Original image after background removal. (B) The power spectrum obtained after performing FFT and the corresponding plot profile. The second peak was further used for analysis, designating the 2 μm distance between single T-tubules.

4.6.3 Heart histology

Masson's Trichrome Staining

Heart histology was performed in collaboration with Prof. Dr. med. Hermann-Josef Gröne, German Cancer Research Center, Heidelberg. Hearts were fixed in 4% PFA overnight at 4 °C and embedded in paraffin prior to histological assessment. For visualization of collagen fibers, sections were subjected to Masson's Trichrome Staining according to standard protocols [14]. Images were taken in random areas of the left ventricle using a brightfield microscope with 20x magnification (Leica DM500, Leica Microsystems, Mannheim, Germany). Collagen was stained blue, muscle and cytoplasm appeared red and nuclei were visualized as being dark brown to black. Both perivascular and interstitial fibrosis were analysed using a quantification software written in QT/C++

based on image processing and segmentation libraries. In a first step, interfering background of all images was masked out by subsequently applying threshold and erosion filters. Further, the fibrotic area was determined using hsv-thresholding with a 10 % tolerance on the hue component, followed by numerical quantification of the percentage area covered. A sample result image is provided in Fig. 10.

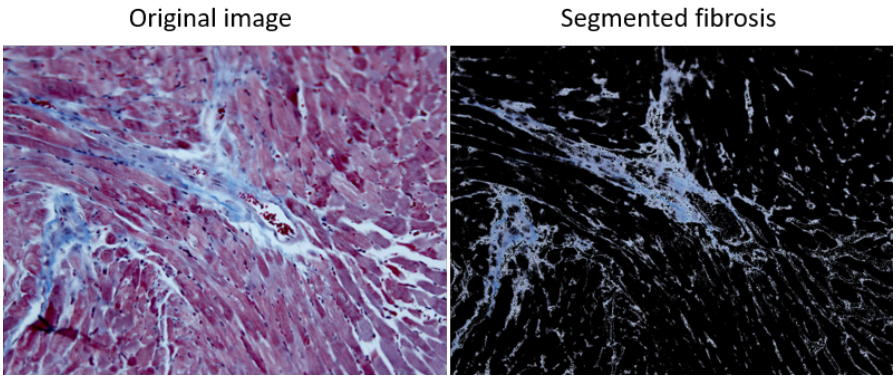

Fig. 10: Quantification of perfentage of fibrotic area. The image on the left represents the original picture of the stained tissue. On the right, the blue region, representing collagen staining, was selected for analysis and the area was calculated.

Hematoxylin-eosin staining

Cardiomyocyte architecture was assessed by H&E (Hematoxylin-eosin) staining of paraffin sections, performed in collaboration with Prof. Dr. med. Hermann-Josef Gröne, German Cancer Research Center, Heidelberg, according to standard protocols [117]. Stained tissue sections were visualised using a brightfield microscope (Leica DM500, Leica Microsystems, Mannheim, Germany). Following the procedure, nuclei appeared blue, while cardiac tissue was stained pink. Cardiomyocytes were identified according to their specific shape and their area on the long axis was measured using ImageJ and normalized to the cell size of sham operated mice.

Verhoeff-van Gieson Staining

Elastic van Gieson staining was performed using Elastic Stain Kit (Sigma Aldrich, Munich, Germany) according to manufacturer's instructions. In brief, 5 μm cryosections were fixed with 4% PFA (paraformaldehyde) and allowed to dry at room temperature. Afterwards, sections were stained with working elastin solution (20 mL hematoxylin solution, 3 mL $FeCl_3$, 8 mL Weigerts iodine solution, 5 mL deionized H_2O) for 10 min

and briefly washed with deionized H_2O. Aortic tissue was then differentiated in 3% $FeCl_3$ for 1 min, rinsed in 95% ethanol and stained with Van Gieson solution for one min. The sections were washed with 95% ethanol and mounted. Images were taken using brightfield microscopy with 10x magnification. Elastin fragmentation was assessed by counting the number of islands of damage by two researchers blinded to the treatment. An island of damage was defined as breaks in two neighbouring elastic fibers surrounded by conjunctive tissue [132].

4.7 Mouse models and techniques

4.7.1 Animal models

Mouse models were used to prove the *in vivo* reproducibility of the results obtained using cell culture models. All animal experiments were carried out under the approval of the regional committees (Regierungsprsidium Karlsruhe, permit numbers G187-11 and G-52/17 for Marfan syndrome project and G180/12 for heart hypertrophy project, applicants Prof. Dr. Klaus Kallenbach, Prof. Dr. Oliver Müller). Animals were kept in the Interfaculty Biomedical Facility (IBF), Heidelberg, under standard conditions with 12h light, 12h night cycle; water and food was offered *ad libitum*.

4.7.2 Aortic grafts transplantation

For the Marfan syndrome project, 6-9 weeks old female mice were used. The animals are underexpressing fibrillin-1 due to a hypomorphic mutation (mgR/mgR), as previously described [183]. Male mice were excluded because they present a significantly lower survival. As comparison we used age-matched wild type littermates.
AAV9SLR-EGFP, AAV9WT and AAV9SLR expressing the hp RNA decoy ODNs were applied at the level of the aorta *ex vivo* by means of a heterotrophic infrarenal transplantation model as previously described [184]. The surgeries were performed by Dr. Rawa Arif and Maximilian Franz, Clinic for Cardiac Surgery, Heidelberg University Hospital. Donor mgR/mgR mice were euthanized with CO_2, the thorax was open and 5 mL of cold sterile saline solution was injected systemically through the left ventricle. The thoracic aorta was gently removed and grafts were incubated with gentle shaking on a tumbling table for 30 min with 50 μL AAV solution (10^{12} virus particles/mL, diluted in NaCl) at room temperature. In order to demonstrate that AAV transduction itself has no effect on elastin structure, mgR/mgR grafts were treated with PBS as a control. Recipient mgR/mgR mice were anesthetized with isoflurane and the abdomen was open. The

infrarenal part of the aorta was visualized under the microscope (25-40x magnification) and vessel clips were placed in between the left renal artery and the aortic bifurcation prior to cutting it. The *ex vivo* transduced aortic graft was implanted, the clips were detached and the abdomen was closed. The following 3 days after surgery, analgesic treatment (Novalgin, Camprofen) was provided. Grafts were removed for analysis 30 days after surgery.

4.7.3 Transverse aortic constriction and echocardiography

Transverse aortic constriction was performed in 10 weeks old C57BL/6N mice for inducing heart hypertrophy which develops into heart failure, as previously described [115]. The surgery was performed in collaboration with Prof. Oliver Müller, Theresa Ruf, Lin Ding, Internal Medicine III, Clinic for Cardiology, Angiology and Pneumology, University Clinic Heidelberg.
The substrain choice was made due to the findings published by Garcia-Menderez *et al* [69], which show that C57BL/6N mice are a better animal model for TAC-induced cardiac hypertrophy than other commonly used substrains, such as C57BL/6J. A 27-gauge needle was used for inducing the stenosis. Successful ligation was confirmed by measuring the right carotid/left carotid flow velocity ratio. Changes in heart function were determined every 2 weeks by echocardiography in non-anesthetised mice using VisualSonics Vevo 2100 imaging system and the 40 Hz MS-550D micro scan transducer. The measurements were performed by an experimenter blinded to the treatment. Long axis and M-mode short axis cine loops were recorded. EF (ejection fraction), FS (fractional shortening) and left ventricular mass was determined using VisualSonics software. The mice were sacrificed by CO_2 asphyxiation 6 weeks after surgery. Heart weight/tibia length ratio was measured as a marker of cardiac hypertrophy, as well as lung weight/tibia length ratio for monitoring heart failure induced lung edema [30]. Furthermore, mice weight was as well tracked every week.

4.8 Statistical data analysis

The statistical data evaluation was made using GraphPad InStat 3.06 software. Differences between 3 or more different groups were assessed using One-way ANOVA, followed by a Tukeys multiple comparison test for particular pairs of groups. Mann-Whitney U test was used to compare two groups. A p value <0.05 was considered significant. *In vitro* experiments were repeated at least 4 times. The mean fluorescence

intensity of at least 20 images/group was analysed in the immunocytochemistry and immunohistochemistry experiments, using ImageJ (FiJi version 1.51p). Gel zymography and Western blot data were evaluated as well using ImageJ. Data are presented as mean $\pm$ SD of *n* individual experiments. Graphs were generated using GraphPad Prism 7 (San Diego, California, USA).

5

Results

5.1 Cloning of the AAV vectors

5.1.1 Digestion of the vectors

Hairpin RNA decoy ODNs were individually cloned into a pDS vector backbone under the control of H1 promoter. Transduced cells were identified by CMV promoter-dependent EGFP expression. Separate vectors containing the sequence of hpRNA decoy ODNs (hpAP-1 cons, hpAP-1 mut, hpNFAT cons, hpNFAT mut) flanked by KasI (5) and XhoI (3) were employed to isolate the insert DNA.
Both pDS vector and the gene synthetized plasmid for each decoy ODN (GeneArt, Thermo Fischer Scientific) were digested with the KasI and SalI enzymes and the resulting DNA was further analysed using agarose gel electrophoresis to prove the successful digestion. As shown in Fig. 11, the detected bands corresponding to the digested vector (5,980 bp) as well as to the insert (164 bp) were cut out and purified using QIAquick Gel Extraction Kit. The pDS vector, kindly provided by Prof. Dr. Oliver Müller, Clinic for Cardiology, Angiology and Pneumology, University Clinic Heidelberg, contained the sequence of an unrelated shRNA, which was detected after KasI and XhoI digestion as a 164 bp band following agarose gel electrophoresis, as demonstrated in Fig. 11. The band corresponding to the pDS vector backbone was identified as the high molecular-weight fragment and was further gel-purified.

5.1.2 Analysis of cloned plasmids

After ligation and transformation steps, single colonies were cultured and plasmid DNA was isolated. In order to show proper ligation and to distinguish self-ligated pDS backbone, SalI digestion was performed, taking into account that the restriction site of this enzyme was present only in the designed insert and not in the initial pDS vector, as shown in Fig. 12.

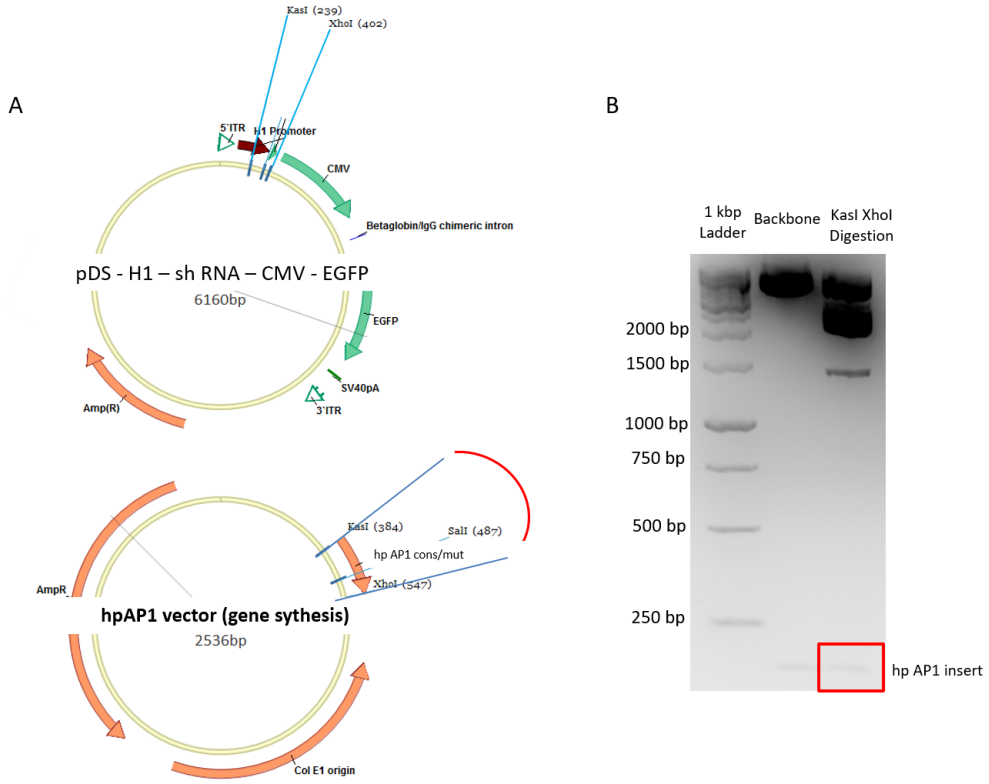

Fig. 11: Cloning strategy for the individual AAV vectors used in the present study. A. Plasmid maps used for backbone and insert isolation respectively. B. Agarose gel detection of plasmid (pDS and RNA decoy ODNs vector) digestion efficiency with KasI and XhoI.

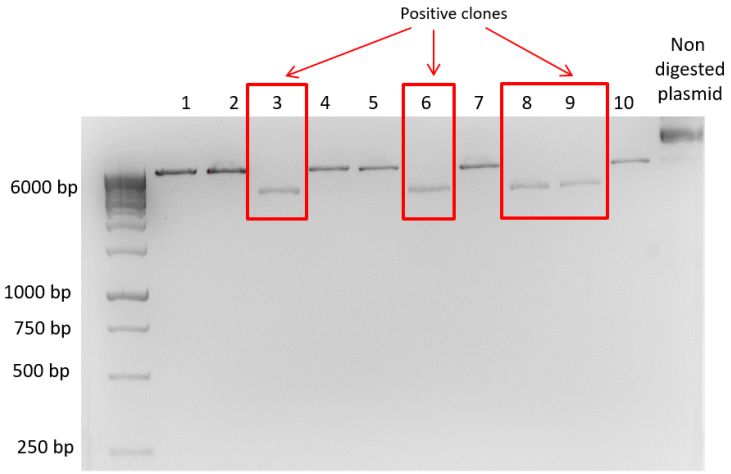

Fig. 12: Confirmation of presence of insert in isolated plasmids. Agarose gel analysis of SalI digested plasmids isolated from picked colonies. The 6,000 bp bands show successful digestion. The non digested plasmid appears as a high molecular weight DNA fragment due to the relaxed structure which migrates with a lower speed than other fragments.

5.2 Marfan syndrome project

5.2.1 "Naked" hpAP-1 decoy ODNs uptake by SMCs

First, hpAP-1 decoy ODNs uptake by aortic SMCs was assessed. For this purpose, primary SMCs isolated from the thoracic aorta of mgR/mgR mice were treated either with Atto-590 fluorescently labelled decoy ODNs alone or with the same amount of DNA pre-incubated with Lipofectamine 3000 as transfection reagent. The distribution of red signal within the cells was analysed by confocal microscopy. The results confirm that 2 h incubation with the labelled hpAP-1 decoy ODNs is sufficient for the decoy uptake by SMCs. On the other hand, when Lipofectamine was pre-mixed with the DNA, a significant lower amount of DNA was detected whithin SMCs, as proven by red fluorescent quantification in Fig. 13.
Moreover, an increased localization of the decoy ODN in the nucleus was observed when the DNA was added alone in the medium, whereas in Lipofectamine-mediated delivery group decoy ODNs were mostly detected inside vesicles. Therefore, in order to assess hpAP-1 decoy ODNs efficiency in SMCs in following experiments, no liposomal transfection reagents were used.

5.2.2 "Naked" hpAP-1 consensus decoy ODN effects on mgR/mgR SMCs

Expression of AP-1 target genes

Having shown that SMCs can be successfully transfected with hpAP-1 decoy ODNs, the analysis of its effect on AP-1 target genes MMP9 and MCP-1 was determined. The two genes have major roles on aortic aneurysm development in Marfan syndrome [92]. MMP9 was already shown to be upregulated in mgR/mgR mice [228] and its deletion decreased the rate of thoracic aortic aneurysms dissection [93]. On the other hand, MCP-1 is a major chemotaxis agent for inflammatory cells and its concentration correlates with disease severity in Marfan patients [164].
In order to induce AP-1 transcription factor family activation, IL-1β was applied to serum depleted SMCs. As expected, 8 h treatment with the stimulus caused a significant increase in the expression of both analysed genes, whereas pre-treatment with hpAP-1 cons decoy ODNs for 2 h led to a significant reduction in the mRNA levels of both MMP9 and MCP-1. The control hpAP-1 mut decoy ODNs had no effect in this context, as shown in Fig. 14, further proving the specificity of the designed decoy ODNs.

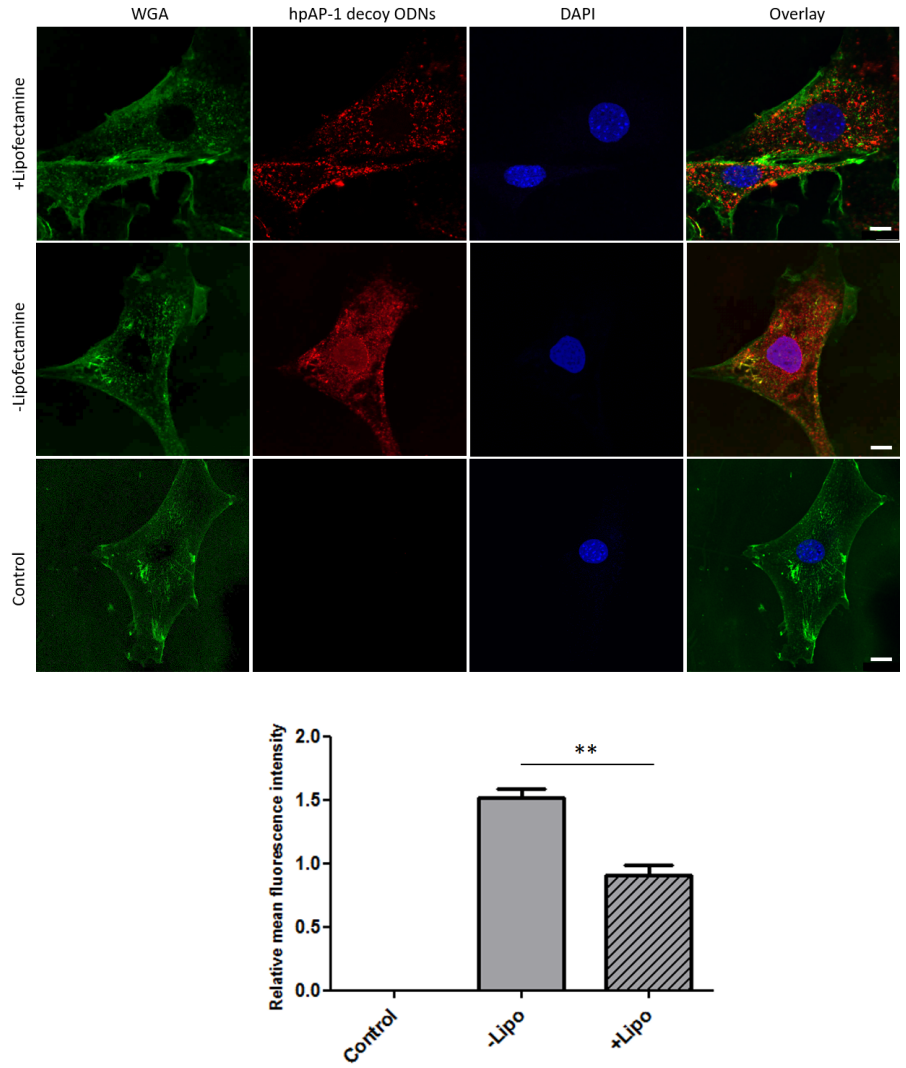

Fig. 13: Hairpin AP-1 decoy ODNs are taken up without auxilliary means by mgR/mgR SMCs. Representative fluorescence images showing the uptake of Atto590 fluorescently labelled hp AP-1 decoy ODN (red) with or without liposomal transfection reagent. Cell membranes were marked with WGA-Alexa488 (green). The graph shows statistical quantification of red signal detected in confocal images, proving that Lipofectamine mediated transfection is less effective than simple decoy ODN addition to cell culture medium. The scale bar represents 10 μm; Lipo: lipofectamine treatment. (n=3, ** p=<0.001).

MMP expression and activity in SMCs

To confirm the results of gene expression analysis on protein level, Western blot experiments were performed using a specific antibody directed to MMP9. As a result, a high molecular weight protein band was detected in mgR/mgR SMCs lysates, which had a higher intensity than the expected 105 kDa band. To prove that the 220 kDa band represents a MMP9 dimer and not a non-specific binding of the antibodies, SMCs were treated with a compound which was validated as a specific MMP9 dimerization

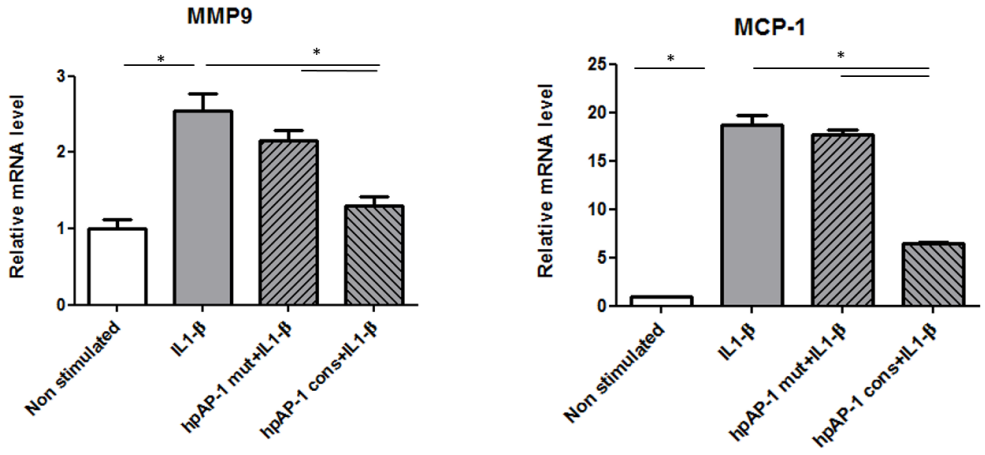

Fig. 14: Hairpin AP-1 consensus decoy ODNs but not the mutated control ODNs significantly decrease the mRNA levels of AP-1 target genes. MMP9 and MCP-1 gene expression was normalised to RPL32 (ribosomal protein L32) as housekeeping gene. (n=5, * $p<0.05$).

inhibitor, by blocking its PEX domain [53]. When SMCs were incubated with this compound for 24 h but not with DMSO as control, MMP9 dimerization was completely abolished and the high molecular band was not present, as depicted in Fig. 15B. This led to the conclusion that in mgR/mgR aortic SMCs MMP9 could be detected mainly as homodimer in SMCs protein lysates, even under denaturing and reducing conditions. Thus further data analysis was made using the 250 kDa protein.

MMP9 expression levels were analysed in SMCs following treatment with hpAP-1 consensous decoy ODNs. As shown in Fig. 15A, MMP9 homodimer expression was significantly decreased by 74% following hpAP-1 cons decoy ODNs application. As expected, the control mutated decoy ODNs had no effect on MMP9 protein level.

Additionally, MMP activity in the cell culture setup was analysed. For this purpose, serum-free cell culture supernatant was subjected to MMP concentration using gelatine beads, followed by gel zymography. In our hands, the 105 kDa band corresponding to the monomeric MMP9 had the highest gelatinolytic activity in mgR/mgR SMCs conditioned medium and was therefore analysed. In consistence with the Western blot results, SMCs treatment with hpAP-1 consensous but not with the mutated decoy ODNs led to a marked decrease of MMP9 proteolytic activity, as shown in Fig. 16A.

In order to evaluate if the activity of non-secreted MMPs follows the same trend, a broad spectrum FRET substrate was employed, which was applied to SMCs in serum free medium. The substrate is cleaved by MMP-1, 2, 3, 7, 8, 9, 12, and 13, leading to the generation of a red fluorescent compound which was further visualized and quantified in confocal images. As demonstrated in Fig. 16B, 24 h incubation with IL-1β significantly

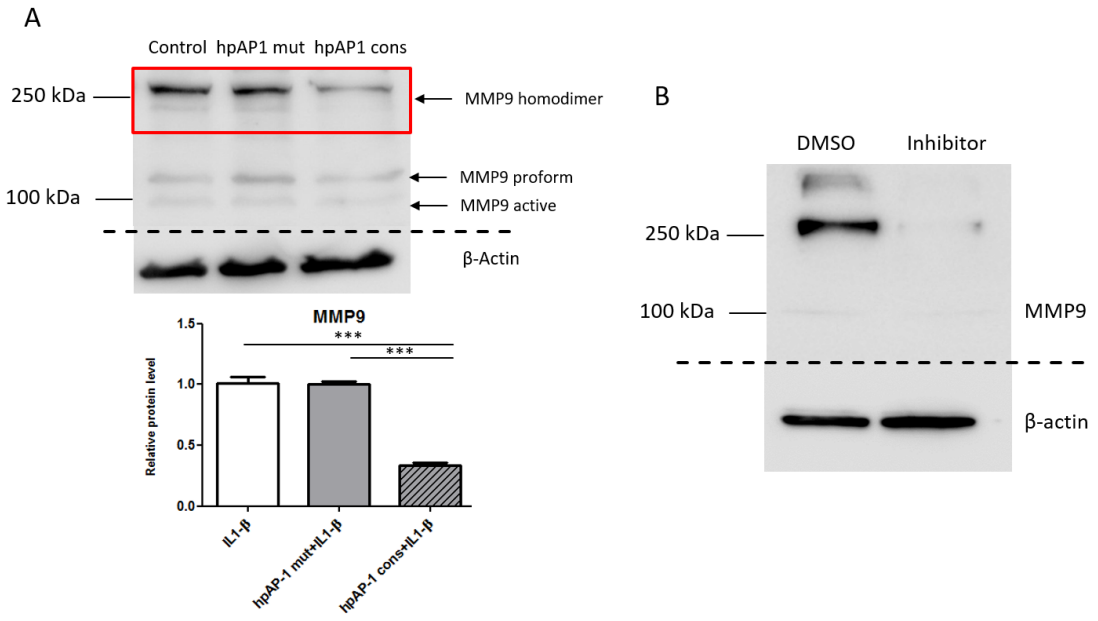

Fig. 15: Hairpin AP-1 consensus decoy ODNs significantlydecrease IL-1β-induced MMP9 protein level in aortic SMCs. (A) MMP9 Western blot analysis of SMCs lysates. β-Actin was used as a loading control and relative protein levels were normalized to IL-1β (20 ng/mL) stimulated SMCs. (n=4, *** p<0.001). (B) Evaluation of the 250 kDa band detected in the Western blot experiments. By using a small molecule which blocks MMP9 dimerization, the high molecular weight homodimer was not detected.

increased MMP activity in SMCs, which was largely diminished by hpAP-1 consensus decoy ODNs application prior to stimulation.
The aforementioned findings demonstrate that AP-1 neutralization through hpAP-1 consensus decoy ODNs can downregulate the mRNA levels of genes controlled by this transcription factor family and activated by IL-1β stimulation. Moreover, decreased MMP9 protein level and activity in SMCs was observed.

Reactive oxygen species generation

An important role in the development and rupture of aortic aneurysms in Marfan syndrome patients was attributed to disturbances in reactive oxygen species (ROS) homeostasis whithin the aortic tissue. ROS are generated by increased TGF-β signalling and were shown to correlate with the rate of aortic aneurysms rupture [29]. Furthermore, AP-1 inhibition was proven to decrease ROS production through reduced NADPH oxidase activity in human aortic SMCs [128]. Therefore, the effect of hpAP-1 consensus decoy ODNs on ROS production in the context of Marfan syndrome was determined.
For this purpose, ROS production was measured by incubating the cells with CM-H2DCFDA after decoy ODNs treatment. The CM-DCF green fluorescence intensity

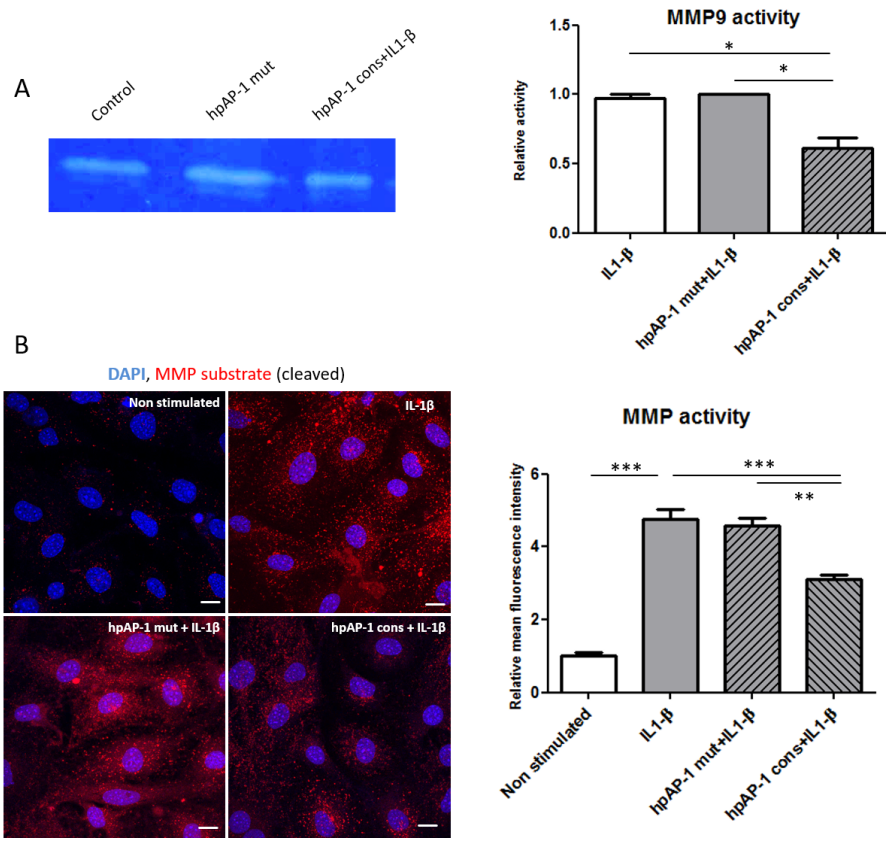

Fig. 16: Hairpin AP-1 consensus decoy ODNs decrease IL-1β-induced MMP activity in aortic SMCs. (A) MMP9 gelatinolytic activity as shown by gel zymography. The graph depicts desitometric analysis of the bands, normalized to IL-1β (20 ng/mL) stimulated group. (n=4, * $p<0.05$) (B). Intracellular MMP activity was analysed using a FRET substrate specific for 12 different MMPs. Red signal represents the fluorescence generated by cleaved substrate and correlates with the total activity of intracellular MMP. The graph shows the statistical quantification of mean red fluorescence intensity of the indicated treatment groups. Cell nuclei were stained with DAPI. The scale bar represents 75 μm, 20 images analysed/group. (n=4, *** $p<0.001$, ** $p<0.01$).

significantly increased in IL-1β stimulated SMCs, as compared to control cells, proving a higher amount of ROS in the presence of the stimulus. However, following 2 h incubation with hpAP-1 consensus decoy ODNs prior to IL-1β addition to the medium, SMCs showed a significant decrease in the level of ROS, as demonstrated by the quantification of fluorescent images in Fig. 17.

Migration rate

In was previously shown that thoracic aneurysms are correlated with phenotypic switch of vascular SMCs, process characterized by increased proliferation, enhanced MMP activity and decreased SMA (smooth muscle α-actin) expression. [129]. Moreover, SMCs

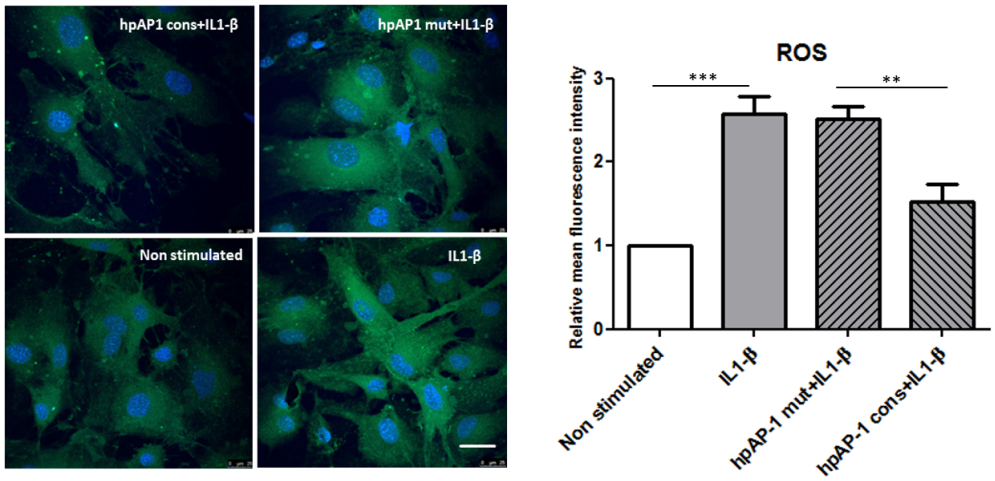

Fig. 17: Hairpin AP-1 consensus decoy ODNs decrease IL-1β-induced ROS production in aortic SMCs. Representative images showing CM-DCF fluorescence, recorded using confocal microscopy on the green channel. Mean fluorescence intensity was analysed and normalized to non-stimulated control. The scale bar represents 75 μm, 20 images analysed/group. (n=4, *** $p<0.001$, ** $p<0.01$).

injury correlates with increased migratory phenotype of the cells. Taking these observations into account, SMC migration rate was analysed in the presence of hpAP-1 decoy ODNs by using ibidi inserts. IL-1β significantly increased the migratory capacity of SMCs. On the other hand, the migration rate of SMCs pre-treated with hpAP-1 consensus decoy ODNs, but not with the mutated control decoy ODNs almost declined to the basal level (Fig. 18).

5.2.3 Transduction efficiency of SMCs with AAV9 modified with targeting capsid peptides

Previous research demonstrated that AAV transduction efficiency and specificity can be markedly improved by the use of targeting capsid peptides [140, 208]. Nevertheless, the transduction efficiency of the AAV serotype 9 with targeting peptide SLRSPP (AAV9SLR) was only shown in human endothelial cells and SMCs *in vitro*. Therefore, we wanted to confirm that AAV9SLR is a suitable vector for transduction of mouse mgR/mgR SMCs. For this purpose, cells were transduced with EGFP expressing AAV9SLR and SMCs were visualised using fluorescence microscopy after 3 days. In addition, AAV9 with 2 other selected peptides were tested, as well as AAV2 with modified capsids. As controls, wild type non modified AAV9 (AAV9WT) and non-transduced SMCs were used. The results in human primary cells could be reproduced in mouse aortic SMCs, namely the targeting capsid peptide SLRSPP significantly improved the transduction efficiency of the wild type vector, as shown in Fig. 19. Using this AAV

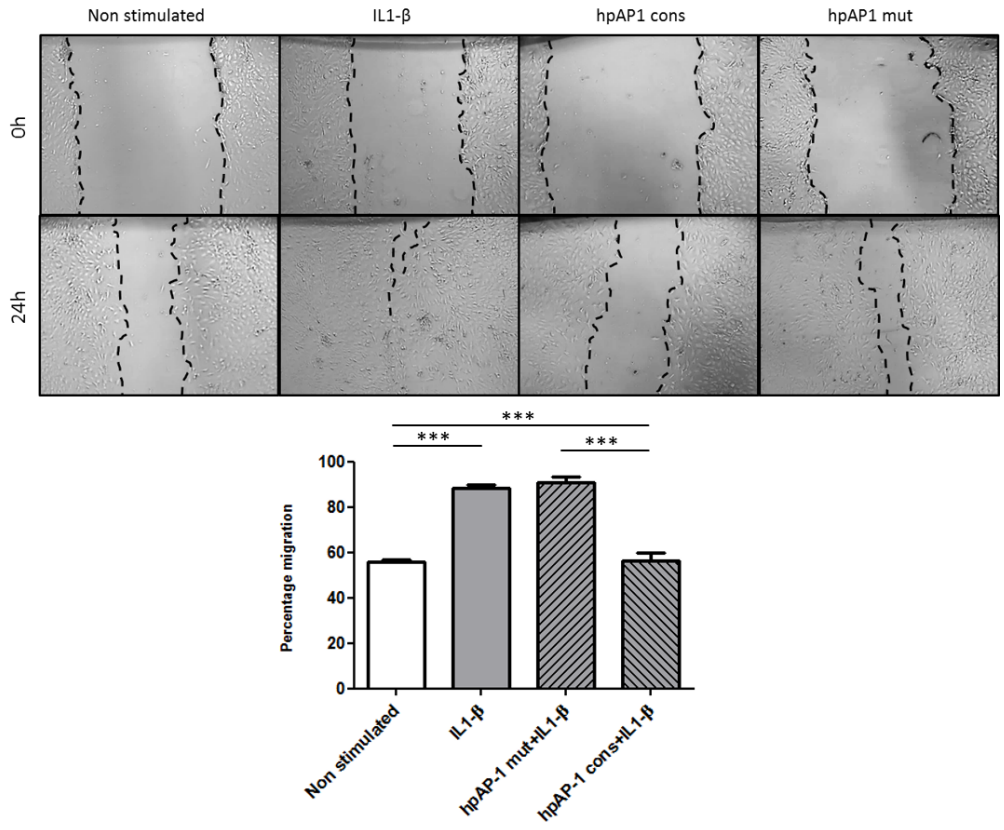

Fig. 18: Hairpin AP-1 consensus decoy ODNs significantly decrease the migration rate of vascular SMCs. Depicted are representative images of SMCs immediately after removal of the inserts (0 h), and after 24 h stimulation with 20 ng/mL IL-1β. The graph shows relative migration rate of SMCs in the 4 treatment groups. (n=4, *** p$<$ 0.001).

construct, a greater than 70% transduction efficiency was achieved on average, while the other serotypes only led to extremely low amount of EGFP positive cells (less than 5%). AAV9WT failed to transduce mgR/mgR SMCs *in vitro*.

Expression of hpRNA decoy ODNs after AAV9SLR transduction

Having identified the most efficient AAV serotype for *in vitro* transduction of primary SMCs, the production of shRNA-expressing vectors was performed. The hpAP-1 consensus and hpAP-1 mutated control decoy ODNs were cloned into the designed plasmids and afterwards AAVs were generated. F.I.S.H. experiments were carried out 3 days after infection to confirm that RNA decoy ODNs are expressed in transduced cells. We used a directly labelled probe with complementary sequence to the hpAP-1 cons decoy ODNs and we showed its specificity *in situ*. The molecular beacon emits no fluorescence as a hairpin structure due to the close proximity of the fluorofore (Cy5) and the quencher (BHQ-2). However, as soon as it hybridizes to its target, namely the hpAP-1

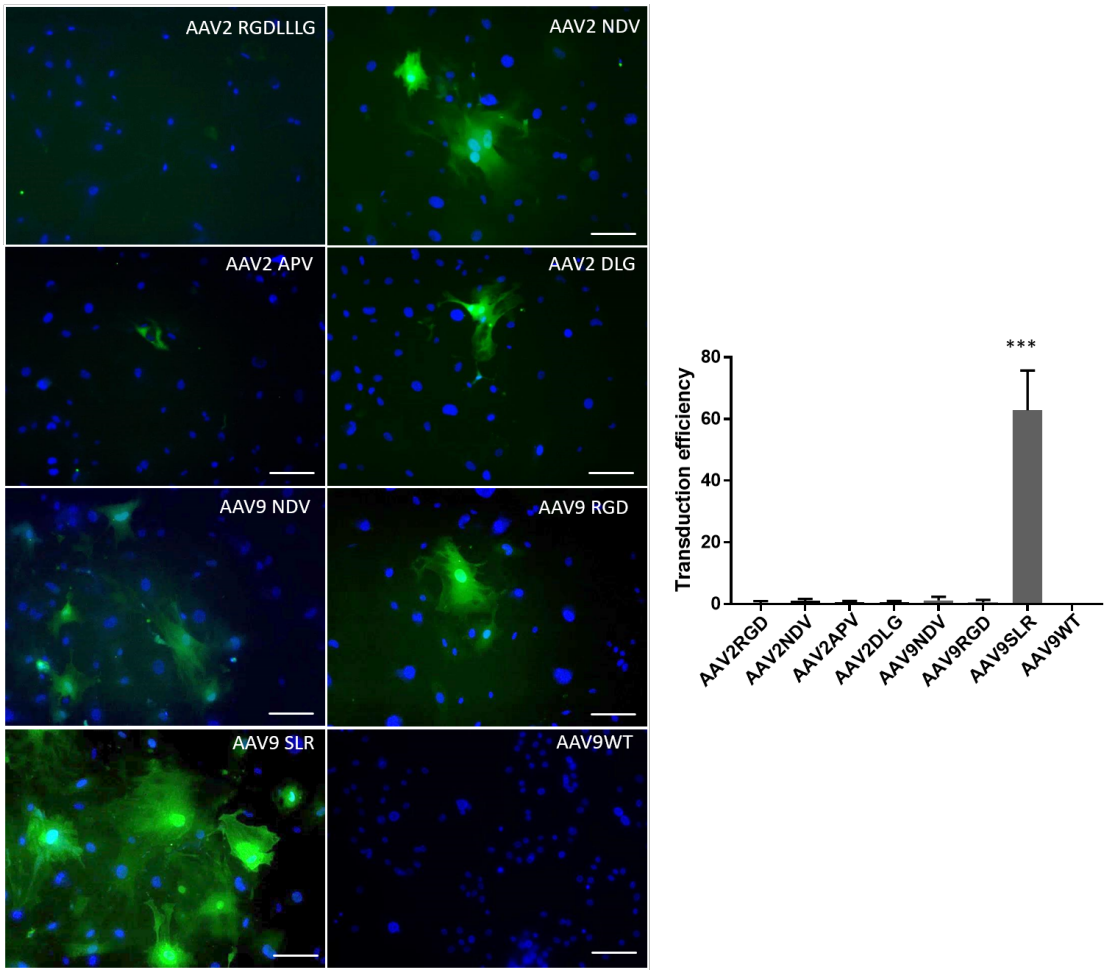

Fig. 19: Transduction efficiency of different AAV serotypes with modified capsid. Representative images of mgR/mgR aortic SMCs 3 days after transduction with tested vectors. EGFP fluorescence (green) was analysed as a marker of transduction efficiency of the indicated vectors and the percentage of transduced cells was calculated. Nuclei were marked using DAPI in order to count the number of cells/field of view. Scale bar represents 82μm. (n=4, *** $p < 0.0001$, compared to AAV9WT.)

consensus RNA decoy ODN, red fluorescence can be detected. After the harsh washing steps during this procedure with hybridization buffer containing formamide, a dramatic loss of the EGFP fluorescence in SMCs was observed. Therefore, EGFP immunocytochemistry was conducted subsequently, in order to identify successfully transduced cells.

Cy5 signal was detected only in EGFP positive cells, showing the accuracy of the method. In contrast, substantially lower or no red fluorescence was found in AAV9SLR EGFP or non-transduced SMCs, as shown in Fig. 20. Hairpin AP-1 RNA decoy ODNs were identified in the nuclei of transduced cells, but they were also expressed in the

perinuclear region.

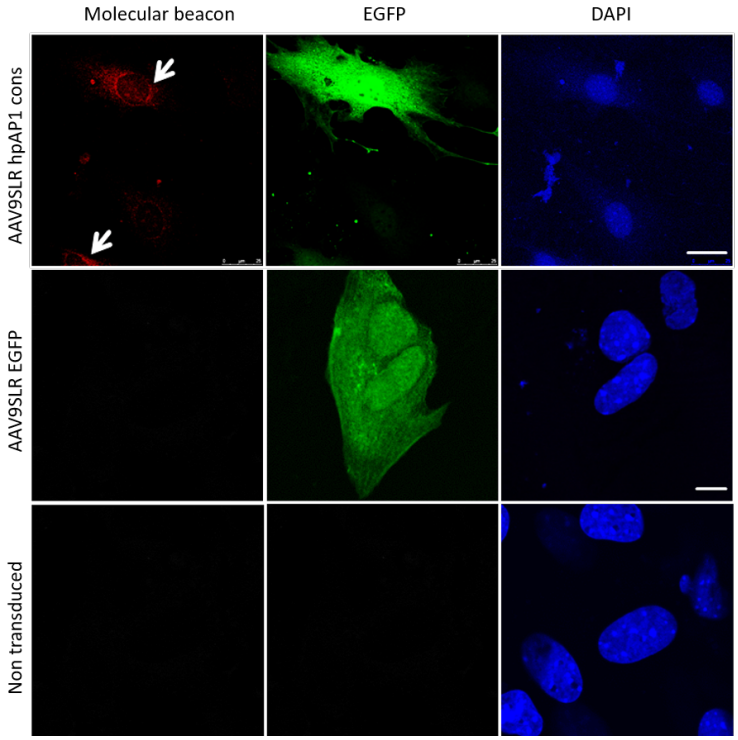

Fig. 20: AAV9SLR-mediated expression of hpAP-1 consensus RNA decoy ODNs in vascular SMCs. Red signal shows F.I.S.H. probe hybridization to its target, proving the generation of shRNA in transduced, EGFP-positive cells (green). Non-transduced SMCs as well as AAV9SLR-EGFP treated cells served as controls . DAPI staining (blue) was employed to visualize the nuclei. The scale bar represents 75 μm. (n=3, exemplary pictures).

5.2.4 Effect of AAV9SLR-mediated hpAP-1 RNA decoy ODNs generation in primary mgR/mgR SMCs

Expression of AP-1 target genes

To further investigate whether AAV9SLR-mediated hpAP-1 consensus RNA decoy ODNs delivery in vascular SMCs is able to neutralize the transcription factor with a similar efficiency as the DNA decoy ODNs, the mRNA levels of MMP9 and MCP-1 was analysed. Similarly to previous experiments, AP-1 was activated by addition of IL-1β to SMCs 3 days after AAV transduction in serum-free medium. As shown in Fig. 21, transduction with AAV9SLR expressing hpAP-1 consensus RNA decoy ODNs resulted in a significant decrease in both genes mRNA expression levels, while the mutated control AAV had no effect on the analyzed AP-1 target genes.

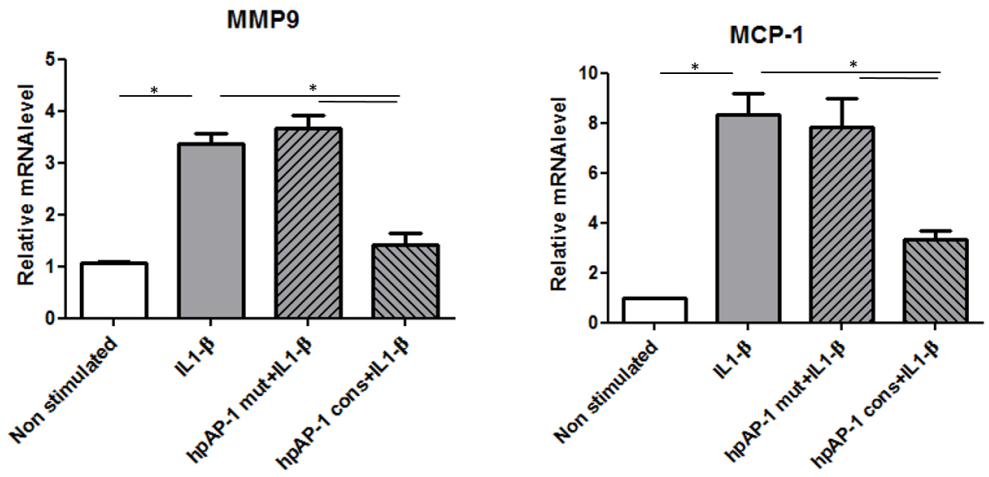

Fig. 21: AAV9SLR-mediated expression of hpAP-1 consensus RNA decoy ODNs significantly decreases AP-1 target genes in vascular SMCs. mRNA levels of MMP9 and MCP-1 were compared to RPL32 as a housekeeping gene. Values were normalized to the non-stimulated controls. (n=4, * $p<0.05$).

MMP expression and activity in SMCs

To further support the mRNA data and to prove efficient AP-1 neutralization by the designed vector, MMP9 protein level was analysed by immunocytochemistry. Red fluorescent signal, corresponding to the MMP9 antibody, was analysed in EGFP positive cells. MMP9 content was significantly higher in IL-1β stimulated SMCs in comparison to non-stimulated cells (Fig. 22). Transduction with hpAP-1 RNA cons decoy ODNs producing AAV9SLR significantly downregulated MMP9 protein level, while the AAV9SLR expressing hpAP-1 mutated RNA decoy ODNs had no effect (Fig. 22). Next, the effect of transduction on secreted and intracellular MMP activity in mgR/mgR SMCs was determined. Gelatine zymography experiments pointed out that AAV9SLR-mediated hpAP-1 consensus, but not mutated RNA decoy ODNs generation led to a dramatic decrease in MMP9 gelatinolytic activity in SMCs supernatant, as shown in Fig. 23A. As is previous experiments, the most prominent band observed in the analysis corresponded to 105 kDa, equivalent to the MMP9 monomer which was further quantified.

Similar results were obtained when a fluorescent broad spectrum MMP substrate was employed to measure the intracellular MMP activity. The main advantage of this technique is that it allows the identification and measurement of the activities of several MMPs expressed by SMCs, i.e. MMP-1, 2, 3, 7, 8, 9, 12, and 13 activities. Moreover, the Ex/Em curves of this substrate is highly compatible to EGFP fluorescence and can be detected in parallel by confocal microscopy. The results of this experiment demon-

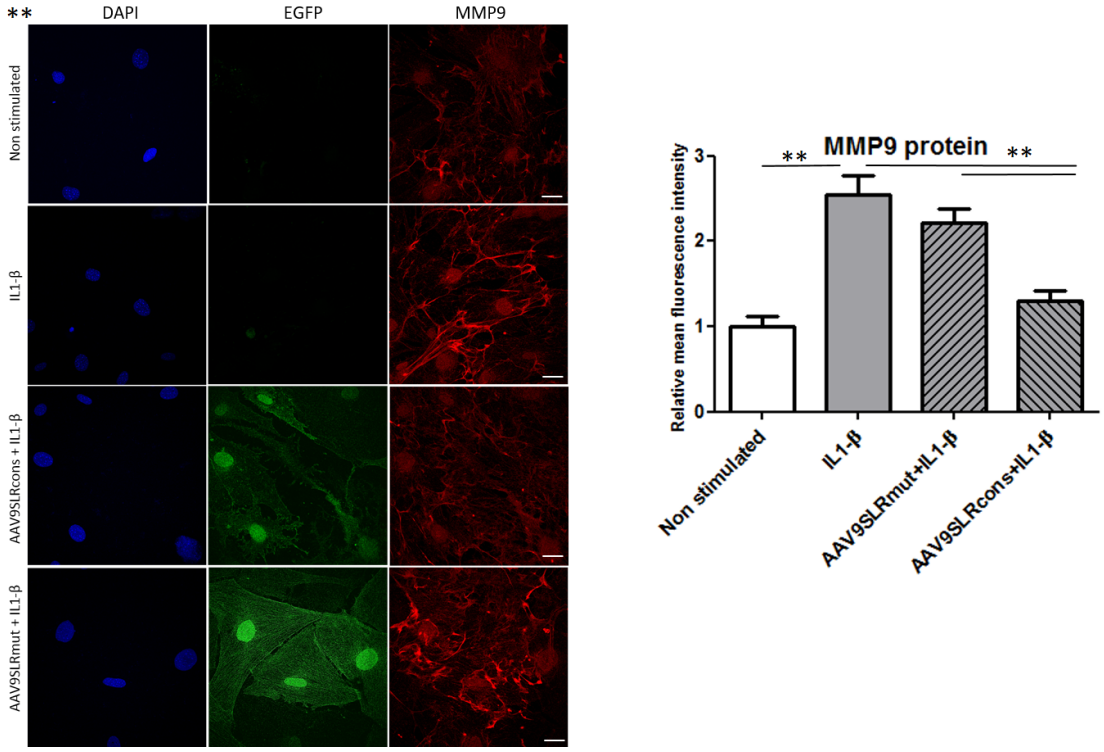

Fig. 22: AAV9SLR-mediated expression of hpAP-1 consensus RNA decoy ODNs significantly decreases MMP9 protein level in vascular SMCs. Detection of MMP9 (red) was made by immunocytochemistry. Successful transduction was confirmed by EGFP fluorescence (green). The graph summarizes the statistical quantification of the mean red fluorescence intensity of individual experiments. Nuclei were visualized by DAPI staining (blue). The scale bar represents 25 μm. (n=4, 20 images analysed/group, ** $p<0.01$).

strate that AAV9SLR-mediated AP-1 neutralization significantly decreased MMP activity, which was brought back to basal conditions, while the mutated control AAV9SLR had no effect on MMP enzymatic activity. Representative images and quantifications are depicted in Fig. 23B.

Reactive oxygen species generation

To determine whether hpAP-1 consensus RNA decoy ODNs delivery in SMCs by AAV9SLR transduction affects the level of ROS in a similar manner as hpAP-1 consensus decoy ODNs application, DHE was used as an indicator of oxidative stress. CM-DCF could not be used as in previous experiments due to the expression of EGFP fluorophore of the AAV9SLR transduced cells, which would interfere with detection of the oxidized dye. Upon entry into the cells, DHE reacts with superoxide ions, yielding oxyethidium. This compound in turn interacts with nucleic acids and emits nuclear red fluorescence which can be detected in parallel with the green signal given by EGFP positive cells. The quantification of DHE oxidation levels shows that AAV9SLR expressing

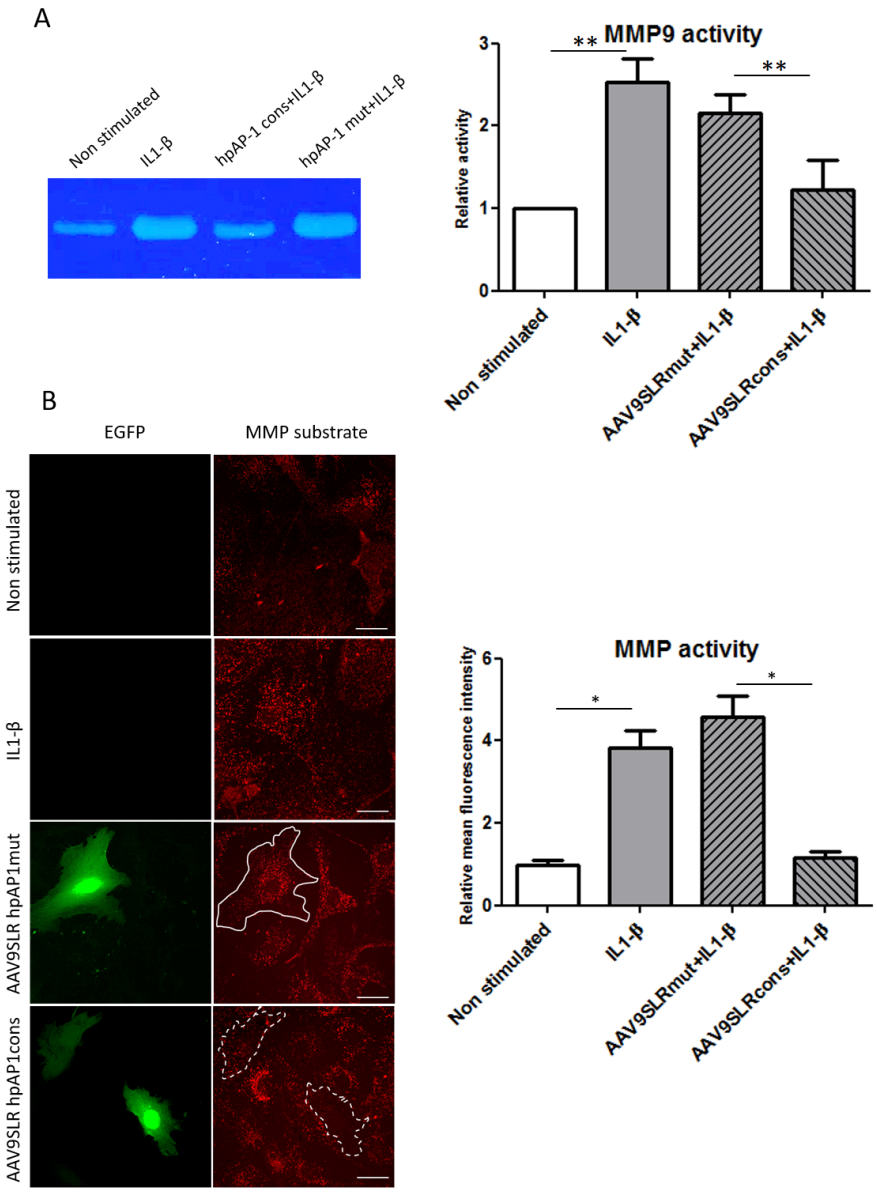

Fig. 23: AAV9SLR-mediated expression of hpAP-1 consensus RNA decoy ODNs significantly decreases MMP activity in vascular SMCs (A) Gelatinolytic activity of MMP9, detected as 105 kDa white bands on Coomassie Brilliant Blue stained zymography gel. The graph shows statistical quantification of relative densitometric analysis of the bands obtained in individual experiments. Values were normalized to the non-stimulated control group (n=4, * $p<0.05$). (B) Representative images of SMCs treated with MMP substrate after AAV9SLR transduction and IL-1β stimulation. Red fluorescence is proportional to the amount of cleaved MMP substrate. Transduced EGFP positive cells (green, underlined with white) were selected for analysis. Scale bar represents 25μm. (n=4, 20 images analysed/group, ** $p<0.01$).

hp AP-1 consensus but not the mutated RNA decoy ODNs can significantly decrease the amount of IL-1β-induced ROS generation by SMCs, as shown in Fig. 24.

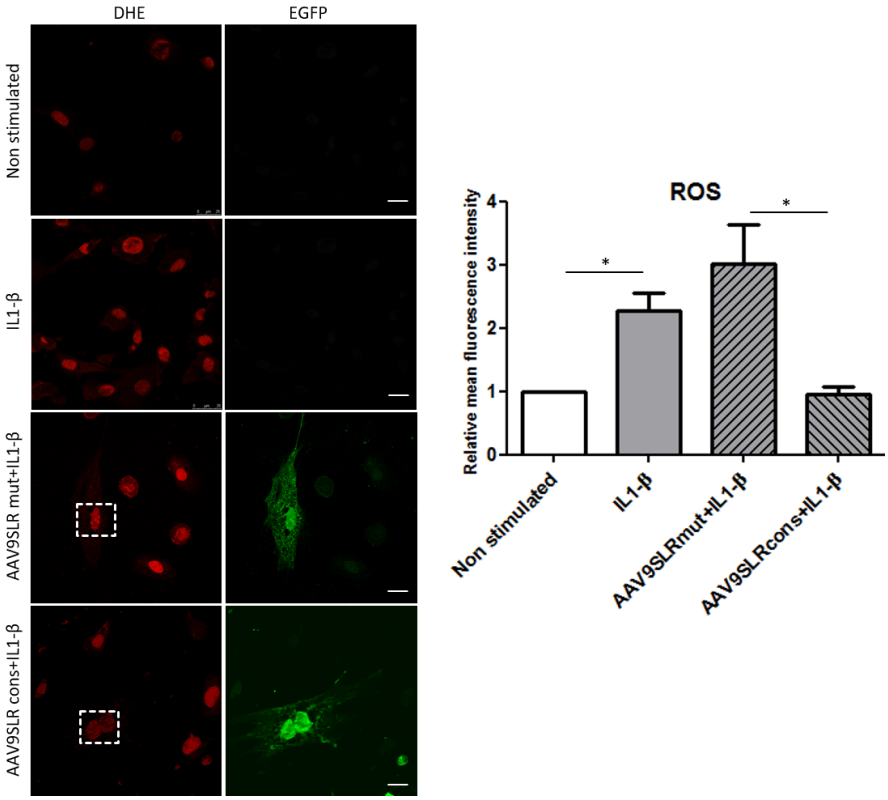

Fig. 24: AAV9SLR-mediated expression of hpAP-1 consensus RNA decoy ODNs decreases the amount of ROS in vascular SMCs. Representative images showing the measurement of superoxide in mgR/mgR SMCs following AAV9SLR transduction. The graph pictures the statistical quantification of relative mean red fluorescence intensity levels as compared to the non-stimulated control. EGFP fluorescence (green) shows successfully transduced cells. Scale bar represents 25 μm. (n=4, 20 images analysed/group, * $p<0.05$).

5.2.5 *Ex vivo* transduction of murine mgR/mgR aortic grafts with AAV9SLR

First, the *in vivo* capacity of AAV9SLR to transduce aortic SMCs was verified by injecting the EGFP expressing vector systemically through the tail vein of mgR/mgR mice. After 30 days, thoracic aortae of injected mice were removed and tested for EGFP expression in frozen sections by immunohistochemistry. Moreover, the aortae were digested and single cell suspensions were prepared and subjected to FACS analysis to determine EGFP fluorescent cells. Nevertheless, no EGFP positive cells, neither SMCs nor endothelial cells, could be detected (data not shown).

Therefore, *ex vivo* treatment of aortic grafts with AAV9SLR-EGFP and wild type AAV9WT-EGFP as a control was performed, followed by infrarenal reimplantation into

recipient mice. This method allows a local application of the vectors to yield a higher AAV transduction rate and the chance of vector neutralization by antibodies in serum is reduced. Under these conditions, successful transduction by AAV9SLR but not by AAV9WT was proven. EGFP expression was found not only in endothelial cells, but also in SMCs, the target cells of this study. An antibody specific for EGFP was used in order to distinguish between elastin fibers autofluorescence on the green channel and EGFP fluorescence. Another reason for EGFP detection by immunohistochemistry was that rapid loss of green fluorescence was observed during fixation and staining procedures. An antibody for CD31 was used to mark endothelial cells. Representative immunohistochemistry images are shown in Fig. 25A.

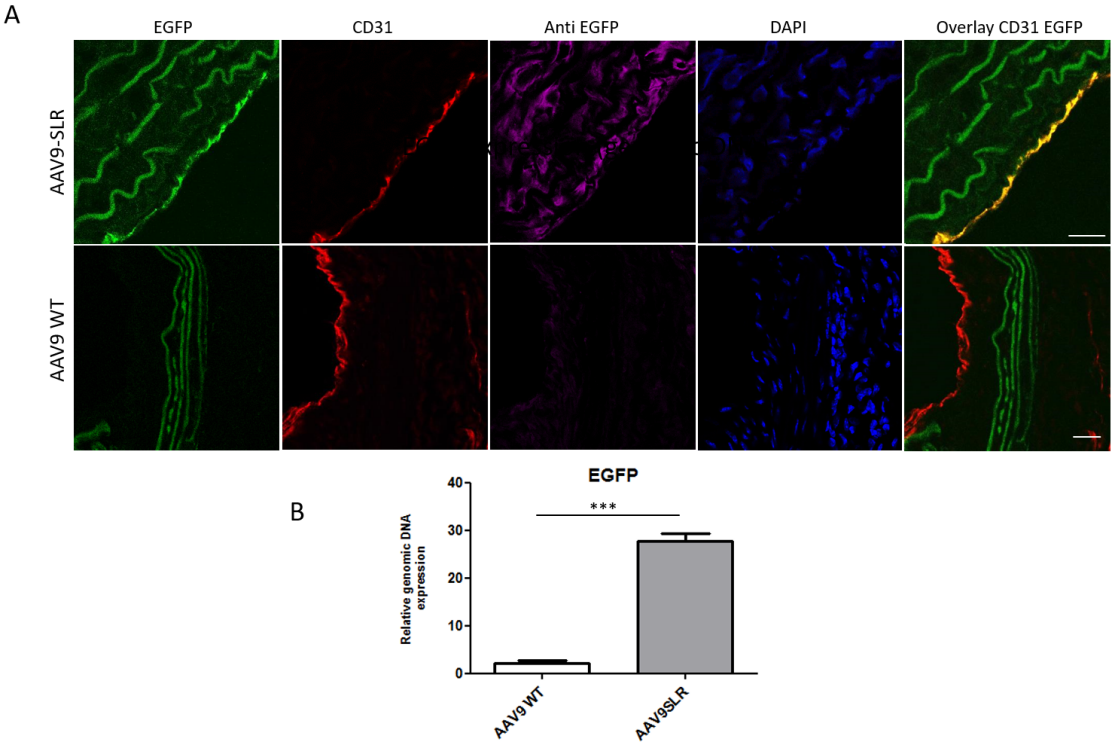

Fig. 25: Capsid peptide SLR significantly enhances *ex vivo* transduction efficiency of AAV9 in mgR/mgR aortic tissue. (A) Illustrative immunohistochemistry images showing EGFP expression (green) in CD31-positive endothelial cells (red), as well as in smooth muscle cells in the media (magenta). (B) EGFP expression on the genomic DNA level is increased in AAV9SLR transduced grafts as compared to AAV9WT treated tissue, 30 days after transduction and reimplantation. Scale bar represents 25 μm. (n=4, *** $<$0.001).

To bring more evidence to support these observations, genomic DNA was isolated from aortic grafts and EGFP expression was analysed by qPCR using specific primers. Through this method, a prominent rise in EGFP expression was demonstrated in AAV9SLR transduced grafts as compared to AAV9WT control treated tissue.

These data demonstrate that AAV9SLR can transduce SMCs of *ex vivo* treated aortic grafts, but fails to infect target cells when administered systemically into the circulation.

5.2.6 Effect of *ex vivo* transduction with AAV9SLR expressing hpAP-1 consensus RNA decoy ODNs

Expression of hpAP-1 RNA decoy ODNs in transduced aortic grafts

After having found a reliable and reproducible method to transduce SMCs in explanted aortic tissue, thoracic aortic grafts were treated *ex vivo* with AAV9SLR expressing hpAP-1 cons RNA decoy ODN, as well as hpAP-1 mut RNA decoy ODNs as a control. The presence of RNA decoy ODNs following vector treatment was first demonstrated by F.I.S.H. For this purpose, the molecular beacon validated in the *in vitro* F.I.S.H. analysis was used. The results point out that aortic grafts treated *ex vivo* with the designed AAV9SLR express high levels of hpAP-1 RNA decoy ODNs, as shown by red fluorescence intensity which is consistent with the amount of probe hybridized to the shRNA. As a negative control a non-transduced graft isolated from a mgR/mgR mouse was used, which showed almost no fluorescence on the Cy5 channel, accounting for the specificity of the method (Fig. 26).

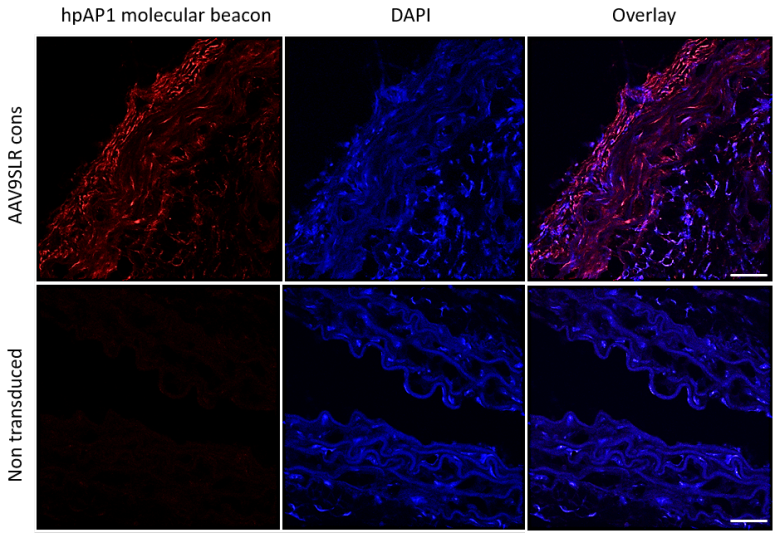

Fig. 26: Hairpin AP-1 RNA decoy ODNs are expressed in *ex vivo* transduced mgR/mgR aortic grafts, four weeks after vector treatment. RNA F.I.S.H. was performed to show shRNA expression in cryosections of AAV9SLR treated grafts, 4 weeks after transduction. DAPI staining (blue) was used to visualize nuclei. Red fluorescence represents hybridized probe to the target. hpAP-1 RNA decoy ODNs were detected both in the nucleus and in the cytoplasm of transduced cells. The scale bar represents 25 μm. (n=4, exemplary images).

Expression of AP-1 target genes in transduced aortic grafts

In order to demonstrate that AAV9SLR-mediated hpAP-1 consensus RNA decoy ODNs delivery in aortic tissue can lead to neutralization of the transcription factor, the mRNA levels of AP-1 target genes were assessed. As previously reported in patient samples [94], MMP9 and MCP-1 mRNA levels were significantly increased in the aorta of mgR/mgR mice which did not receive AAV treatment, as compared to WT controls (Fig. 27). Similar to the results of *in vitro* experiments, transduction with AAV9SLR expressing the mutated form of decoy ODNs had no effect on the analysed genes (Fig. 27). Remarkably, AAV9SLR-mediated generation of hpAP-1 cons RNA decoy ODNs in aortic grafts led to a significant decrease in both analysed AP-1 target genes.

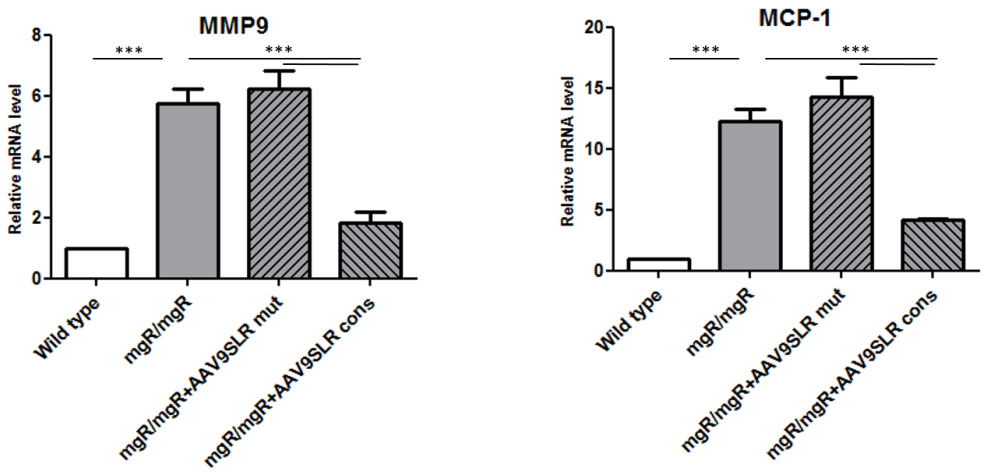

Fig. 27: AAV9SLR-mediated delivery of hpAP-1 consensus RNA decoy ODNs significantly decreases AP-1 target genes in *ex vivo* transduced mgR/mgR aortic grafts. MMP9 and MCP-1 mRNA levels of AAV9SLR transduced aortic grafts were normalised to RPL32 as housekeeping gene and normalized to aortic samples isolated from age matched wild type mice. (n=6, *** $p < 0.001$).

MMP2 and MMP9 protein levels in transduced aortic grafts

Having shown a clear and significant effect of AAV9SLR-mediared hpAP-1 consensus RNA decoy ODNs generation on AP-1 target gene expression, the protein levels of gelatinases were further investigated in transduced tissue. Thus, immunohistochemistry was performed for assessment of MMP2 and MMP9 in treated grafts. The experiments revealed that both MMP2 and MMP9 protein levels were significantly increased in non-treated mgR/mgR thoracic aorta as well as in mutated AAV9SLR transduced grafts in comparison to control (Fig. 28). In consistence with the mRNA results, a dramatic decrease in the expression of both gelatinases was noted in thoracic aortae treated with

active AAV9SLR expressing hpAP-1 consensus RNA decoy ODNs. Representative images and analysis are shown in Fig. 28.

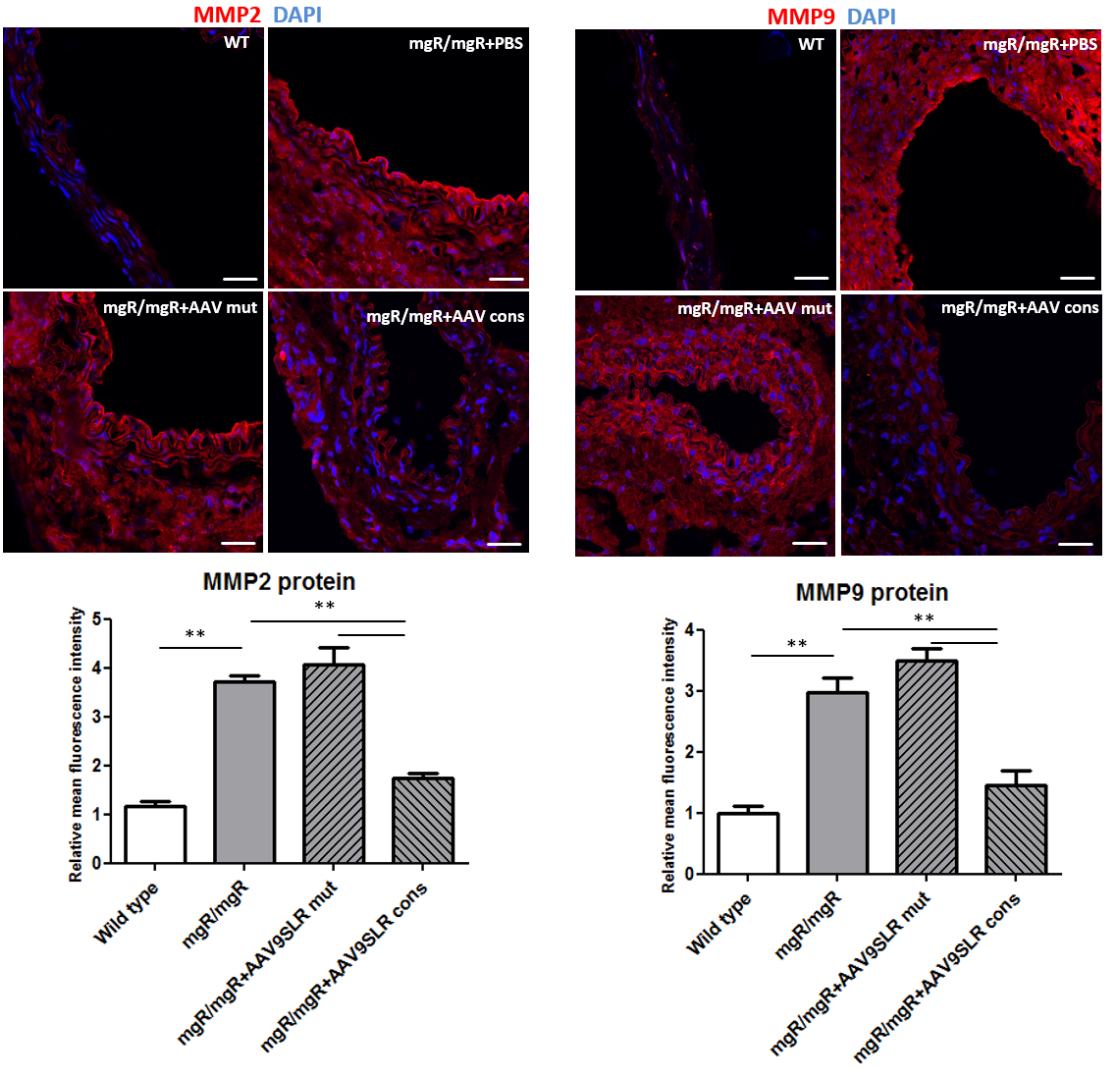

Fig. 28: AAV9SLR-mediated expression of hpAP-1 consensus RNA decoy ODNs significantly decreases MMP2 and MMP9 protein levels in *ex vivo* transduced mgR/mgR aortic grafts. Illustrative images of immunohistochemistry experiments showing MMP2 and MMP9 immunohistochemsitry (red). DAPI staining (blue) was used to mark nuclei. Relative mean fluorescence intensity was analysed and normalized to values of the WT control mice. The scale bar represents 25 μm. (n=6, 20 images analysed/ treatment group, ** $p < 0.01$).

MMP12 protein level in transduced aortic grafts

MMP12 or macrophage elastase was another target protein investigated in the context of Marfan syndrome. The importance of MMP12 in the dissection of aortic aneurysm was previously shown [187]. MMP12 does not only cleave elastin, but also other components

of the extracellular matrix such as collagen and laminins and hence can be an important factor in the development of elastin fragmentation noted in Marfan syndrome.
To determine which cell types express MMP12 in aortic tissue isolated from mgR/mgR mice, co-staining with SMA was performed. Immunohistochemistry analysis showed that MMP12 was expressed not only by SMCs cells in the media, but also by cells in the adventitia. (Fig. 29).

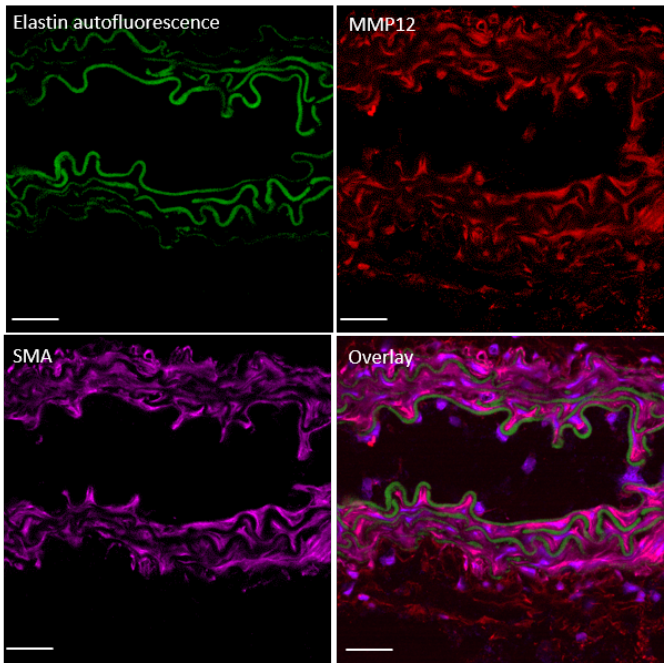

Fig. 29: MMP12 protein expression in mgR/mgR aorta. Representative fluorescent images of MMP12 immunohistochemistry analysis (red) and SMA (magenta) in Marfan aortic frozen. Overlay with DAPI (blue) and elastin autofluorescence (green) is shown. Scale bar represents 50 μm. (n=3, exemplary images).

Having shown a high MMP12 protein expression in the thoracic aorta of mgR/mgR mice, the level of this elastase was evaluated following viral treatment. As shown in Fig. 30, MMP12 protein level in mgR/mgR mice is remarkably increased in comparison to WT controls. Moreover, immunohistochemistry experiments proved that AAV9SLR expressing hpAP-1 consensus but not mutated RNA decoy ODNs caused a significant 2-fold decrease in MMP12 protein levels of mgR/mgR aortic grafts.

MMP activity in transduced aortic grafts

To test whether transduction with AAV9SLR expressing hpAP-1 consensus RNA decoy ODNs has an effect not only on MMP protein level in aortic grafts but also on total MMP activity, the tissue was treated with the previously used FRET substrate. Cryosections

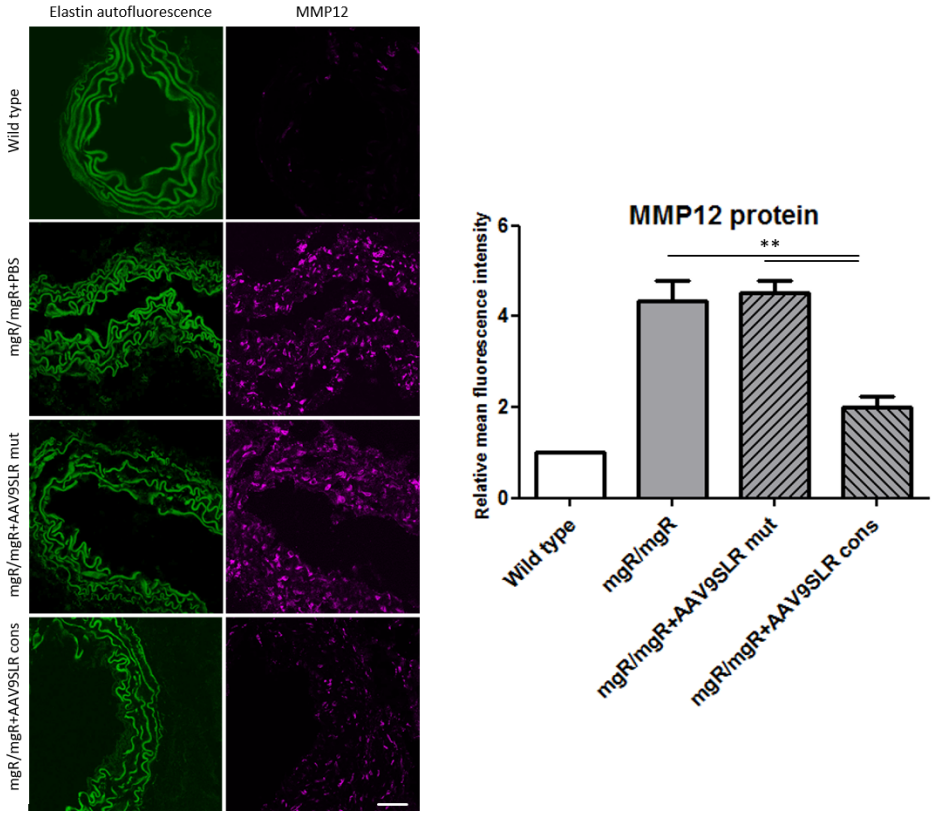

Fig. 30: AAV9SLR-mediated delivery of hpAP-1 consensus RNA decoy ODNs significantly decreases MMP12 protein level in *ex vivo* transduced grafts. Representative MMP12 (magenta) immunohistochemistry images and statistical quantification of the mean fluorescence intensity, normalized to the WT control mice. Elastin autofluorescence was recorded on the green channel. Scale bar represents 50 μm. (n=6, 20 images analysed/group, ** $p < 0.01$).

were incubated at 37 °C in Ca^{2+}-containing buffer, to allow substrate degradation and red fluorescence intensity was measured. A red signal was observed in target SMCs, but non-specific binding of the substrate to elastin fibers was noted, which could not be successfully eliminated by washing steps. Therefore, the fluorescent intensity which does not overlay with the green autofluorescence of elastin fibers was analysed.
Consistent with the MMP immunohistochemistry analysis, this experiment showed that mgR/mgR aortic frozen sections, as well as AAV9SLR control treated grafts present elevated MMP activity in comparison to the wild type cryosections. However, AAV9SLR-mediated neutralization of AP-1 led to a pregnant decreased MMP activity in SMCs, as shown in Fig. 31.

Reactive oxygen species generation in transduced aortic grafts

Having previously demonstrated that transduction with AAV9SLR expressing hpAP-1 consensus RNA decoy ODNs has a beneficial effect on IL-1β-induced oxidative stress *in*

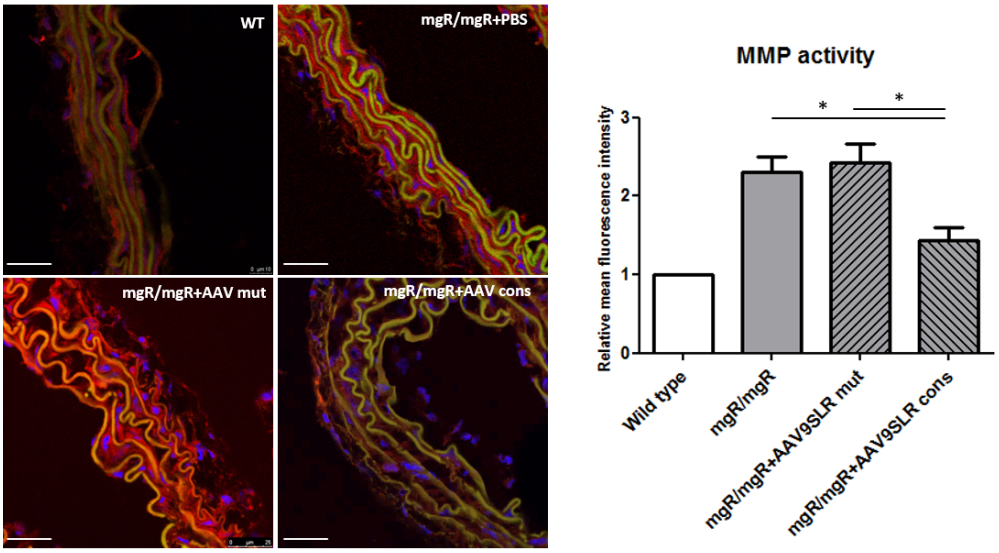

Fig. 31: AAV9SLR-mediated expression of hpAP-1 consensus RNA decoy ODNs significantly decrease MMP activity in *ex vivo* transduced mgR/mgR aortic grafts. Representative images depicting the fluorescence of cleaved MMP substrate in aortic cryosections (red). Elastin fibers were detected by imaging the autofluorescence on the green channel. Nuclei were detected by DAPI staining (blue). The graph shows statistical quantification of relative mean red fluorescence intensity of the different treatment groups. MMP activity was normalized to the values of WT control cryosections. Scale bar represents 25 μm. (n=6, 20 images analysed/group, * $p< 0.05$).

vitro in SMCs, we next investigated if a similar result can be obtained in *ex vivo* treated grafts. *In situ* ROS detection in cryosections using DHE showed a significant decrease in the amount of superoxide ions following AP-1 neutralization. The cryosections of wild type aortic tissue showed no DHE fluorescence, as depicted in Fig. 32.

ZO-1 protein level in transduced aortic grafts

Low protein levels of tight junctions such as ZO-1 (zonula occludens-1) in endothelial cells was shown to be related to aneurysm formation. Moreover, a decrease in the number of tight junctions is correlated with infiltration of inflammatory cells, especially monocytes [199]. In accordance with these results, a much higher transduction efficiency of SMCs in aortic grafts of mgR/mgR mice was observed, in comparison to WT mice, proven by EGFP immunohistochemistry (Fig. 33). Endothelial cells, visualized by CD31 staining, were transduced efficiently in both mgR/mgR and WT mice. These results show an increased permeability of the endothelial cell layer in mgR/mgR mice, allowing the viral vector to reach the media.

We then wanted to investigate whether the endothelial barrier permeability is caused by disruption of ZO-1 protein in mgR/mgR aorta. As hypothesised, ZO-1 immunohistochemistry proved a significant 60% decrease in ZO-1 protein level in endothelial cells

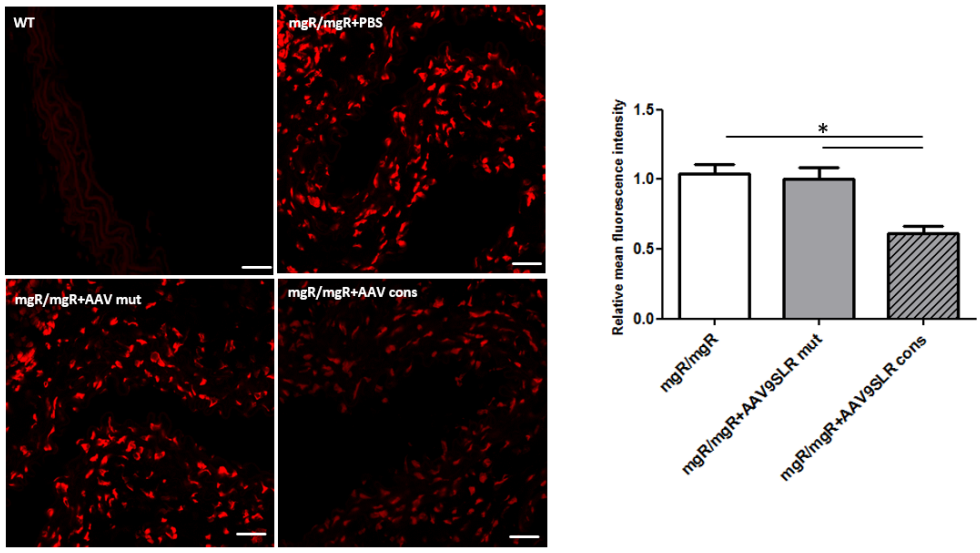

Fig. 32: AAV9SLR-mediated expression of hpAP-1 consensus RNA decoy ODNs significantly diminishes the amount of ROS generated in *ex vivo* transduced mgR/mgR aortic grafts. DHE nuclear fluorescence (red) was quantified in the indicated treatment groups and normalized to non-treated mgR/mgR DHE mean fluorescence intensity. Scale bar represents 25 μm. (n=6 for mgR/mgR mice, 20 images analysed/group, * $p < 0.05$).

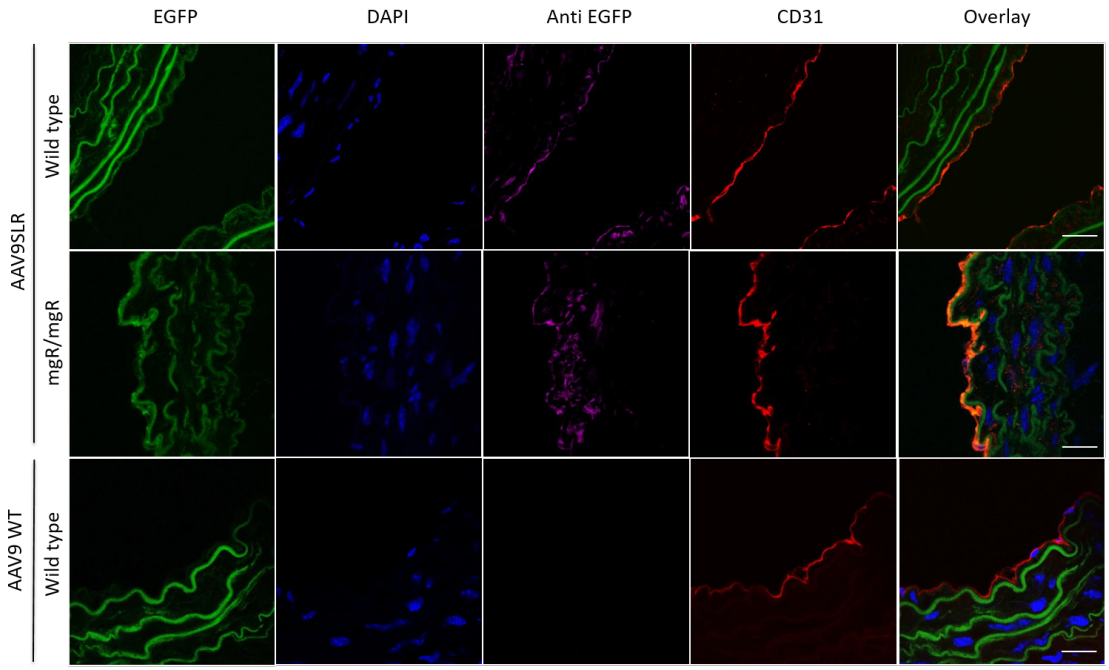

Fig. 33: *Ex vivo* transduction of aortic grafts with AAV9SLR-EGFP in wild type and mgR/mgR mice. Endothelial cells were labelled using CD31 antibody (red). EGFP immunohistochemistry (magenta) was used to show successful transduction. DAPI marks nuclei (blue) and elastin autofluorescence (green) was visualized in the green channel. The scale bar represents 25 μm. (n=3, exemplary images.)

of mgR/mgR mice, as compared to wild type controls. A co-staining with CD31 antibody was used to label endothelial cells specifically, as pictured in Fig. 34. Since ZO-1

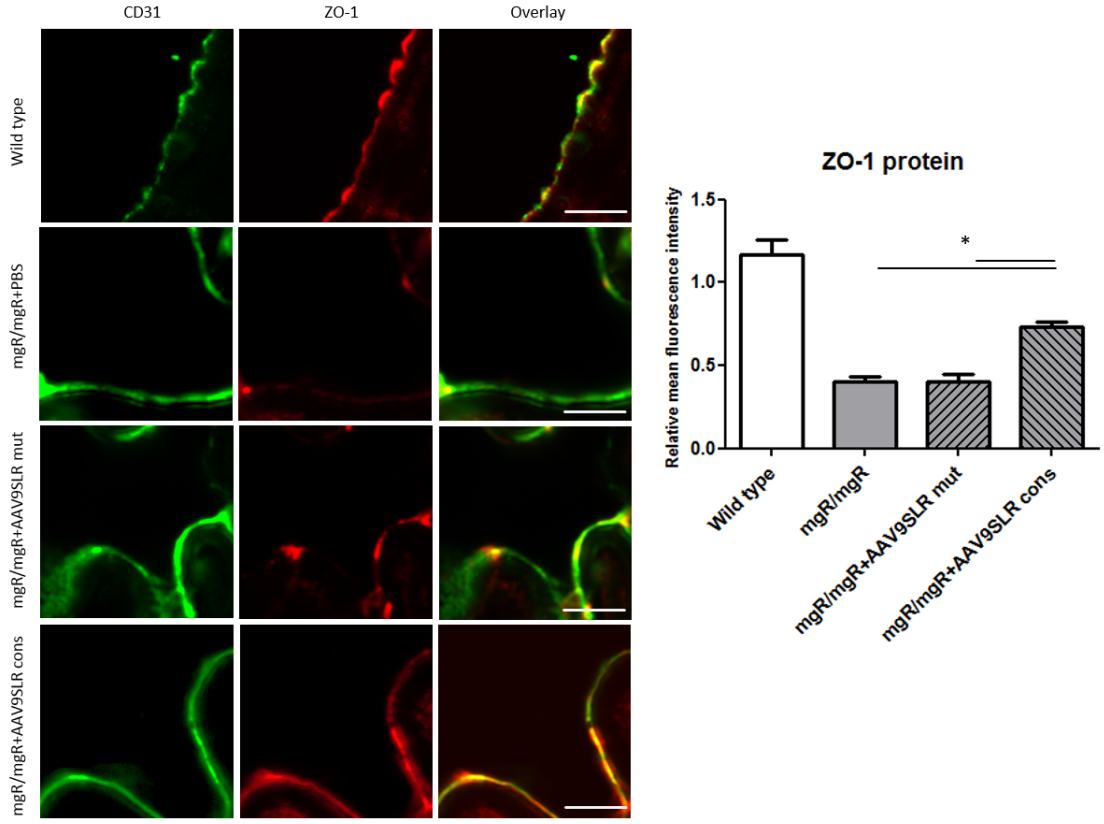

Fig. 34: AAV9SLR-mediated expression of hpAP-1 RNA decoy ODNs significantly increase ZO-1 protein level in *ex vivo* transduced mgR/mgR aortic grafts. Representative images showing ZO-1 immunohistochemistry in WT as well as mgR/mgR mice. CD31 (green) and ZO-1 (red) overlay was performed to assess ZO-1 protein expression in endothelial cells. The graph represents the statistical quantification of fluorescence images. The scale bar represents 75 μm. (n=3 for WT mice, n=6 for mgR/mgR mice, 20 images were analysed/group, * $p < 0.05$).

protein level is downregulated by oxidative stress [165] and is a substrate for MMPs [199], the next question was whether ZO-1 protein level can be restored in endothelial cells following AAV9SLR-mediated AP-1 neutralization. The results show that indeed, generation of hpAP-1 RNA decoy ODNs by AAV9SLR transduction in aortic grafts led to a marked increase in ZO-1 protein level as compared to controls (Fig. 34).

Monocyte infiltration into the thoracic aorta

The pro-inflammatory component of Marfan syndrome has already been well established [164]. The thoracic aorta of Marfan patients, as well as mgR/mgR mice present

a strong infiltration of monocytes and T cells, which secrete MMPs and in turn contribute to formation of elastin breaks. After having found that treatment with the designed AAV9SLR expressing hpAP-1 consensus RNA decoy ODNs can significantly downregulate MCP-1 which acts as a chemoattractant for inflammatory cells, it was hypothesized that in transduced grafts the level of macrophages is also reduced.
For this purpose, F4/80 immunohistochemsitry was performed and macrophage density in aortic grafts was analysed. As previously reported, [164] most of the macrophages were detected in the adventitia of mgR/mgR mice, whereas the sections of WT mice presented no inflammatory cells (Fig. 35). The density of F4/80 positive cells was not affected by treatment with control AAV9SLR, while transduction with AAV9SLR expressing hpAP-1 cons RNA decoy ODNs resulted in a significant 38% decrease in the infiltration of macrophages.

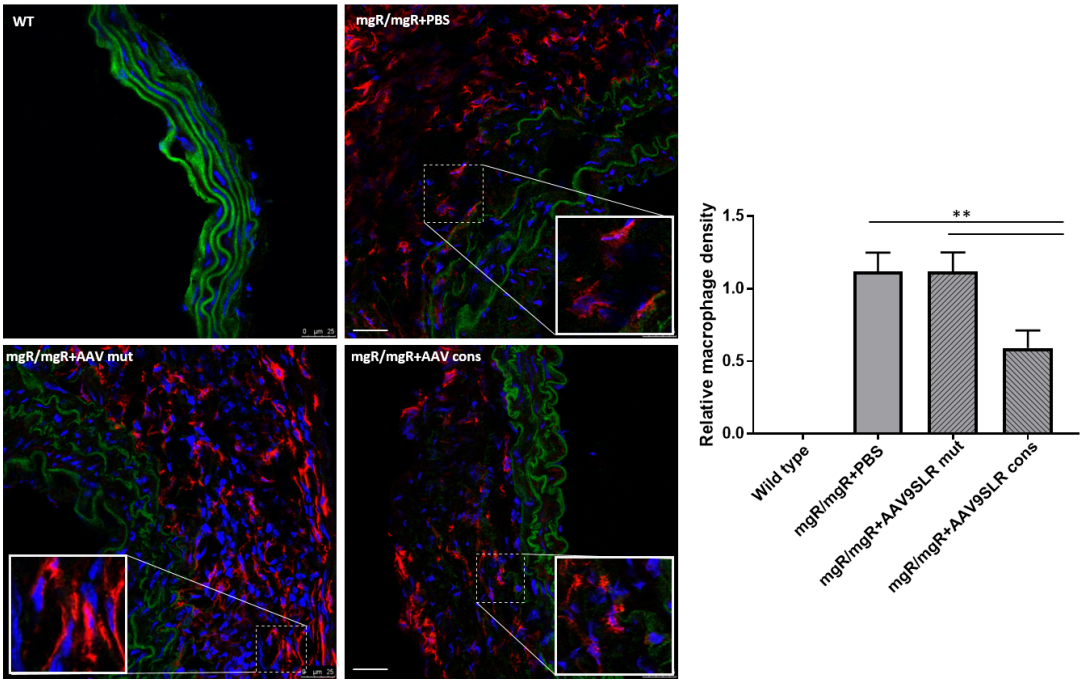

Fig. 35: AAV9SLR-mediated expression of hpAP-1 RNA decoy ODNs significantly decrease the macrophage infiltration in the adventitia of *ex vivo* transduced thoracic aortae. Representative images showing F4/80 immunohistochemistry (red), used to mark macrophages. Elastin autofluorescence was recorded in the green channel and DAPI (blue) was used to mark cell nuclei. The graph shows relative macrophage density in the adventitia, normalized to WT control counts. The scale bar represents 50 μm. (n=6, 20 images analysed/group, ** < 0.01).

Effect of AAV9SLR-mediated decoy ODNs expression on aortic elastolysis

To explore the effect of AAV9SLR-mediated hpAP-1 RNA consensus decoy ODNs generation on elastin architecture of aortic mgR/mgR grafts, elastic van Gieson staining was carried out and the degree of fragmentation was measured. As a read-out, the number of islands of damage was counted, as previosly described [132]. An island of damage was considered as a defined area where an elastin break can be detected, surrounded by conjective tissue.
In non-treated as well as in AAV9SLR control transduced mgR/mgR cryosections, a high number of islands of damage was observed. On the other hand, grafts treated with AAV9SLR expressing hpAP-1 consensus RNA decoy ODNs showed a significant decrease in the occurrence of islands of damage. These findings show that AAV9SLR-mediated AP-1 neutralization can inhibit elastin loss in mgR/mgR mice and therefore stabilize the aortic aneurysms dissection, which is a characteristic feature of Marfan syndrome.

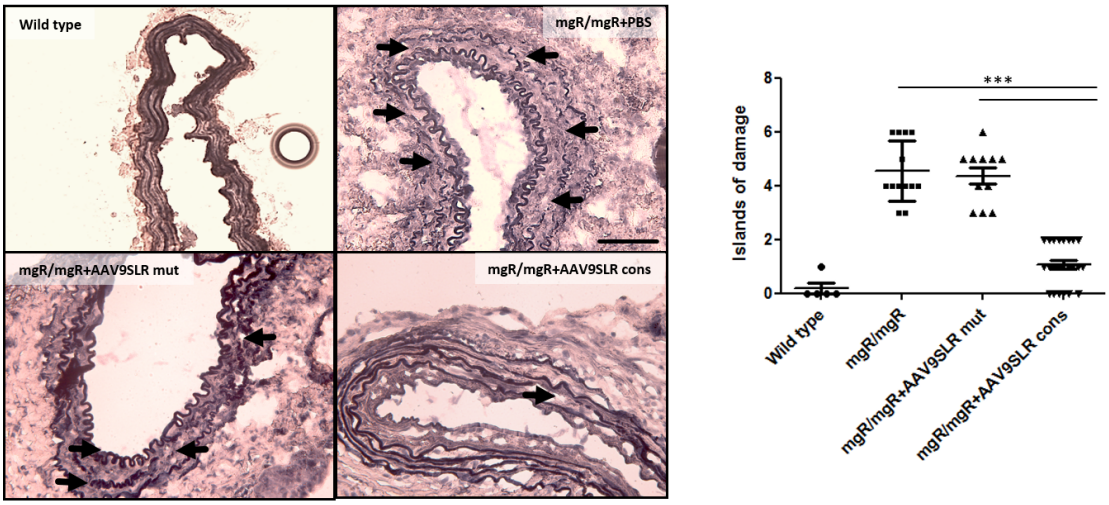

Fig. 36: AAV9SLR-mediated expression of hpAP-1 consensus RNA decoy ODNs significantly improve elastic fiber structure in *ex vivo* transduced mgR/mgR thoracic aortae. Representative images of elastin van Gieson histologic stainings and statistical quantification of the frequency of islands of damage per field of view, shown by black arrows. Scale bar represents 50 μm. (n=6 for mgR/mgR mice, 30 images analysed/group, *** $p< 0.001$).

Activation of KLF4 in aortae of mgR/mgR mice

Other transcription factors besides AP-1 could play major roles in aortic aneurysm formation and dissection in Marfan syndrome. One candidate which was described in literature is KLF4 [196]. In order to determine the activation pattern of KLF4 (Kruppel-like

factor 4) in aortic frozen sections isolated from mgR/mgR mice, imuunohistochemistry using a specific antibody was performed. Following DAPI staining, the percentage of positive cells was calculated. The quantification shows a clear increase in KLF positive nuclei in mgR/mgR mice as compared to wild type aortae, as demonstrated in Fig. 37.

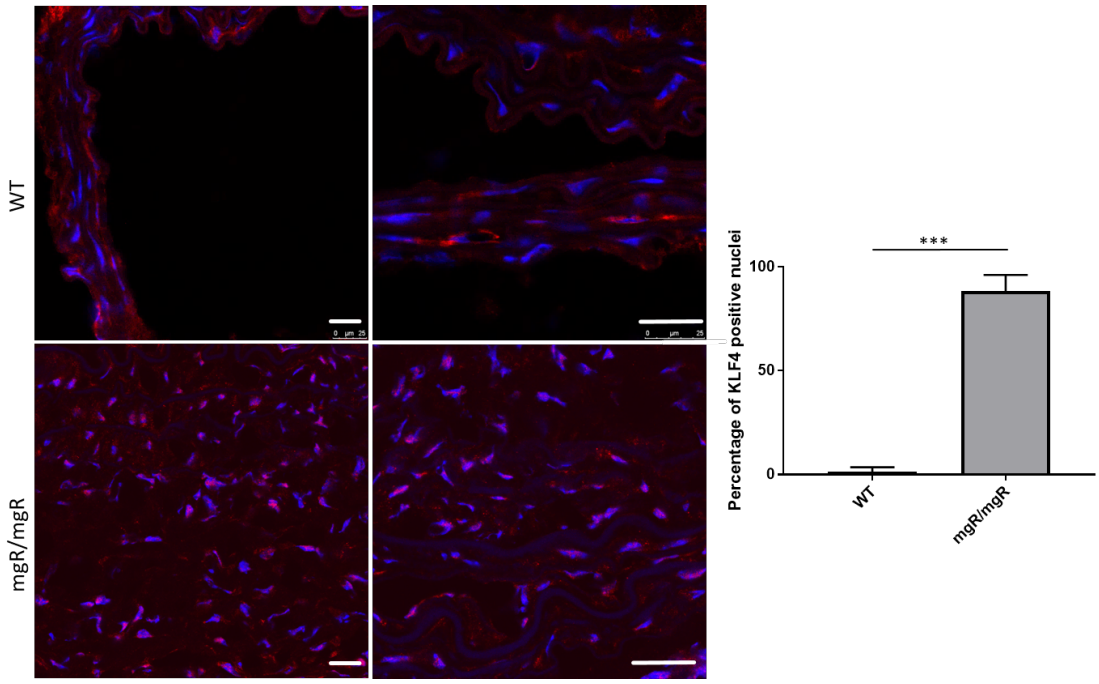

Fig. 37: KLF4 nuclear translocation is increased in mgR/mgR aorta. Representative images showing KLF4 immunohistochemistry (red) and DAPI (blue). The statistical quantification of the percentage of KLF4 positive nuclei in the two groups is shown. Scale bar represents 25 μm. (n=3, 12 images analysed/group, *** $p < 0.001$).

5.3 Heart hypertrophy project

5.3.1 ”Naked” hpNFAT decoy ODNs uptake by cardiomyocytes

First, cardiomyocyte ability to take up hpNFAT decoy ODNs was analysed. For this purpose, HL-1 cells, neonatal as well as adult cardiomyocytes were treated with Atto-590 labelled hp decoy ODNs at a final concentration of 10 μmol/L in complete Claycomb medium. After 2 h, cells were fixed with PFA and the membranes were marked using WGA. Confocal images show that hpNFAT decoy ODNs can be efficiently taken up without any auxiliary means by cardiomyocytes. Red fluorescence was detected in the nuclei, as well as in the cytoplasm, as depicted in Fig. 38.
Next, the effect of Lipofectamine-mediated decoy ODN delivery in HL-1 cells was ad-

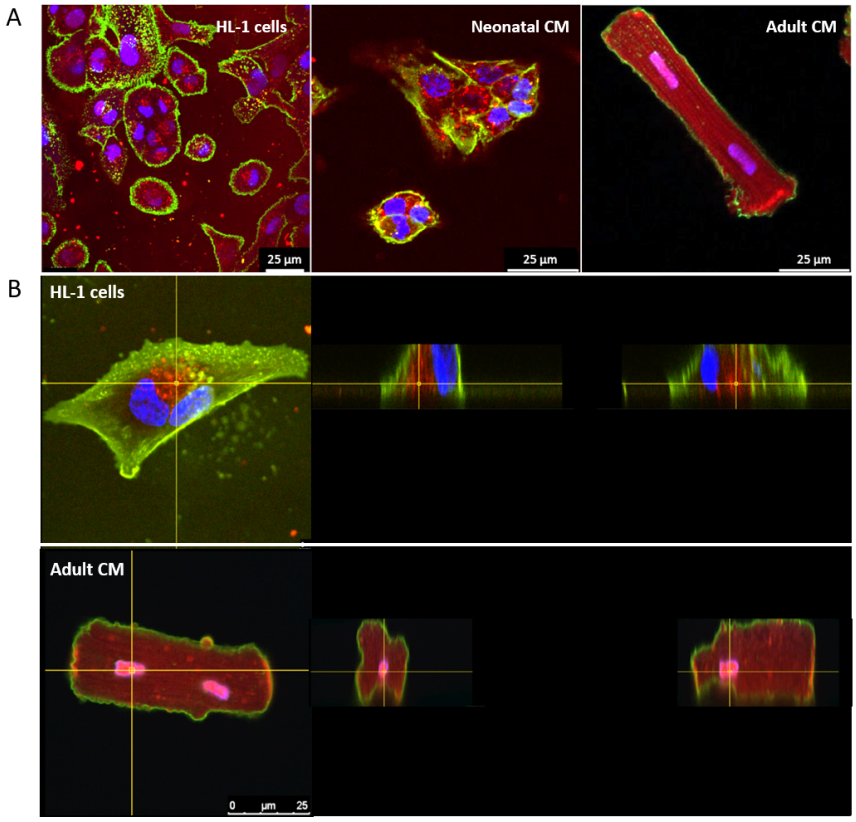

Fig. 38: Hairpin NFAT decoy ODNs are taken up by cardiomyocytes without auxilliary means. (A) Representative images of cardiomyocytes treated with Atto590-hpNFAT decoy ODNs (red) for 2 h and stained with WGA (green). DAPI (blue) was used to mark cell nuclei. (B) Three dimensional reconstruction of Z-stack confocal images showing nuclear and cytoplasmic localization of the decoy ODNs. The scale bar represents 25 μm. (n=4, exemplary images).

dressed. Atto-590 labelled hpNFAT decoy ODNs were incubated with the transfection reagent prior to addition to cell culture medium and the localization of red fluorescent signal was assessed. As shown in Fig. 39, the efficiency of uptake through direct application of the ”naked” decoy ODNs was significantly higher than the efficacy obtained using the liposomal reagent. Consequently, for the next experiments no transfection reagents were used for hpNFAT decoy ODNs delivery in cardiomyocytes.

5.3.2 ”Naked” hpNFAT decoy ODNs effect on cardiomyocyte hypertrophy

Fetal gene program

Having proven that decoy ODNs can be taken up by HL-1 cells and primary cardiomyocytes, the next aim was to analyse the effect of NFAT1-4 neutralization on ET-1 induced hypertrophy. Cells were treated with the active hpNFAT consensus decoy ODNs, as well as control hpNFAT mutated decoy ODNs for 2 h after serum deprivation and

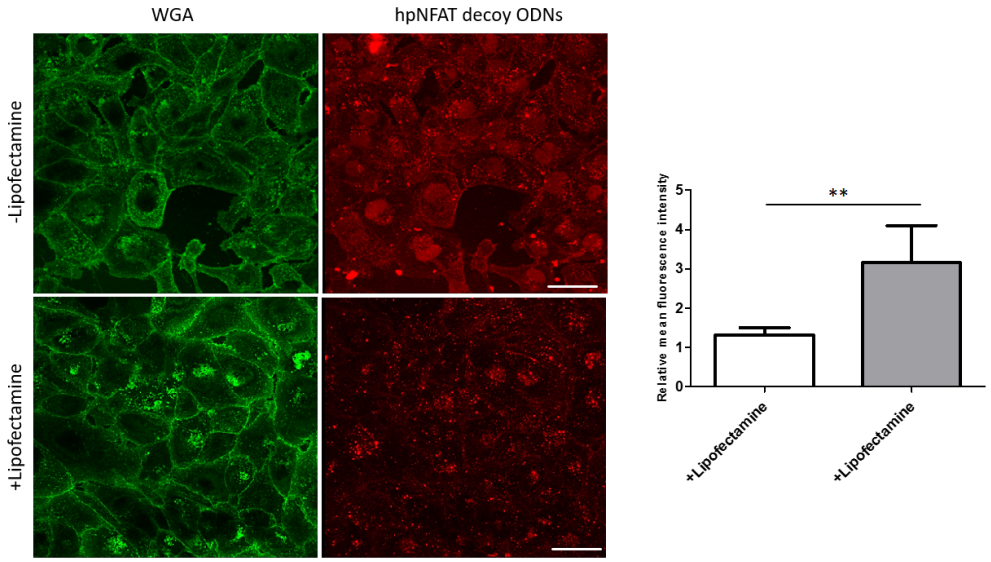

Fig. 39: Lipofectamine-based transfection does not improve hpNFAT decoy ODNs uptake by HL-1 cells. Representative images of Atto-590 labelled hpNFAT decoy ODNs (red) transfection with and without Lipofectamine. Membranes were stained with WGA, visualized on the green channel. The graph summarises statistical quantification of mean red fluorescence intensity of images in the two treatment groups. The scale bar represents 25 μm. (n=4, 20 images analysed/group, ** $p< 0.01$).

stimulated with 100 nmol/L ET-1 for 24 h. As a read-out, expression of fetal genes ANP and BNP was analysed. In addition, BNP protein levels in the supernatant and in HL-1 cell lysates were measured.

As expected, exposure to ET-1 for 24 h led to an increase in fetal gene expression (Fig. 40A). NFAT1-4 neutralization by hpNFAT consensus decoy ODNs application prior to stimulation decreased the expression of the two analysed pro-hypertrophic genes. On the other hand, application of the inactive hp NFAT mutated decoy ODNs had no effect on the investigated genes, as shown in Fig. 40A.

Similar to the mRNA results, a significant increase in BNP protein level was detected by ELISA follwing 24 h ET-1 stimulation, as compared to control, while hpNFAT cons decoy ODNs supplementation prior to ET-1 stimulation normalized BNP concentration to the basal level, both in cell lysates and in supernatant. No significant effect on BNP protein was observed in hpNFAT mutated decoy ODNs treated HL-1 cells, as depicted in Fig. 40B.

Given the clear effect of the hpNFAT consensus decoy ODNs on ET-1 induced pro-hypertrophic markers in HL-1 cell line, its efficiency in primary cardiomyocytes was further investigated. For this purpose, isolated murine primary neonatal cardiomyocytes were used. Comparable to the previous results, ET-1 induced a significant re-activation

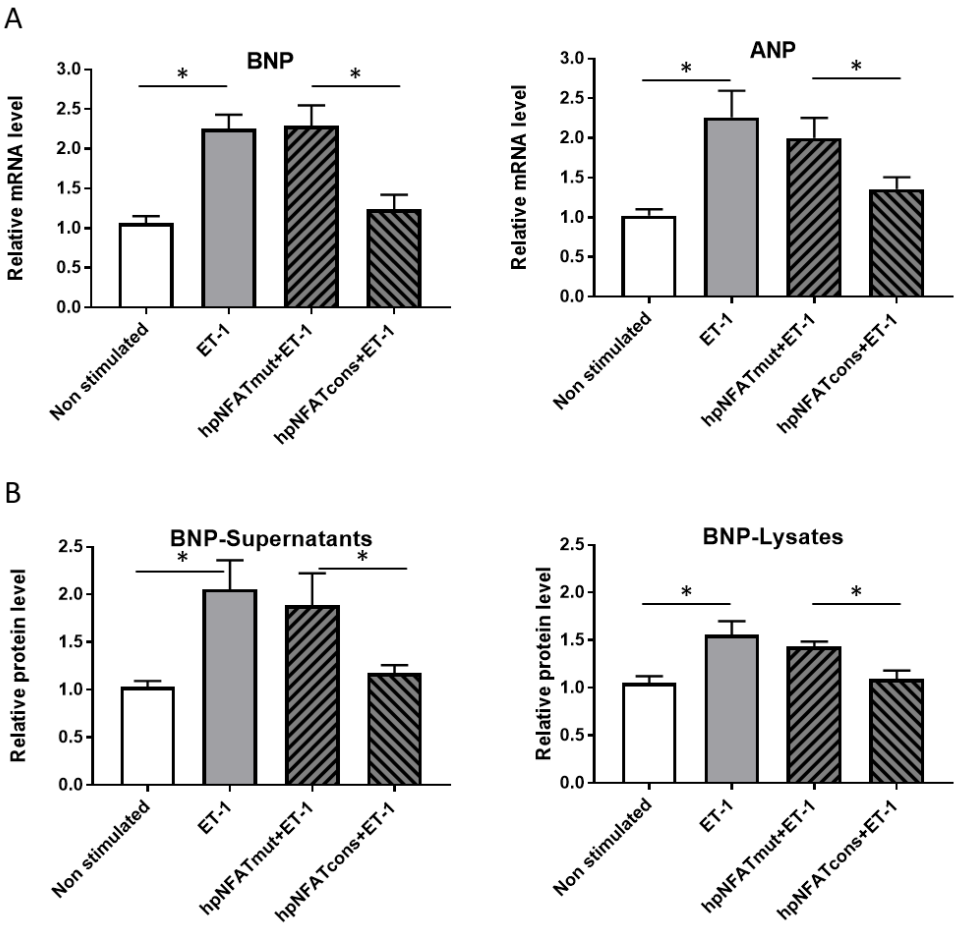

Fig. 40: Hairpin NFAT consensus decoy ODNs decrease ET-1 induced fetal gene program in HL-1 cells. (A) mRNA levels of ANP and BNP were analysed in HL-1 cardiomyocytes as markers of ET-1 (100 nmol/L) induced hypertrophic response. Gene expression was normalizeed to RPL32 as a housekeeping gene. (B) BNP protein levels were measured in HL-1 cells supernatants and lysates using ELISA and reported to the concentration measured in non-stimulated control cells. (n=4, * $p < 0.05$).

of the fetal gene program, which was abolished with hpNFAT cons decoy ODNs supplementation in the medium 2 h before ET-1 stimulation, as depicted in Fig. 41.

Protein translation level

Hypertrophic growth of cardiomyocytes is accompanied by an increased rate of total protein translation rate [83]. Therefore, the effect of hpNFAT decoy ODNs on this parameter was investigated by employing the non-radioactive SUnSET assay. First, HL-1 cells were treated with increasing concentrations of puromycin, ranging from 0.1 to 100 μmol/L in order to determine the optimal concentration of the compound to be further used. Using high amounts of puromycin (> 50 μmol/L), a significant decrease in viable

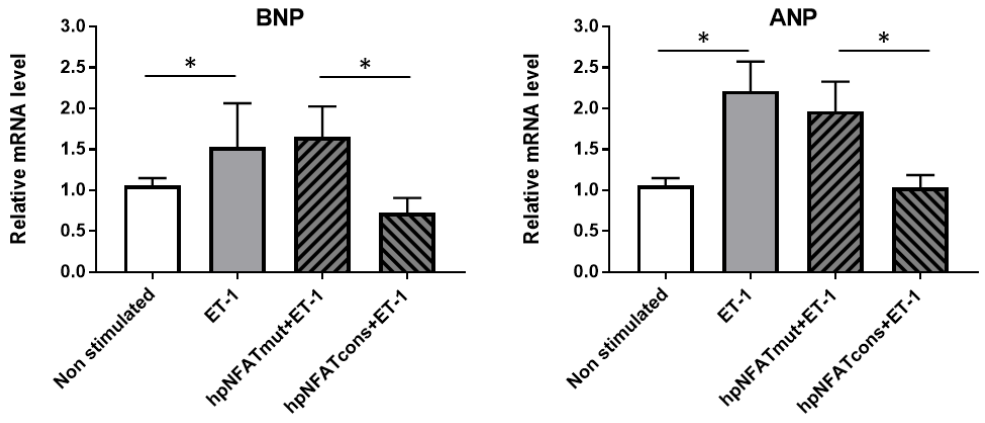

Fig. 41: Hairpin NFAT consensus decoy ODNs decrease fetal gene program in neonatal cardiomyocytes. Statistical quantification of ANP and BNP mRNA levels in neonatal cardiomyocytes in the indicated treatment groups. RPL32 was used for gene expression normalization and non-stimulated HL-1 cells served as a control. (n=4, * $p < 0.05$.)

cells was observed, as proven by Alamar Blue assay (data not shown). On the other hand, when less than 1 μmol/L puromycin was added to the medium, low fluorescent signal was detected following anti-puromycin immunocytochemistry. Consequently, 10 μmol/L puromycin was chosen for subsequent experiments.
HL-1 cells were treated with hpNFAT decoy ODNs for 2 h in serum-free medium and stimulated with ET-1 for 24 h. Afterwards, cardiomyocytes were subjected to puromycin treatment and the amount of nascent proteins was detected by immunofluorescence methods using a specific anti-puromycin antibody.
Exposure of HL-1 cardiomyocytes to the pro-hypertrophic stimulus ET-1 in serum-free medium led to a significant increase in protein translation level, as shown in Fig. 42. Pre-incubation with hpNFAT conensus decoy ODNs triggered a significant decrease of ET-1 induced protein translation rate, while the hpNFAT mutated decoy ODNs had no effect. Taken together, these results demonstrate that hpNFAT consensus decoy ODNs reduce ET-1 induced HL-1 cells hypertrophy by decreasing the fetal gene program, and additionally affecting cellular metabolism characteristic for hypertrophic growth.

5.3.3 AAV6 effect on cardiomyocyte hypertrophy

Fetal gene program

After having demonstrated that hpNFAT consensus decoy ODNs can attenuate the hypertrophic changes induced by ET-1, the next aim was to investigate whether the same effect can be achieved by expression of hpNFAT RNA decoy ODNs through AAV6

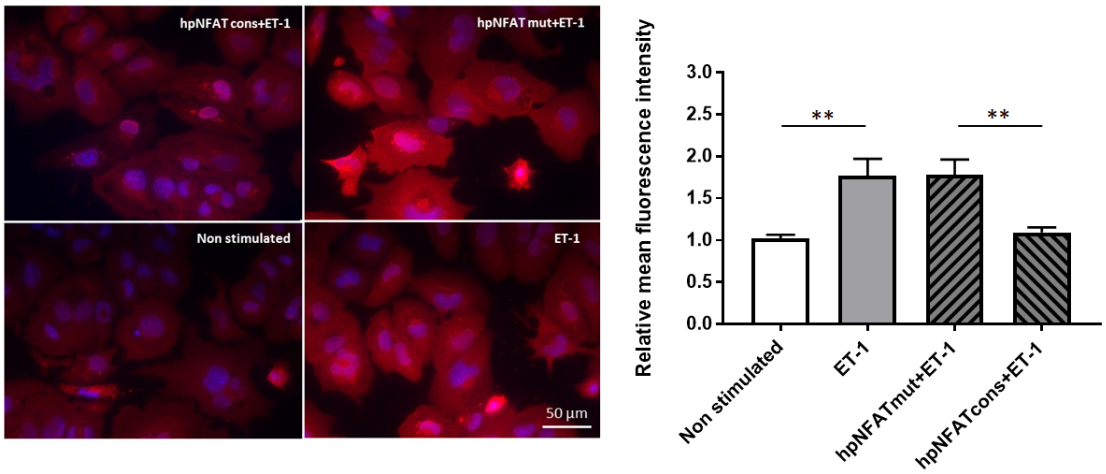

Fig. 42: Hairpin NFAT consensus decoy ODNs decrease the level of total protein translation in HL-1 cells. Representative images showing anti puromycin immunocytochemistry in different treatment groups. A Cy5 labelled secondary antibody (red) was used and nuclei were marked by DAPI staining (blue). The graph summarizes the statistical quantification of mean red fluorescence intensity in the indicated treatment groups. (n=4, 20 images analysed/tretament group, ** $p < 0.01$)

transduction. Therefore, AAV6 generating hpNFAT consensus as well as mutated RNA decoy ODNs were produced. Using AAV6 at MOI=10^5 vp/cell, the transduction efficiency measured as EGFP positive cells by fluorescence microscopy was determined to be 80% in HL-1 cells. In addition, cell viability after transduction was not influenced by AAV6 treatment, as indicated by Alamar Blue assay (data not shown). Three days after vector treatment, HL-1 cells were stimulated with ET-1 100 nmol/L for 24 h after serum-deprivation.

The results of gene expression analysis show that AAV6 expressing hpNFAT consensus RNA decoy ODNs markedly reduced the expression of fetal gene program represented by ANP and BNP almost to basal level, as shown in Fig. 43. In a similar manner, BNP protein level in HL-1 cells supernatant was significantly downregulated after transduction with hpNFAT consensus RNA decoy ODNs producing AAV6. The control AAV6 expressing a mutated form of the RNA decoy ODNs had no effect, neither on the analysed genes nor on BNP protein level (Fig. 43).

Protein translation level

The effect of AAV6-mediated hpNFAT RNA decoy ODNs delivery on ET-1 induced protein translation level was further analysed by SUnSET assay as measured before in Chapter 5.3.2. For this purpose, AAV6 transduced cells were treated with puromycin after 24 h ET-1 stimulation. The analyses of confocal fluorescence images following

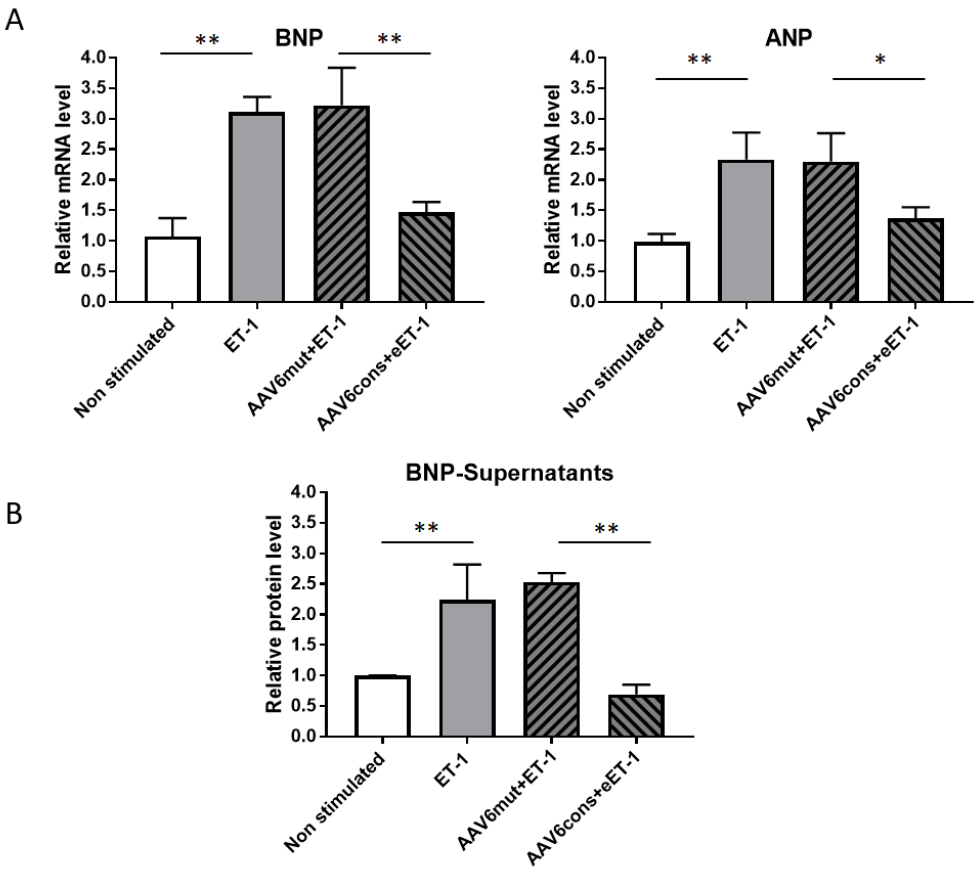

Fig. 43: AAV6-mediated delivery of hpNFAT consensus RNA decoy ODNs decreases ET-1 induced fetal gene program in HL-1 cells. A. Fetal genes ANP and BNP was analysed on mRNA level in AAV6 transduced HL-1 cardiomyocytes. The analysis was made using RPL32 as a housekeeping gene for mRNA expression analysis. (n=5, * $p< 0.05$, ** $p< 0.01$). B. BNP protein level in cardiomyocyte supernatants was measured using ELISA and values were normalized to the BNP concentration of non-stimulated control cells. (n=4, * $p<0.05$, ** $p<0.01$).

immunostaining with anti-puromycin antibody confirmed, similarly to previous experiments, that ET-1 application caused a pronounced increase in total protein translation rate as compared to non-stimulated control. On the other hand, NFAT1-4 neutralization caused a significant reduction in the rate of protein translation. Treatment with the control mutated AAV6 did not affect this parameter, as shown in Fig. 44.

5.3.4 NFAT5 activation in the presence of hp decoy ODNs

The designed hpNFAT decoy ODNs has high specificity to NFAT1, NFAT2, NFAT3 and NFAT4, but does not neutralize NFAT5 due to its different binding matrix. NFAT5 is a critical transcription factor for heart development and response to hyperosmotic stress. Consequently, knockout of this transcription factor causes embryonic lethality and abnormal cardiomyocyte function [127]. Moreover, hearts isolated from NFAT5 knock-out

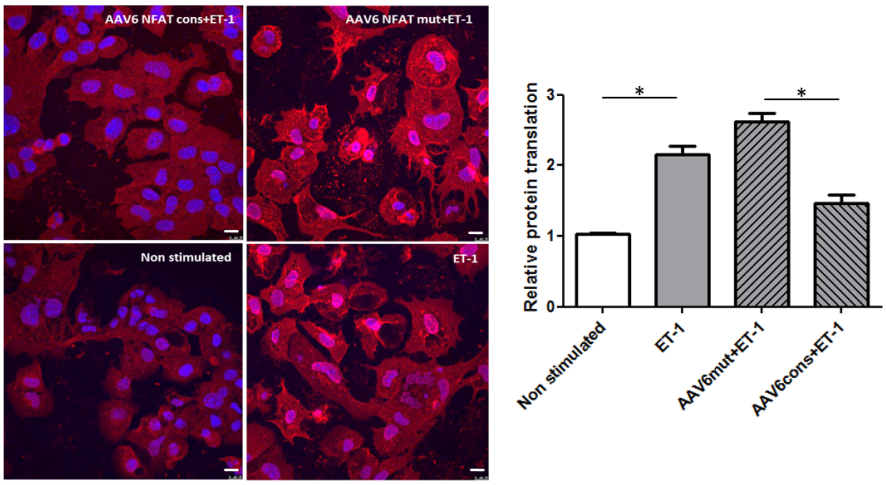

Fig. 44: AAV6-mediated expression of hpNFAT consensus RNA decoy ODNs decrease ET-1 induced protein translation rate. Representative confocal images showing anti-puromycin staining (red) in HL-1 cells. A Cy5 labelled secondary antibody (red) was used in the present experiment. Nuclei were labelled with DAPI (blue). The graph represents the statistical summary of mean red fluorescence intensity of indicated treatment groups. Non-stimulated cells served as controls. Scale bar represents 10 μm. (n=4, 20 images were quantified/group, ** $p<0.001$).

embryos present with decreased cardiomyocyte density and extreme thinning of the ventricular wall [127].

Taking into account the major role of this transcription factor in cardiomyocyte physiology, the expression and activation of NFAT5 in the presence of NFAT1-4 neutralizing "naked" hp decoy ODNs as well as RNA decoy ODNs delivered through AAV6 transduction was further addressed. For this purpose, HL-1 cells were treated with the hpNFAT decoy ODNs or transduced with AAV6 expressing hpNFAT RNA decoy ODNs and afterwards subjected to hyperosmotic stress induced by LiCl 100 mmol/L treatment.

As expected, the analysis of immunofluorescence images showed a dramatic close to 5-fold increase in nuclear NFAT5 translocation in response to LiCl treatment (Fig. 45A). Moreover, the results demonstrate that neither hpNFAT decoy ODNs treatment, nor transduction with the designed AAV6 had an effect on NFAT5 activation, as depicted in the quantification of NFAT5 positive nuclei in Fig. 45A.

To further support these data, the mRNA levels of NFAT5 target genes SMIT and HSP70 were analysed. qPCR analysis revealed a significant increase the mRNA levels of both investigated genes following LiCl exposure, which was not affected by NFAT decoy ODNs pre-treatment or AAV6 transduction, as shown in Fig. 45B.

These data demonstrate that NFAT5 nuclear translocation and function is not impaired by the hpNFAT decoy ODNs or hpNFAT RNA decoy ODNs.

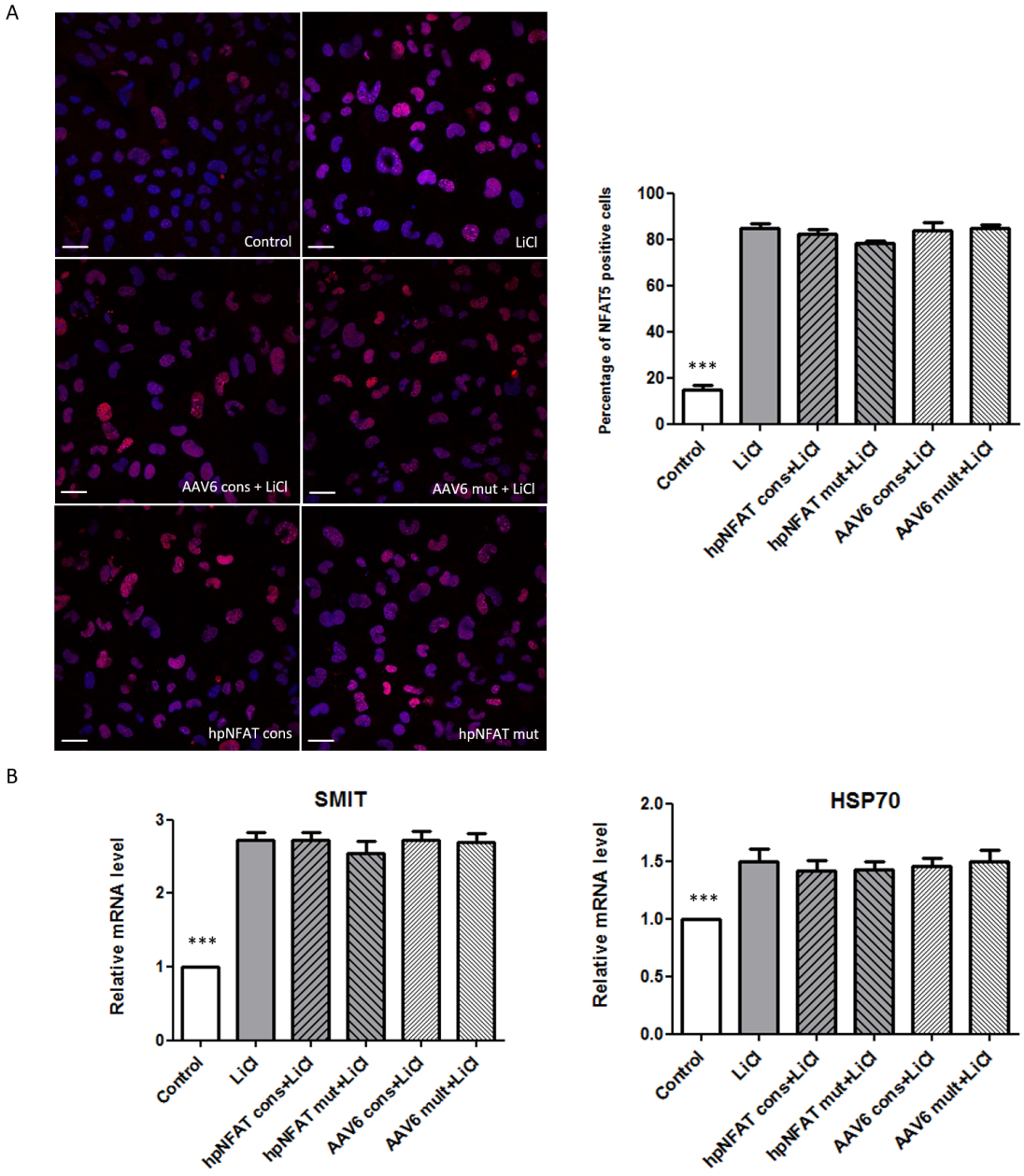

Fig. 45: Hairpin NFAT consensus decoy ODNs do not affect NFAT5 translocation and function under hyposmotic stress induced by LiCl treatment. (A) Analysis of NFAT5 distribution in HL-1 cells subjected to hypertonic stress (100 mmol/L LiCl). The graph shows statistical quantification of NFAT5 (red) positive nuclei, marked using DAPI (blue) staining. Scale bar represents 25 μm. (n=4, 20 images analysed/group, *** $p<0.001$).(B) Gene expression analysis of NFAT5 target genes SMIT (sodium/myo-inositol cotransporter) and HSP70 (heat shock protein 70). RPL32 was used as a housekeeping gene and the measurements were normalized to the control non-treated cells. (n=4, ** $p<0.01$).

5.3.5 *In vivo* hpNFAT RNA decoy ODNs effect

The *in vitro* experiments indicate reduced ET-1 induced hypertrophic response of cardiomyocytes treated with both hpNFAT consensus decoy ODNs and AAV6 expressing hpNFAT consensus RNA decoy ODNs. In order to prove the *in vivo* efficiency of the designed AAV, heart hypertrophy was induced by transverse aortic constriction (TAC) The surgery was performed by Theresa Ruf and Lin Ding, Internal Medicine III, Clinic for Cardiology, Angiology and Pneumology, University Clinic Heidelberg. AAV9 was previously shown to be the most effective virus serotype to transduce cardiomyocytes *in vivo* following systemic tail-vein injection [95]. Hence, the delivery of hpNFAT RNA decoy ODNs was made by using this virus serotype (10^{12} genomic particles/mouse) 2 weeks before surgery, in order to allow the generation of RNA decoy ODNs into the tissue. The survival rate after TAC was 95% (19 surviving mice out of 20). One mouse in the control AAV9 injected group lost a significant amount of weight, developed drastic dilated heart failure with extremely low ejection fraction (20%) and died 5 weeks after surgery.

EGFP and RNA decoy ODNs expression after transduction

Successful cardiomyocyte transduction by AAV9 was demonstrated employing EGFP immunohistochemistry 2 weeks after injection. As shown in Fig. 46A, EGFP protein was detected in the myocardium of both AAV9-injected groups, while control PBS treated mice did not present any EGFP signal in cardiomyocytes. These data suggest that cardiomyocyte transduction can be achieved by systemic tail-vein injection of AAV9.
The next aim was the detection of hpNFAT RNA decoy ODNs in the cardiomycytes of AAV9 injected animals. Hence, 5 μm heart frozen sections were subjected to RNA F.I.S.H. The detection of shRNAs was carried out using a molecular beacon with complementary sequence of the decoy ODNs and which emits red fluorescence when bound to the target. As a control, heart cryosections of PBS-injected mice were used. As presented in Fig. 46B, hpNFAT RNA decoy ODNs were expressed in the tissue isolated from AAV9 injected mice, while samples of PBS treated mice presented no fluorescence signal.

Effect of AAV9 injection on heart function

Having determined that AAV9 systemic application leads to cardiomyocyte transduction and subsequently to hpNFAT RNA decoy ODNs production, its effect on heart function was further investigated.

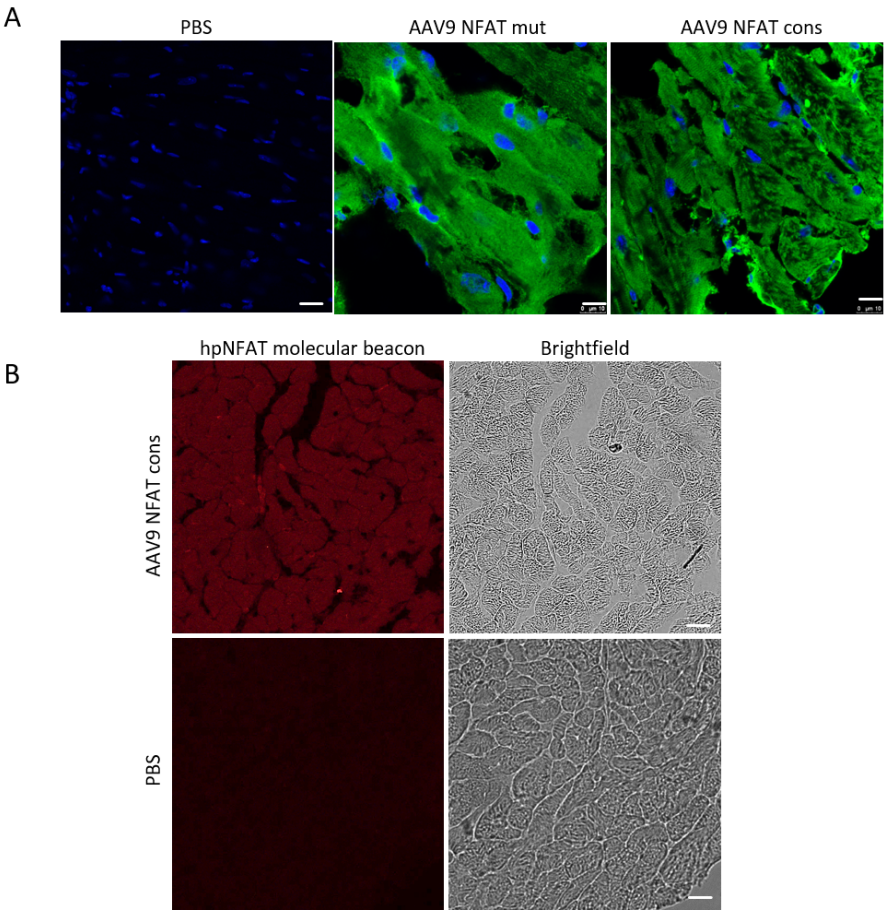

Fig. 46: Transduction efficiency of cardiomyocytes of AAV9 injected mice, 2 weeks after virus injection. (A) Representative images showing EGFP immunohistochemistry (green) performed in heart cryosections. (B) Detection of hpNFAT consensus RNA decoy ODNs in heart cryosections by F.I.S.H. Red fluorescence corresponds to hybridization of the probe to the target and proves the generation of decoy ODNs. Scale bar represents 10 μm. (n=3 for PBS injected mice, n=8 for AAV9 injected groups, exemplary pictures).

Echocardiography was performed 2 weeks after AAV9 injection, to analyse the effect of the designed AAV9 before TAC-induced heart hypertrophy. As shown in Fig. 47, AAV9 expressing neither hpNFAT consensus, not mutated RNA decoy ODNs had any effect on the ejection fraction at baseline. Consistently, no differences were observed in the calculated LV mass values.

Having established that AAV9 expressing hpNFAT decoy ODNs does not affect heart function on the basal level, TAC was performed in AAV9 injected mice and the effect of NFAT1-4 neutralization in this heart hypertrophy model was analysed. Mice were sacrificed 6 weeks after surgery.

Since a high variation of body weight was observed between groups (Fig. 49), the ratio heart weight/tibia length (HW/TL) was used as an established readout for myocardial

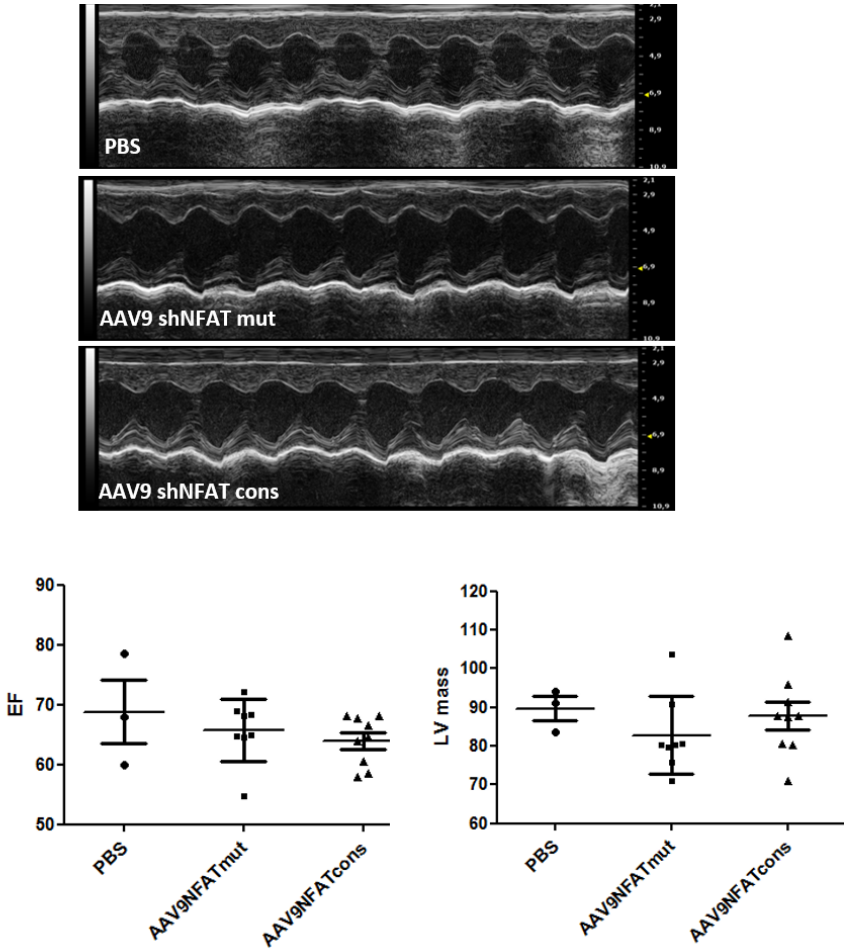

Fig. 47: Echocardiographic assessment of heart function in AAV9 injected mice prior to hypertrophy induction by TAC. Representative M-mode echocardiograms and analysis of ejection fraction as a functional cardiac parameter and LV mass on basal level. EF: ejection fraction; LV: left ventricle. (n=3 for PBS injected group, n=8 for AAV9 injected groups).

hypertrophic growth [206]. The measurements showed that AAV9 mediated hpNFAT consensus RNA decoy ODNs expression significantly reduced left ventricular hypertrophy (HW/TL) as compared to PBS treated group, while the mutated control AAV9 had no effect. Moreover, heart failure induced lung edema was analysed. In accordance to HW/TL measurements, the results prove a dramatic improvement of this parameter by a significant decrease in the group treated with AAV9 expressing hpNFAT consensus RNA decoy ODNs,as compared to controls (Fig. 48A).

Follow-up echocardiography showed as well an amelioration of heart function parameters after NFAT1-4 neutralization by RNA decoy ODNs. As expected, stenosis of the transverse aorta by surgery led to a significant increase in LV mass. Correspondingly, heart function severely deteriorated, as demonstrated by a dramatic decrease in EF, as

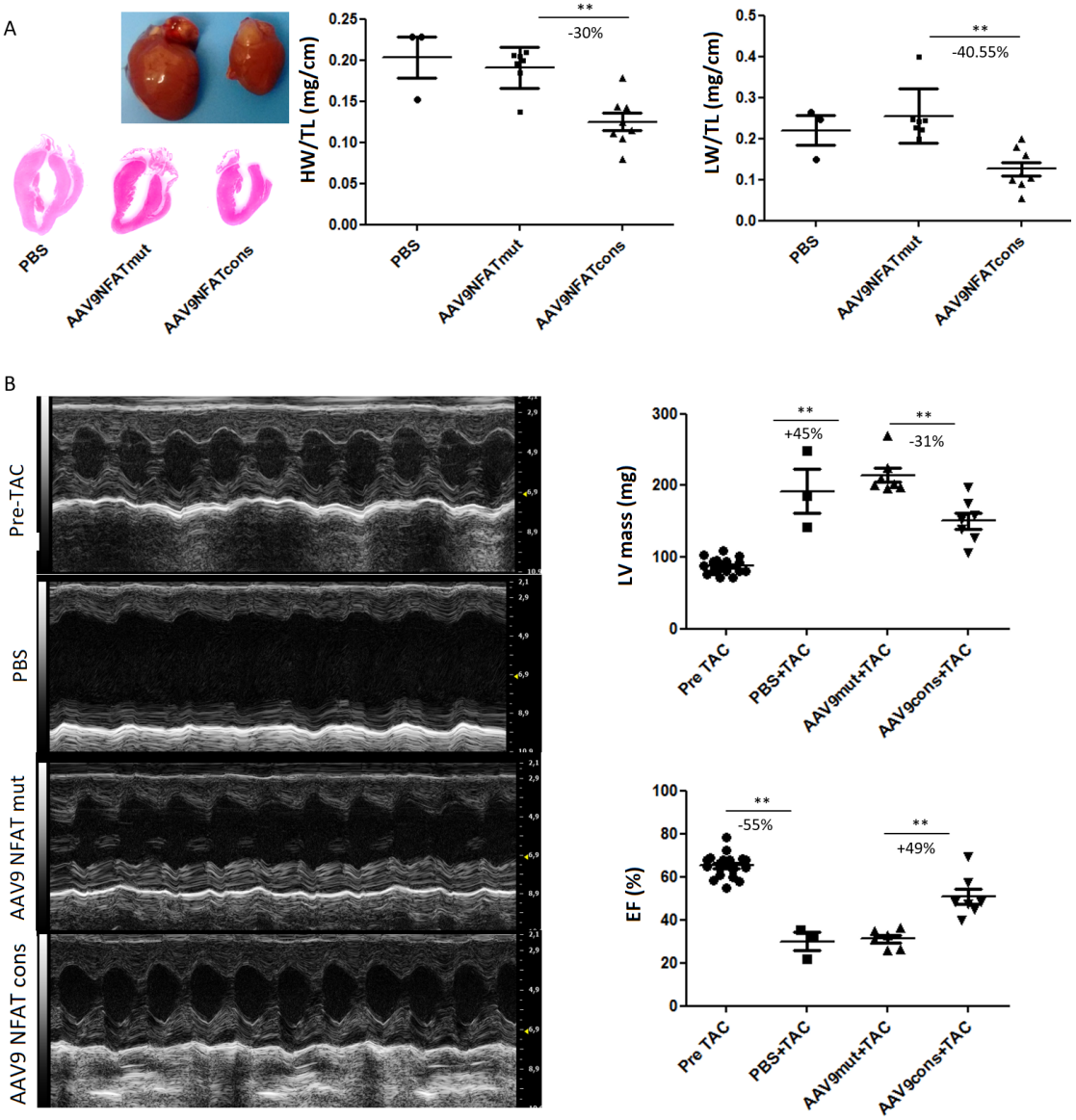

Fig. 48: AAV9-mediated generation of hpNFAT consensus RNA decoy ODNs decreases TAC-induced heart hypertrophy (A) The graphs summarize the statistical quantification of markers of heart hypertrophy (HW/TL) and heart failure (LW/TL). The pictures on the left show gross morphology of the different AAV9 injected groups after TAC. (n=3 for PBS injected group, n=8 for AAV9 injected groups, ** $p<0.01$). (B) Representative M-mode echocardiograms of control mice and of animals subjected to TAC. On the right, the graphs present statistical analysis of calculated LV (left ventricle) mass and EF (ejection fraction). (n=3 for PBS injected group, n=8 for AAV9 injected groups ** $p<0.01$; HW: heart weight, TL: tibia length, LW: lung weight, LV: left ventricle, EF: ejection fraction).

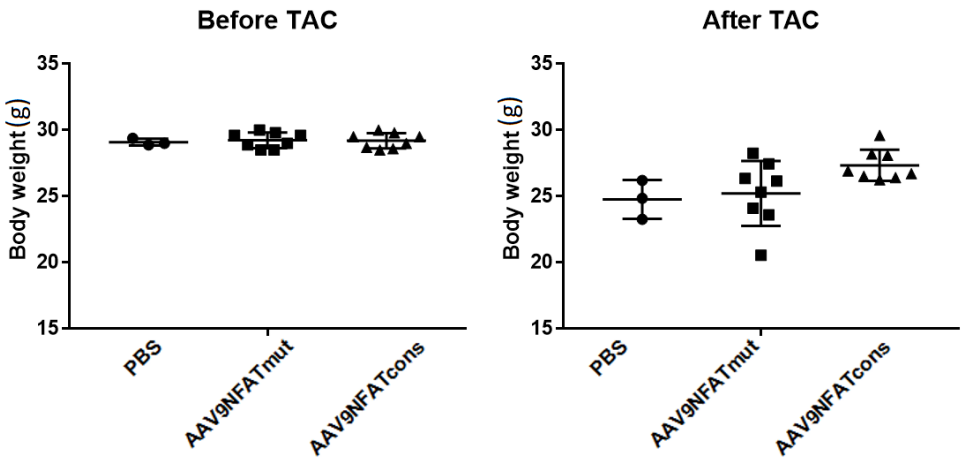

Fig. 49: Mice body weight measurements before and after TAC surgery. (n=3 for PBS injected group, n=8 for AAV9 injected groups)

compared to pre-TAC values. However, the injection of AAV9 expressing hpNFAT consensus RNA decoy ODNs, but not the mutated control had a beneficial effect on both LV mass and EF (Fig. 48). Thus, echocardiographic measurements confirm that hpNFAT cons RNA decoy ODNs can successfully improve cardiac performance 6 weeks post TAC.

5.3.6 Effect of AAV9 injection on phospholamban phosphorylation status

Phospholamban (PLN) is an important regulator of cardiac contractility and inhibits SERCA Ca^{2+} release. Under pathological stress conditions, PLN is phosphorylated by protein kinase A (PKA) at serine 16 (Ser16) [62]. Hence, the phosphorylation status of PLN was further addressed in protein extracts isolated from AAV9 transduced hearts, using Western blot analysis. As a measure of protein load Ponceau staining was used, due to the different expression of commonly used internal controls in diseased cardiac tissue, as previously described [54].

The quantification of Western Blot results (Fig. 50) indicates that AAV9 expressing hpNFAT consensus RNA decoy ODNs significantly decreased the phosphorylation state of PLN by 72% in comparison to the PBS treatment. As in the previous experiments, the control AAV9 injection prior to TAC had no effect on the level of phosphorylated PLN.

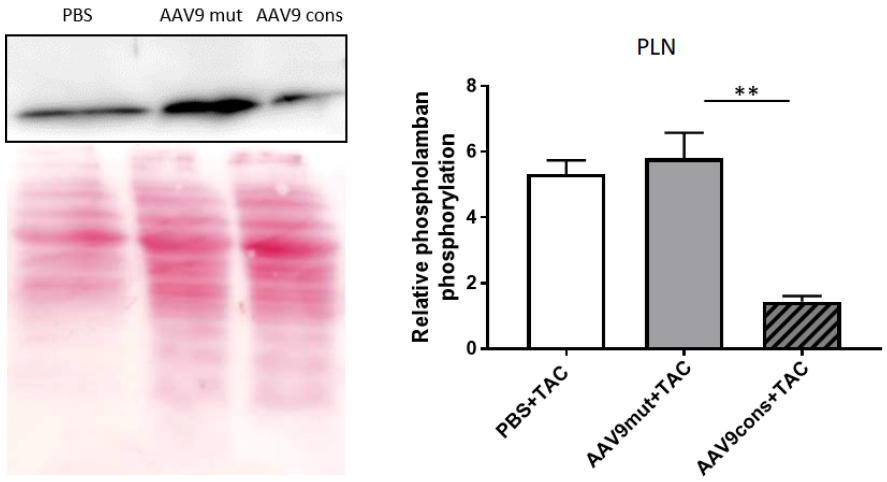

Fig. 50: AAV9-mediated expression of hpNFAT consensus RNA decoy ODNs decreases the phosphorylation level of PLN (Ser16) in heart tissue. Western blot analysis using a specific antibody that recognises the phosphorylated PLN at Ser16. Ponceau staining was used as a loading control. (n=3, ** $p<0.01$).

Effect of AAV9 injection on fetal gene program

Next, the effect of AAV9 injection on pro-hypertrophic markers ANP, BNP and RCAN-1 was examined. As expected, 6 weeks of pressure overload induced a significant increase in the expression of fetal genes in the myocardium, as compared to sham-operated group. Notably, AAV9-mediated delivery of hpNFAT cons RNA decoy ODNs prior to TAC could significantly decrease the mRNA levels of the three analysed genes. (Fig. 51A).

In addition, BNP protein level was measured in the heart tissue, as well as in plasma isolated from treated mice by ELISA. Remarkably, prophylactic injection of AAV9 expressing hpNFAT consensus RNA decoy ODNs significantly reduced BNP plasma level as shown in Fig. 51B. The control AAV9 had no effect in this context. Similarly, BNP protein level in plasma isolated from mice subjected to TAC was shown to be 3-fold diminished in the group which received gene therapy.

Effect of AAV9 injection on cardiac fibrosis

Fibrosis is a hallmark of heart failure and is associated with collagen deposition, contributing to impairment of heart function. It was previously shown that fibrosis is another factor that leads to TAC-induced cardiac pathology [225].

At first, fibrosis markers were analysed on mRNA level in heart tissue. The results confirmed a significant increase in mRNA levels of fibrosis markers collagen-3, TGF-β and

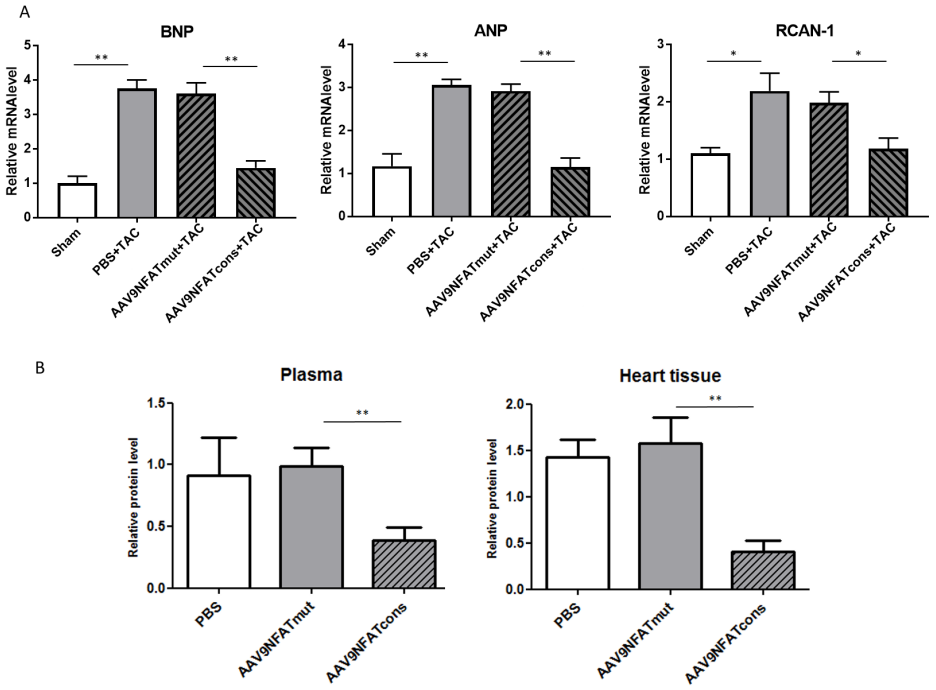

Fig. 51: AAV9-mediated delivery of hpNFAT consensus RNA decoy ODNs into the myocardium decreases the expression of TAC-induced pro-hypertrophic markers. (A) Gene expression analysis of ANP, BNP and RCAN-1 in the heart tissue, using RPL32 as a housekeeping gene. Values were normalized to sham-operated mice as control. (B) BNP protein level was measured by ELISA in plasma and heart protein extracts. (n=3 for sham and PBS injected groups, n=8 for AAV9 injected groups, * $p<0.05$, ** $p<0.01$)

CTGF in the hearts of mice subjected to TAC and injected with PBS (Fig. 52A). However, when mice were injected with AAV9 expressing hpNFAT consensus RNA decoy ODNs prior to TAC, a significant decrease in remodelling-associated genes were observed, as demonstrated in Fig. 52A.

Next, collagen deposition was analysed by Masson's Trichrome staining in heart sections. Fibrosis was observed to be associated with blood vessels (perivascular fibrosis), but interstitial fibrosis in between cardiomyocytes was as well noted in myocardium of TAC-treated animals.

The results prove intense fibrosis in hearts isolated from PBS and AAV9 control injected mice, while AAV-mediated NFAT1-4 neutralization prior to *in vivo* hypertrophy induction significantly reduced the area of collagen deposition, as depicted in Fig. 52B. These data support the gene expression analysis, proving the beneficial effect of AAV9 mediated hpNFAT consensus RNA decoy ODNs on collagen deposition in the myocardium of mice subjected to TAC.

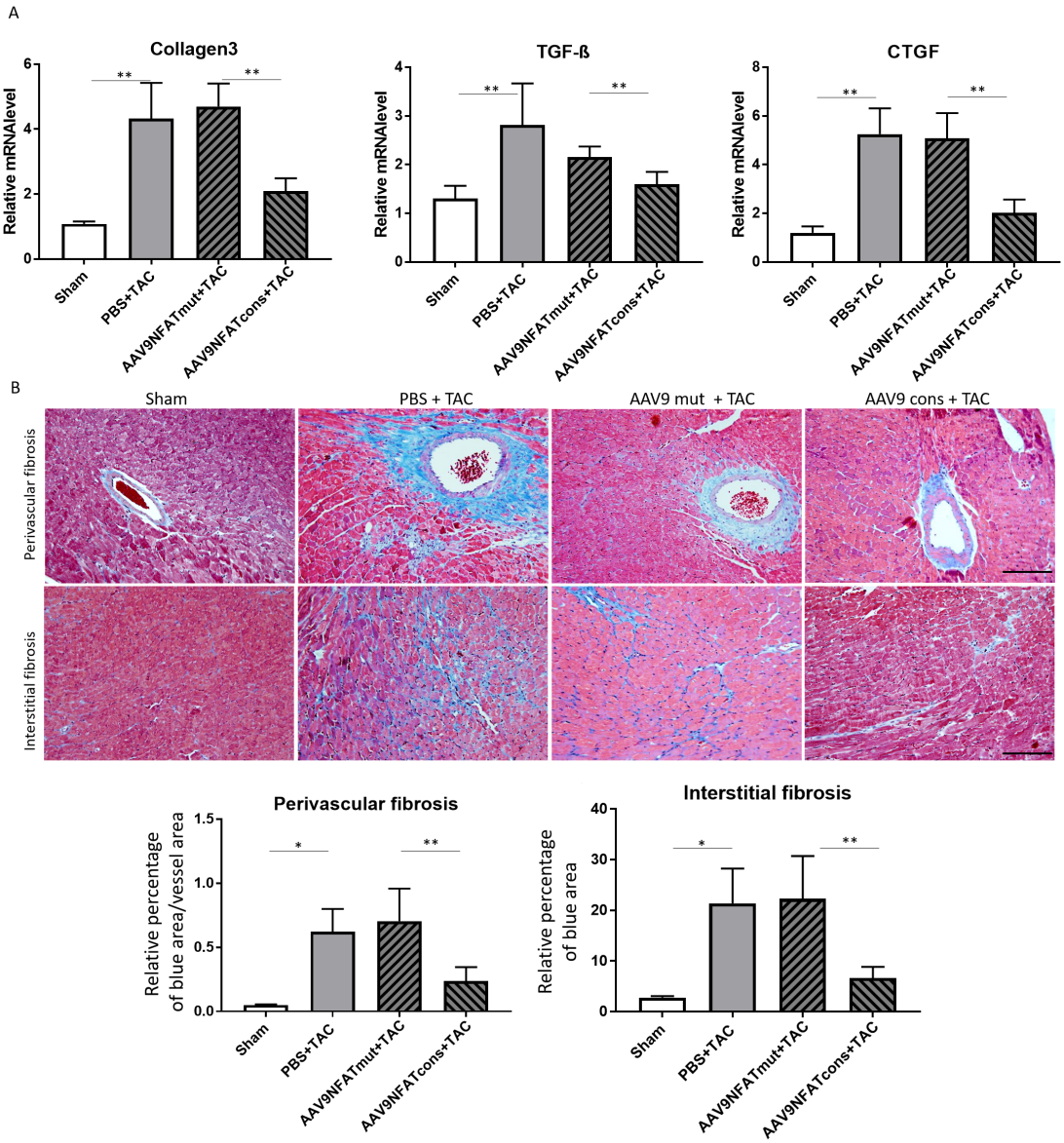

Fig. 52: AAV9-mediated delivery of hpNFAT consensus RNA decoy ODNs into the myocardium decreases fibrosis markers in heart sections. (A) mRNA levels of fibrosis markers collagen 3, TGF-β and CTGF in cardiac tissue. Gene expression was normalized to RPL32 as a housekeeping gene (n=3 for sham and PBS injected groups, n=8 for AAV9 injected groups, * $p<0.05$, ** $p<0.01$). (B) Representative left ventricular cross sections revealing perivascular and interstitial fibrosis. The graphs present the statistical quantification of the percentage of fibrosis (blue area) in myocardium of mice of different treatment groups. Scale bar represents 20 μm. (n=3 for sham and PBS injected groups, n=8 for AAV9 injected groups, * $p<0.05$, ** $p<0.01$).

Effect of AAV9 injection on β-MHC protein level

Heart hypertrophy is characterized by re-activation of the β isoform of the myosin heavy chain, which is expressed under normal conditions in the late stages of embryonic development [167]. Therefore, the relative amount of this protein was analysed as an additional marker of hypertrophic response in the 3 different treatment groups. Immunohistochemical analysis demonstrated that PBS, as well as the control AAV9 injected mice re-expressed β-MHC in cardiomyocytes, as depicted in Fig. 53, whileAAV9-mediated hpNFAT RNA decoy ODNs expression significantly reduced the levels of this protein with 49$\pm$ 9% as compared to the control.

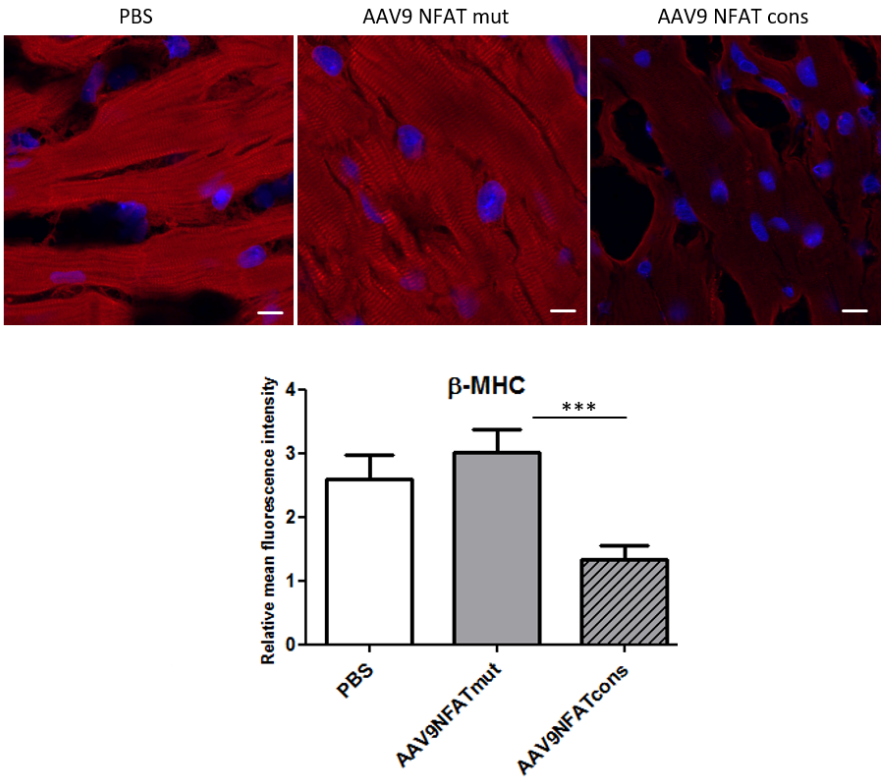

Fig. 53: AAV9-mediated delivery of hpNFAT consensus RNA decoy ODNs into the myocardium reduces β-MHC protein level. Representative images depicting β-MHC immunohistochemistry (red) in heart cryosections. Nuclei were stained with DAPI (blue). The graph shows the statistical summary of the quantification of mean red fluorescence intensity in different treatment groups. The scale bar represents 10 μm. (n=3 for PBS injected groups, n=8 for AAV9 injected groups, 20 images analysed/group. *** $p<0.001$)

5.3.7 Effect of AAV9 injection on protein translation rate

Cardiomyocyte hypertrophy involves an accelerated protein translation rate which can be determined, as shown in the *in vitro* experiments, by using the non-radioactive SUn-

SET assay. This method was further applied for the detection of total protein translation level in heart tissues of different treatment groups.
Analysis of confocal images revealed a dramatic decrease in mean fluorescence intensity of the cryosections of mice injected with AAV9 expressing hpNFAT consensus RNA decoy ODNs (Fig. 54). As in previous experiments, the control AAV9 had no influence on the rate of protein translation.

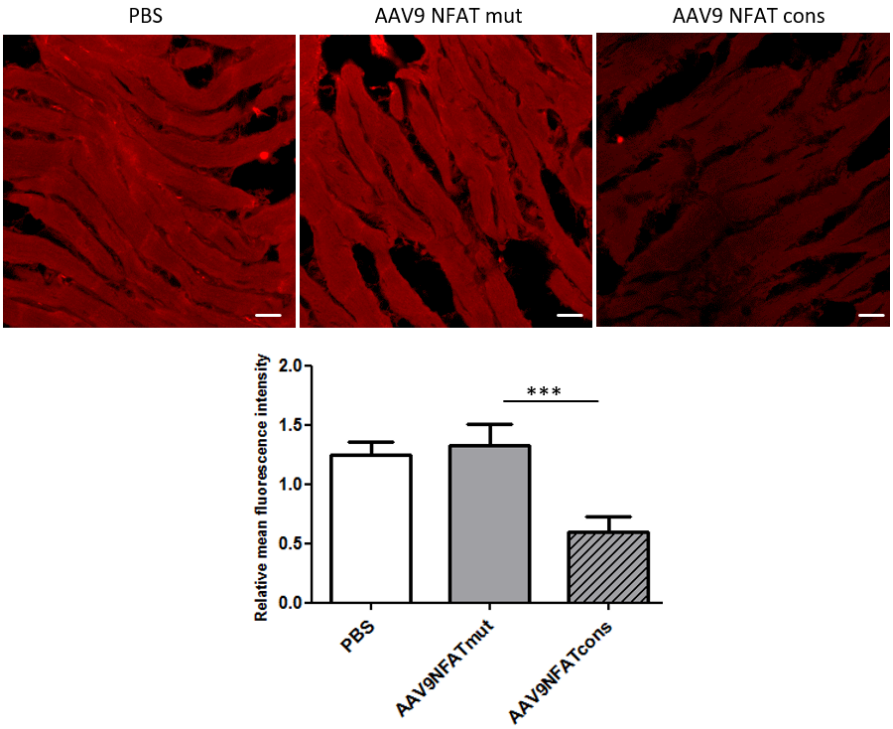

Fig. 54: AAV9-mediated delivery of hpNFAT consensus RNA decoy ODNs decreases the rate of protein translation. Representative images of anti-puromycin immunohistochemistry (red) which correlates with the total protein translation rate. The graph depicts the quantification of mean red fluorescence intensity of confocal images in different treatment groups. Scale bar represents 20 μm. (n=3 for PBS injected groups, n=8 for AAV9 injected groups, 20 images analysed/group. *** $p<0.001$).

5.3.8 Effect of AAV9 injection on cardiomyocyte size

Next, cardiomyocyte hypertrophy was addressed directly by measuring cell size. In this respect, 5 μm thick frozen sections were treated with WGA to label specifically cell membranes. Prior to staining, cardiomyocyte orientation was analysed. Both long and short axis were considered for quantification, to have a two dimensional assessment of cell size. The results clearly confirm that AAV9-mediated hpNFAT consensus RNA decoy ODNs expression can normalize cardiomyocyte size in TAC-subjected mice. Cells

were significantly smaller than cardiomyocytes in the control groups in both width and length. Injection with AAV9 expressing the mutated control RNA had no effect on cardiomyocyte size, as shown in Fig. 55.

To further confirm cell size measurements, hematoxilin-eosin staining was performed

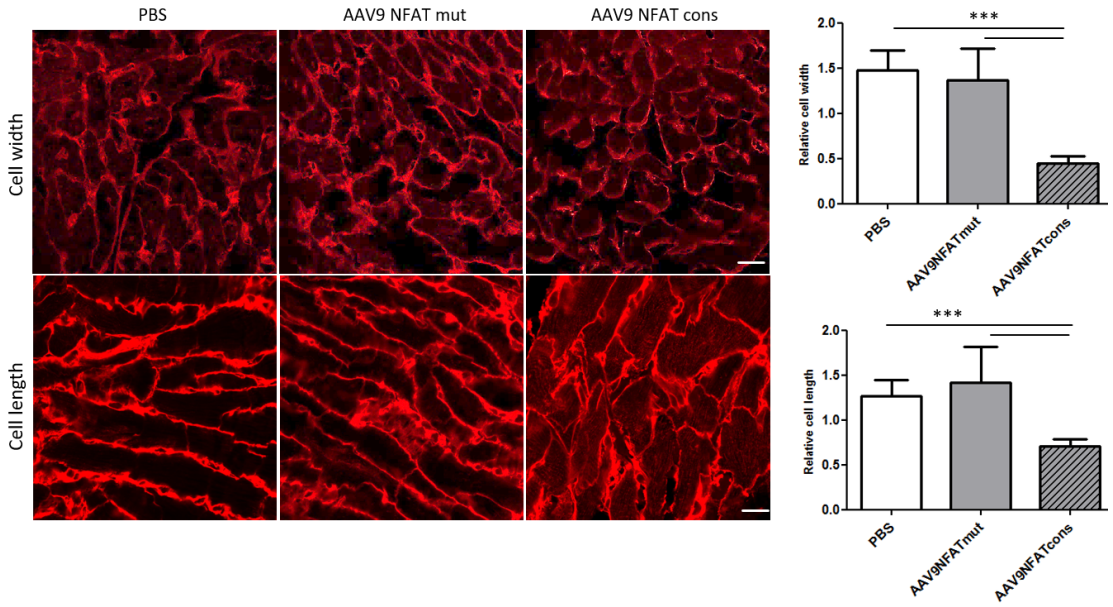

Fig. 55: AAV9-mediated delivery of hpNFAT consensus RNA decoy ODNs decreases cardiomyocyte dimensions. Representative images of WGA stainings (red), labeling cell membranes of cells in short and long axis. Cardiomyocyte width and length were analysed using ImageJ. Scale bar represents 20 μm. (n=3 for PBS injected groups, n=8 for AAV9 injected groups, 20 images analysed/group, *** $p < 0.001$).

and relative cardiomyocyte area was analysed. As expected, TAC induced a significant increase in cell area as compared to sham operated mice (Fig. 56). Moreover, the changes in left ventricular wall dimensions, assessed by echocardiography were validated by this technique, as an increased left ventricular wall thickness was observed following TAC (Fig. 56). However, injection of AAV9 expressing hpNFAT consensus RNA decoy ODNs two weeks before TAC had a favourable effect on heart architecture, as proven in decreased left ventricular wall thickness and reduced cardiomyocyte size as compared to the controls (Fig. 56).

5.3.9 Effect of AAV9 injection on T-tubule organization

In healthy cardiomyocytes, the T-tubule system is highly organized, with regular spacing distance of approximately 2 μm, which is essential for excitation-contraction coupling. It was previously shown that T-tubule remodelling accompanies the transition from heart

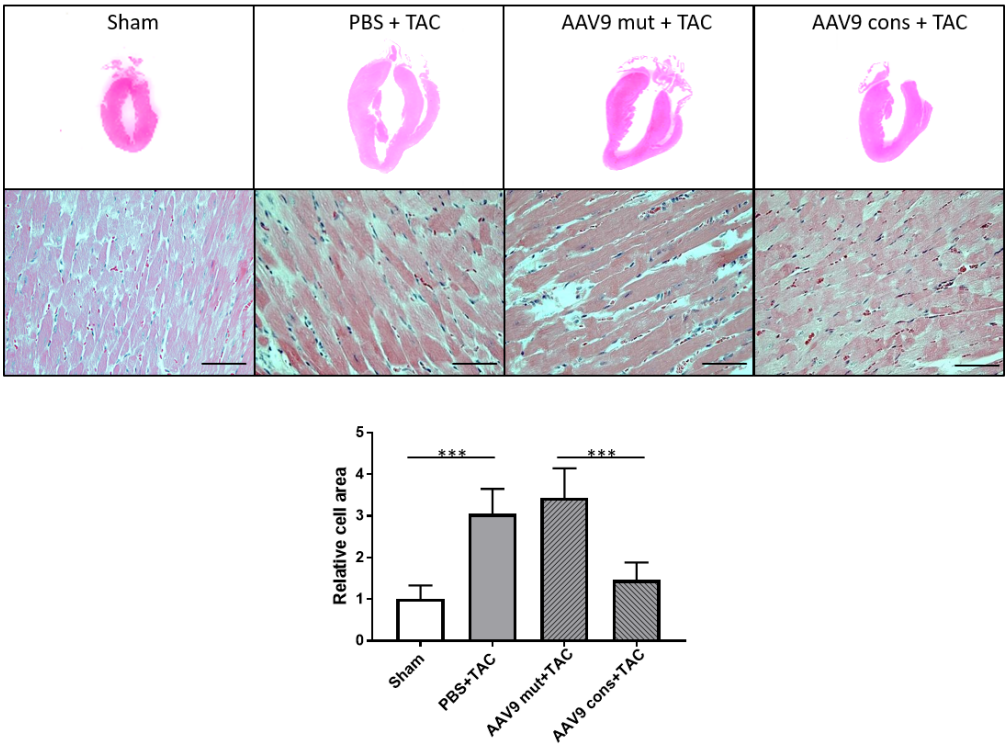

Fig. 56: AAV9-mediated delivery of hpNFAT consensus RNA decoy ODNs reduces left ventricular and cardiomyocyte size. Representative images of H&E stainings of heart sections after TAC, as well as sham operated control mice. The graph shows relative cell area calculated using ImageJ. Values were normalized to the sham group. Scale bar represents 10 μm. (n=3 for PBS injected groups, n=8 for AAV9 injected groups, 15 images analysed/group, *** $p< 0.001$).

hypertrophy to heart failure, and this process was observed in various models of pressure overload [215]. Therefore, the next aim was to determine whether prophylactic AAV9-mediated NFAT1-4 neutralization can prevent the pathological reorganization of the T-tubules which precedes heart failure.

As expected, TAC led to a dramatic decrease in T-tubule regularity and density in cardiomyocytes, as shown in Fig. 57. Similarly, the control AAV9 injected mice presented with a disrupted T-tubule system. AAV9-mediated hpNFAT consensus RNA decoy ODNs expression in cardiomyocytes led to a regular occurrence of T-tubules, as shown by plotting the fluorescence intensity profile of WGA staining, depicted in Fig. 57A. T-tubule frequency was then analysed by already established regularity markers T-index, tubularization percentage and T-power. T-index was defined as the percentage of T-tubule area in cardiomyocytes. Cells presenting T-index above 2 were considered tubular, and the percentage of tubulated myocytes was further analysed (percentage tubularization). T-power was considered to be the frequency at which the 2 μm regu-

lar T-tubule pattern is observed, and was calculated by plotting the power spectrum of Fourier transformed images (Fig. 57 C). The results of the analysis of these parameters show a significant increase in T-index, percentage of tubular cells and T-power in cardiomyocytes of mice receiving gene therapy.
These observations conclude that T-tubule network organization can be rescued by NFAT1-4 neutralization in the context of TAC-induced left ventricular dysfunction. Moreover, these results support the conclusions of previous experiments, suggesting the beneficial effect of the designed AAV9 expressing hpNFAT consensus RNA decoy ODNs on heart hypertrophy and heart failure *in vivo*.

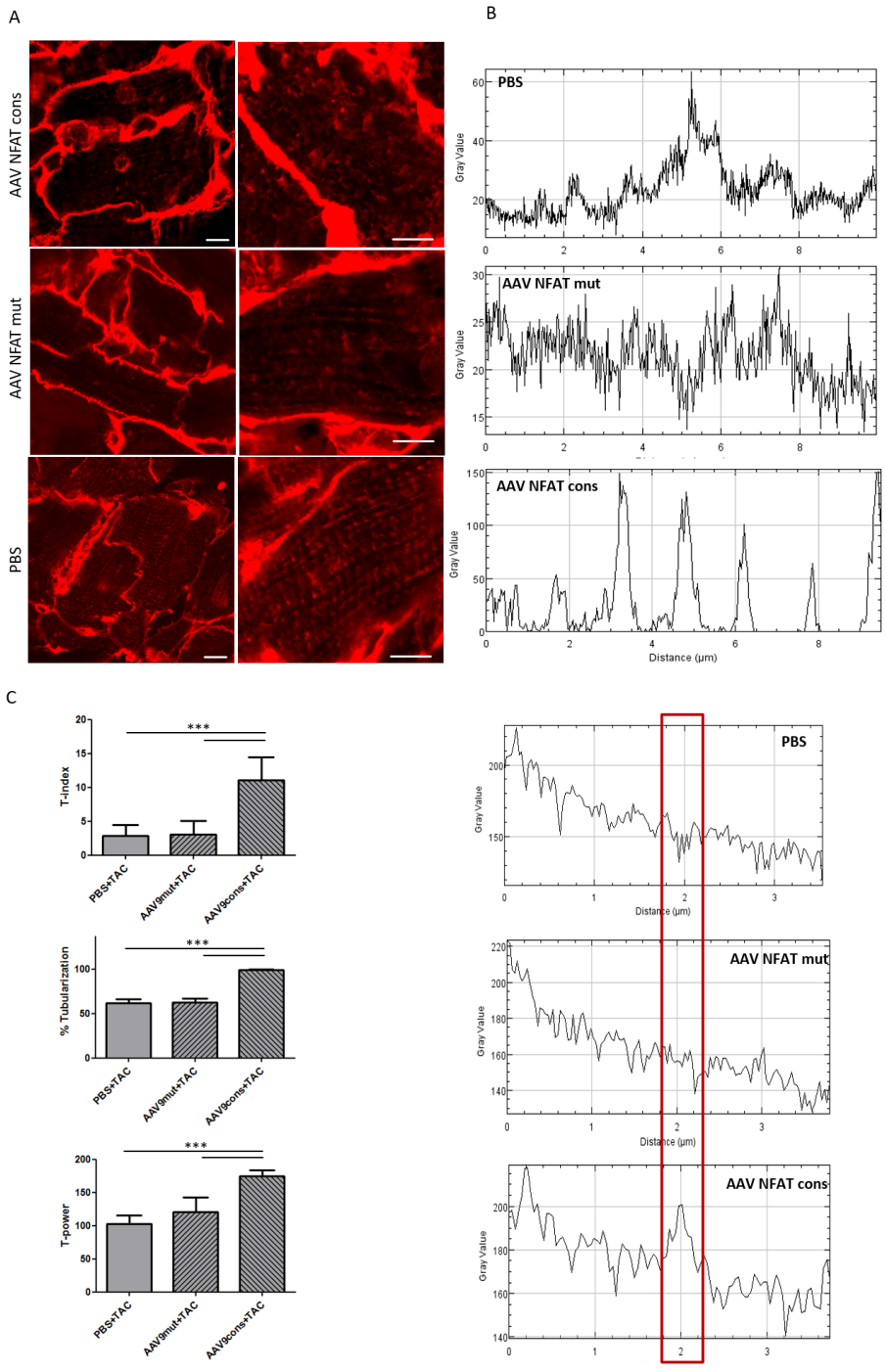

Fig. 57: AAV9-mediated delivery of hpNFAT consensus RNA decoy ODNs improves T-tubule organization in cardiomyocytes. (A) Representative images of WGA stainings (red) of myocardium cryosections. Note, that the high red fluorescence background observed in confocal images of the stained tissue next to cell membrane is due to fibrotic areas around cardiomyocytes. (B) Plot profile of WGA stainings showing the regularity of the T-tubule system. (C) Statistical quantification of T-index, percentage of tubulated cells and T-power. The graphs on the right represent the plots obtained after Fourier transformation, showing the frequency of T-tubules at different distances. Scale bar represents 25 μm. (n=3 for PBS injected groups, n=8 for AAV9 injected groups, 30 images were taken/ group with different magnifications, *** $p< 0.001$).

6

Disussion

6.1 Marfan syndrome

6.1.1 Clinical importance

The main mortality risk of patients suffering from Marfan syndrome is thoracic aortic aneurysm formation and dissection. Current treatment options such as β-blockers or aortic root replacement offer only a temporary solution to this cardiovascular complication and do not provide a long-term treatment. Additionally, conflicting results were published regarding the benefit of β-blockers on the survival rate of the patients [70]. Furthermore, a trend but not a significant beneficial effect on thoracic diameter was shown by β-blocker therapy in children and adolescents with Marfan syndrome [67].
Prevastin, a HMG-CoA reductase inhibitor was shown to reduce aortic dilatation in a mouse model for Marfan syndrome by downregulating MMP expression in the aortic wall [132]. It has been recently shown that losartan, an angiotensin II type 1 receptor blocker can be successful in improving, but not fully normalising the architecture of the elastic fibres in the aorta of mgR/mgR mice [80]. However, when losartan was administered to patients suffering of Marfan syndrome, the observed benefits could not be reproduced for all types of fibrillin-1 mutations [63]. Therefore, the need for a therapeutic strategy for Marfan syndrome is still actual.
The approach investigated in this study provides the possibility to achieve a long term delivery of the AP-1 decoy ODNs in aortic smooth muscle cells, which can be translated into a new therapy for prevention of aortic aneurysm formation and dissection in patients suffering from Marfan syndrome. Moreover, the current study supports the central role of AP-1 in the development of aortic aneurysms in the context of Marfan syndrome.

6.1.2 The role of AP-1 in aortic aneurysm dissection

Defective fibrillin-1 protein leads to the pathological phenotype of Marfan syndrome, through dysfunctional TGF-β signalling [149], mechanism explained in detail in the Introduction. By using the mgR/mgR mouse model for this disease [183], the critical pathways of elastin fragmentation in the aortic wall have been revealed [156]. It was previously shown that mgR/mgR mice present with severe elastolysis in both thoracic and abdominal aorta and are affected by thoracic aneurysm rupture, which limits their lifespan [183]. The mice show increased MMP activation, inflammatory cells recruitment and elastin degradation, which are typical events that lead to aortic dilatation [21, 183, 156].

The role of MMPs in the progression of aortic aneurysm development in the context of Marfan syndrome has already been established [35, 34, 94]. MMPs degrade a high variety of extracellular matrix components, such as collagens, elastin, fibronectin and gelatine [190] and consequently lower the stability of the aortic wall. Additionally, aortic samples isolated from Marfan patients were proven to contain highly active MMP9 and MMP2 [146]. Downregulation of MMPs in mgR/mgR mice by treatment with doxycycline, a non-specific MMP inhibitor increased the life span of Marfan mice and decreased the incidence of aneurysm dissections. Moreover, a significant improvement in the elastic fiber architecture was observed [35]. MMP2 and MMP9 were proven to decrease SMCs contractility, increase cell apoptosis and promote elastin fragmentation in the context of thoracic aneurysm in mgR/mgR mice [34].

The AP-1 transcription factor family has been shown to play a pivotal role in MMP regulation [11]. In a previous study, a significant increase in AP-1 transcription factor activity was shown in aortic SMCs isolated from mgR/mgR mice, in comparison to wild type aortic SMCs [4]. Increased AP-1 nuclear translocation resulted in increased MMP2 and MMP9 protein levels in these cells [4]. AP-1 activity is increased in the presence of TGF-β [211], which could be one of the reasons for the elevated MMP expression levels detected in mgR/mgR aorta. Interestingly, losartan was shown to decrease AP-1 activity, which can be one explanation for its therapeutic effect observed in mgR/mgR mice [172]. A similar mechanism was noted for statins, which inhibit AP-1 nuclear translocation and downregulate target genes in SMCs and endothelial cells [47].

Taking into account the major role of AP-1 in aortic aneurysm progression through upregulating MMP expression as well as inflammatory cytokines [182], the use of a decoy ODN neutralizing this transcription factor family could be translated into a therapeutic approach for preventing aortic aneurysm dissection, as shown in our previous study

[4]. Treatment of SMCs as well as aortic grafts with decoy ODNs which neutralize AP-1 downregulated the expression of MMP9 and MMP2, as well as the gelatinease activity in the tissue, which was as well observed in the present study. Moreover, a beneficial effect on the elastin structure in mgR/mgR aortic cryosections was noted. These data suggest the central role of the transcription factor in the vessel wall remodelling, characteristic for Marfan syndrome. In addition, the results attest the potential of AP-1 decoy ODNs to improve the structure of elastic fibers in the aorta and the possibility of using this nucleic acid drug preventing aortic dissection that is prototypic for Marfan syndrome [4].
AP-1 decoy ODNs have already been employed in pre-clinical testing in the treatment of cardiovascular complications. For example, they were proven effective in decreasing neointima proliferation in a minipig angioplasty model by reducing ET-1 expression [20]. Moreover, AP-1 neutralization by means of *ex vivo* treatment with decoy ODNs was found to be protective against rejection in an allogenic rat heart transplantation model [189].

6.1.3 Novelty of the study

The present study provides a novel strategy for preventing aortic dilatation and dissection in the context of Marfan syndrome by aortic transduction with AAV9SLR [208] expressing shRNA-based decoy ODNs that neutralize AP-1. The designed AAV vector causes expression within the target cells of a hpAP-1 decoy ODN as shRNA, under the control of H1 promoter. The innovation of this concept is the continuous production of the hpAP-1 RNA decoy ODN in the transduced tissue. Consequently, a single application of the AAV vector is enough for the long-term expression of the active compound in transduced cells, making this a suitable therapeutic approach and constituting an improvement to the method published in our previous study [4].
Prior research proves that the intracellular production of transcription factors decoy ODNs by means of plasmid or viral vectors is a feasible method of decoy ODN delivery in cells. By using a ssDNA expression vector, the generation of any ssDNA was proven possible [31]. Initially, this approach was used in the present study to deliver hpAP-1 decoy ODNs in SMCs. Although this strategy was shown to be effective in downregulation of AP-1 target genes (data not shown), the designed vector leads to reverse transcriptase translation, which may be a disadvantage for further clinical testing due to its possible side effects. To overcome this drawback, a new strategy was described in the literature [226]. The NF-κB transcription factor decoy ODNs were generated as shRNA and successfully inhibited the expression of downstream genes *in vitro* [226].

Nevertheless, *in vivo* experiments did not show so far the possibility of using this strategy for therapeutic purposes. This study uses of a similar approach, in order to achieve hpAP-1 RNA decoy ODNs production in SMCs.
By using *in vitro* primary aortic SMCs isolated from fibrillin-1 deficient mgR/mgR mice, as well as *in vivo* methods, successful decoy ODNs production and AP-1 target genes downregulation, as well as positive effects on elastin breaks could be shown.

6.1.4 Hairpin AP-1 decoy ODNs delivery

The ability of cultured cells to take up "naked" decoy ODNs has already been demonstrated [33]. The main advantage of this approach is that cells can incorporate the decoy ODNs without any auxiliary means and rapidly neutralize the transcription factor. In contrast to the antisense ODNs, which are transfected into cells by endocytotic pathway [68], the mechanisms for decoy ODNs uptake are distinct and consist of carrier-mediated and receptor-mediated delivery [86]. The results of this study prove that cationic transfection reagents like Lipofectamine3000 do not improve the nuclear localization of the hpAP-1 decoy ODNs, confirming the already published data [8]. Furthermore, liposomal mediated transfection led mostly to cytosolic localization of the fluorescent decoy ODNs, which were mostly localized into liposomal complexes. Afterwards, the decoy ODNs are most likely degraded through the lysosomal pathway [66]. In contrast, treatment with "naked" decoy ODNs led to mostly nuclear delivery of the active compound and could immediately exert its role in transcription factor neutralization.
The suitable method of delivery of decoy ODNs *in vivo* depends on the targeted organ. Systemic administration is, in most cases, the preferred method of administration. Indeed, the systemic application of decoy ODN containing the promoter binding site for NF-κB, designed to have a ribbon-circular structure to improve stability, was used in a mouse abdominal aneurysm model. The DNA molecules were detected in the abdominal aortic wall after tail-vein injection, leading to decreased elastin fragmentation and reduced the gelatinease activity of MMP9 and MMP2 [135]. Nevertheless, the blood flow in the thoracic aorta is presumably too high and therefore it allows inadequate amount of time to pass the endothelial barrier and reach SMCs, the target cells in the present study.
On the other hand, local aplication of the nucleic acid reduces the risk of degradation and decreases the side effects caused by nonspecific site of action. At the same time, it allows an accurate dosage of delivery of the active compound for a fast therapeutic effect. Decoy ODNs were locally applied at the level of the lungs [118], eyes [98] or

skin [144].

Viral mediated approach of decoy ODN delivery is an effective and targeted option for transcription factor neutralization for treatment of diverse pathologies. AAVs are the most frequently used gene delivery vehicles for therapeutic approaches due to of their non-pathogenic nature and low immunogenity, as well as long-term transduction efficiency [145]. In the present study, hpAP-1 RNA decoy ODNs were delivered in SMCs by using AAV serotype 9 with modified capsid. The vector was directed to human endothelial cells *in vitro* and was shown to be significantly more effective in transducing the target cells as compared to the wild type AAV9 [208]. Importantly, the rate of AAV9SLR neutralization by AAV antibodies contained in human sera was dramatically reduced, confirming that the vector is a feasible tool for gene therapy [208]. The ability of AAV9SLR to transduce endothelial cells was already proven by intradermal injection of the vector particles [120]. However, this study is the first to show successful SMCs transduction by AAV9SLR in mgR/mgR mice.

Initially, the evaluation of transduction efficiency of AAV9SLR in the aorta was made by tail-vein injection of the AAV9SLR vector expressing EGFP. Nevertheless, the green fluorescent marker was detected neither in SMCs, nor endothelial cells. This could be, as in the case of "naked" decoy ODNs, due to the high flow velocity in the thoracic aorta, not permitting sufficient contact time of the AAV with the tissue in order to allow successful transduction. Therefore, the application of the viral construct was further performed *ex vivo* and treated grafts were next implanted into mgR/mgR mice in a model of renal aortic transplantation, as previously described [184], [4]. This method allowed the successful transduction of both endothelial cells and SMCs in the aorta, as shown by CD31 and EGFP immunohistochemistry experiments. Moreover, by using RNA F.I.S.H method, hpAP-1 RNA decoy ODNs could be detected in transduced cells.

6.1.5 The importance of inflamation in aortic aneurysm development

The role of ROS in the pathogenesis of aortic aneurysms has already been investigated [131]. ROS increase MCP-1 secretion by SMCs in the aortic wall, thereby stimulating macrophage infiltration and increasing the migratory capacity of SMCs [177]. Additionally, increased oxidative stress and pro-inflammatory cytokines such as IL-6 and IFN-γ (Interferon-γ) were found to be present in biopsies isolated from patients undergoing surgery after thoracic aortic aneurysm [57]. Furthermore, it has been demonstrated that the aorthopathy observed in Marfan syndrome is partly due to the high amount of ROS generated in SMCs and macrophages, which was proven to be caused by increased TGF-β signalling [170], through activation of NOX4 (NADPH oxidase-4) [193]. NOX4 was

shown to be transcriptionally regulated by AP-1 and SMCs treatment with a decoy ODN that neutralized the transcription factor led to decreased accumulation of ROS [128]. In accordance with this study, the treatment with AAV9SLR neutralizing AP-1 could significantly reduce the level of ROS produced in aortic grafts of mice which received viral treatment.

Pro-inflammatory cytokines and oxidative stress enhance SMCs migration rate, as shown by primary cultures isolated from Marfan syndrome patients [40]. The data presented here show that AP-1 activation through IL1-β treatment can induce both the level of ROS production and the migration rate of primary SMCs, which could be decreased by hpAP-1 decoy ODNs treatment.

On the inflammatory level there is evidence that macrophage infiltration is an early event that leads to aneurysm development in the context of Marfan syndrome [76]. Macrophages can enhance the rate of elastin degradation through MMP secretion [164]. Elastin fragmentation leads to secretion of elastin-derived peptides, which in turn act as a chemotactic agent for macrophages [75]. In agreement with these results, mgR/mgR mice treatment with a monoclonal antibody against the elastin binding domain could decrease inflammatory cells infiltration, accompanied by decreased MMP activity in the aorta of mgR/mgR mice [77].

Moreover, TGF-β signalling and inflammatory pathways were shown to be highly activated in aorta of Marfan patients [164]. In the same study, immune cells infiltration was observed in both aortic adventitia and media, and plasma analysis showed increased concentration of pro-inflammatory cytokines, such as M-CSF (Macrophage colony stimulating factor), MCP-1, IL-8, IL-17 and INF-γ. The high number of macrophages present in aortic specimens of Marfan mice lead, in turn, to an increased expression level of the macrophage elastase MMP12 which further contributes to the elastic laminae degradation and consequently to the aneurysm development [187]. The results of the present study show that *ex vivo* treatment with AAV9SLR expressing hp AP-1 RNA decoy ODNs decreased the amount of macrophages in the adventitia of fibrillin-1 underexpressing mice. Similar to previous studies targeting inflammation in Marfan syndrome by indomethacin treatment [78], our data show that MMP12 protein level in aortic cryosections of treated mice was as well downregulated, which correlated with less elastin breaks in the media. These results indicate that AP-1 neutralization by the designed AAV can alter the pro-inflammatory environment which precedes aortic aneurysm dissection.

6.1.6 Endothelial permeability in Marfan syndrome

Ex vivo treatment of mgR/mgR aortic grafts with AAV9SLR led to transduction of not only endothelial cells, but also SMCs of the media, proving the ability of the vector to pass the endothelial cell layer. This observation is consistent with the previous study [4], which showed the ability of AP1 decoy ODNs to reach SMCs in mgR/mgR grafts. In contrast, aortic grafts isolated from wild type mice showed high transduction efficiency of endothelial cells, but considerably reduced EGFP positive SMCs as compared to mgR/mgR grafts. This can be explained by a dysfunction in the endothelial cell layer in the aorta of mgR/mgR mice, which was already addressed in the literature [184]. Plasma of Marfan syndrome patients was shown to contain high amounts of endothelial cells-related products von Willebrand factor antigen and thrombomodulin, proving indirectly an endothelial dysfunction [19].
Endothelial hyperpermeability was shown to be correlated with inflammatory cell recruitment in various models of vascular diseases [111]. Gelatinases MMP9 and MMP2 were shown to be responsible for the endothelial tight junction protein ZO-1 degradation in brain vessels [213]. In the current study, we demonstrated that aortic samples from Marfan mice present decreased ZO-1 protein level in CD31 positive endothelial cells, which can be a direct explanation for the observed endothelial cell dysfunction. However, by transduction with AAV9SLR expressing hpAP-1 RNA decoy ODNs, the tight junction expression could be rescued and brought to similar protein levels as the ones detected in the wild type controls. These results could further explain the therapeutic effect of the designed AAV9SLR transduction and could be an additional reason for the decreased macrophage numbers infiltrating the treated aorta.

6.1.7 Targeting other transcription factors for treatment of Marfan syndrome

The present study proves the importance of the transcription family AP-1 in the pathogenesis of aortic aneurysms in the context of Marfan syndrome. However, the significance of other transcription factors should be further considered in order to identify in more depth the molecular basis of this disease and to advance new therapeutic strategies. One protein of interest is KLF4. Although the role of this transcription factor was mostly elucidated during embryonic development [56] as well as in stem cell populations [237], its function in SMCs was less studied. It is known that the deletion of this transcription factor is beneficial in the context of abdominal aortic aneurysms development in both elastase and angiotensin II infusion models [175]. SMCs specific deletion of KLF4 decreased the pro-inflammatory cytokines MCP1, TNF-α, CCL12 (Chemokine (C-C

motif) ligand 12), and IL-23 in the aortic wall and the number of elastin breaks was significantly reduced in these mice in abdominal aneurysm models. Moreover, KLF4 was shown to be highly upregulated and activated in samples isolated from human aortic aneurysms [175]. KLF4 was also shown to have a major role in artherosclerosis pathogenesis by increasing the pro-inflammatory environment in the plaques. Interestingly, SMCs conditional knockout of KLF4 led to a dramatic decrease in plaque size and increased plaque stability, accompanied by a reduced number of pro-inflammatory cells in the vessel wall [186].
A recent study using SMCs differentiated from iPSCs (induced pluripotent stem cells) derived from Marfan patients also points out the importance of KLF4 in the progression of the disease [72]. KLF4 was significantly increased on mRNA and protein levels in Marfan syndrome lines, and silencing this transcription factor with siRNA led to increased deposition of fibrillin-1 *in vitro*. These data validate KLF4 as another key target that leads to the phenotype shown by Marfan patients, but also for other vascular diseases with inflammatory component.
It was previously demonstrated that KLF4 expression on the basal level is extremely low, but it is rapidly induced after injury [122]. The reduced KLF4 expression level detected by immunohistochemistry in this study further confirms this observation. In contrast, mgR/mgR aortic cryosections presented significantly increased nuclear translocation of KLF4 into the nucleus, showing the activation of the transcription factor in mgR/mgR SMCs.
The activity of other transcription factors such as SMAD family were shown to correlate with the severity of thoracic aneurysms in Marfan syndrome [90] and hence decoys downregulating downstream pathways could be analysed as therapeutic nucleic acid drugs.

6.1.8 Limitations and perpectives

The main limitation of this study is the mode of application of the viral vector in aortic grafts. Since AAV9SLR was unable to transduce SMCs after tail vein injection, we used heterologous transplantation model to reimplant treated grafts. This method is however impossible to translate into practice in the clinical context. Nevertheless, this procedure allowed us to show the effects of AAV9SLR-mediated AP-1 neutralization on the elastin fibers architecture and can be used as a proof of principle study. For further translation projects, a new viral application method should be developed. One possibility of transfection with hpAP-1 decoy ODNs or of transduction with AAV9SLR expresing hpAP-1 RNA decoy ODNs would be using a celulose-based delivery sheet, as previously de-

scribed [134]. In addition, a hydrogel-based delivery system was also shown to be an appropriate vehicle for DNA transfection into the vessel wall [229]. The hydrogel sheet could be placed around the thoracic aorta, in the areas where aneurysm formation is evident, and could inhibit its development and dissection.
Furthermore, because of the delivery method we employed, the effect of AAV9SLR cons on the survival rate of mgR/mgR mice could not be addressed. It was previously shown [156] that the survival rate of homozygous mgR/mgR mice is poor, due to vascular complications, specifically aortic aneurysms. Starting with as early as 6 weeks of age, mgR/mgR mice present fragmented elastin fibers at the level of the aorta, with immune cells infiltration and medial calcification, which later develop into aortic aneurysms.
In addition, the active AAVs could be applied at different stages of the disease to determine the best time point of transduction to obtain the best results, which could be a valuable step before translation into further clinical studies.
The mgR/mgR mouse model for Marfan syndrome is a valuable tool for pre-clinical testing of AAV transfer at the level of the aorta. Nonetheless, large animals model for Marfan syndrome have already been described [205]. The fibrillin-1 mutant pigs recapitulated the features of Marfan syndrome observed in humans and the similarities between pigs and humans are closer from a physiological point of view. The fibrillin-1 mutant pigs present scoliosis, a feature of Marfan patients, and the histopathology of the aorta is similar to the one observed in mgR/mgR mice and patients. Using large animal models would make surgical procedures much easier to execute. For example, the use of a dispatch catheter was already shown to be a feasible way to deliver a viral vector in a pig coronary artery [224]. This method allowed as well the transfection of decoy ODNs into the coronary arteries of minipigs in a model of stent angioplasty [20].
In addition, the possibility of using decoy ODNs neutralizing other transcription factors important in aneurysm formation could be further assessed. KLF4 activation, described in detail in the previous section, was shown in mgR/mgR aorta. Decoy ODNs for KLF4 are already described [163], and their efficiency could be tested in Marfan syndrome model.

6.2 Heart hypertrophy

6.2.1 Clinical importance

Heart hypertrophy represents the response of myocardium to stress conditions, such as pressure or volume overload or neurohormonal stimuli and represents one of the leading causes of death in Western countries. This process is an adaptive series of events

which lead to increased heart size due to cardiomyocyte growth [64]. Although myocardial hypertrophy can help in decreasing wall stress, it can lead to a dilated stage, with decompensated function and heart failure. The mechanisms of decompensation include loss of cardiomyocytes through apoptosis, necrosis and autophagy. Consequently, myocyte replacement with myofibroblasts and intense remodelling of the heart occurs, accompanied by reduced contractility [48]. Recently, therapeutic strategies focused on reversing or even blocking the hypertrophic response, which was shown to inhibit heart failure, even when pressure overload persisted [106]. In the case of translational studies in human patients, other virus serotypes were confirmed to successfully transduce cardiomyocytes following intracoronary administration, for instance AAV1.
Traditional pharmacological treatment options include intervention with β-adrenergic receptor antagonists, inhibitors of angiotensin II and diuretics, all with good short-term response. However, the 5-year survival is below 50% [155]. Therefore, new therapeutic strategies are necessary to be established.

6.2.2 Novelty of the study

Therapeutic DNA oligonucleotides have already been tested in the treatment of heart hypertrophy in various models. Antisense oligonucleotides directed against LIF (leukemia inhibitory factor) and CT-1 (cardiotrophin-1) could downregulate AngII (angiotensin-II)-induced hypertrophic response *in vitro* [176]. However, their effects in a heart failure animal model was not analysed. Inhibition of phospholamban, a SERCA2a inhibitor through systemic injection of antisense oligonucleotides improved heart function in a pressure-overload mouse model [138]. Although effective, this approach could lead to side effects due to the systemic administration route, which is not specific for the target organ.
AAV mediated oligonucleotide expression in the myocardium could improve the distribution of the nucleic acid into target cells. The advantages of recombinant AAVs is the ability of transducing both dividing and non-dividing cells, inducing the expression of the gene of interest without inducing an immune response. Furthermore, several AAV serotypes were shown to have tropism for the heart [91]. AAV-mediated angiotensinogen antisense delivery was shown to reduce heart hypertrophy in a spontaneous hypertension mouse model [103].
The therapeutic effect on myocardium infarction of an NF-κB decoy ODNs has been previously shown [139]. Treatment with the active compound, but not the scrambled control before occlusion or immediately after reperfusion could decrease the infarction size and reduce the inflammatory response [139]. On the other hand, GATA4 decoy

ODNs failed to reduce ET-1-induced hypertrophic response in neonatal rat cardiomyocytes [159], suggesting that this transcription factor is not essential for the development of hypertrophy. GATA4 factor activity was shown to be correlated with the expression of other transcription factors, including NFAT and MEF2 [105]. This could constitute one of the reasons for unsuccessful reduction of hypertrophic markers and underlines the complexity of the molecular mechanisms leading to heart failure.
In consistence with the present study, NFAT inhibition was proven to be an effective method of treatment of pressure overload induced heart hypertrophy [112]. The administration of VIVIT, an inhibiting peptide after TAC led to decreased fetal gene program, reduced myocardium weight and improved heart function in comparison to control animals. Nevertheless, the administration of high peptide doses could be problematic for further clinical translation. Moreover, because of the short half-life of this compound, repeated injection of VIVIT is required. In contrast, the approach suggested in this study involves the single systemic injection of the AAV9 for continuous production of the decoy ODNs in target tissue, i.e. the myocardium, which is an advantage in comparison to previous published studies.
The study offers a new preventive one-time treatment for heart hypertrophy and decompensated heart failure. This involves the AAV9-mediated delivery of hp RNA decoy ODNs that reduce NFAT transcriptional activity. After one-time injection, decoy ODNs are continuously expressed in transduced cells as shRNAs bearing the consensus binding site in the promoter region of this transcription factor and can therefore downregulate the expression of target genes involved in hypertrophic response. This is, to our knowledge, the first AAV-mediated approach for NFAT transcription factor neutralization as a therapeutic approach for heart hypertrophy. By using cardiomyocyte cell models, successful decrease in NFAT-regulated genes was proven. Importantly, a beneficial effect on heart function was shown in TAC model of pressure overload.

6.2.3 Regulation of fetal gene program in heart hypertrophy

Synthesis of natriuretic peptides ANP and BNP is increased in the late fetal and early neonatal development stages, remarkably decreasing in the adult myocardium [25]. The reexpression of fetal gene program is a common characteristic of failing myocardium, representing a reliable marker of heart dysfunction. Several studies showed the correlation between BNP plasma levels and prognosis of heart failure patients [203]. Raised BNP protein concentration detected in plasma correlate with the severity of heart disease and mortality rate. BNP was shown to decrease following therapy [104].
The role of NFAT in the BNP reexpression in the hypertrophied myocardium has been

previously addressed [207]. Following nuclear translocation, NFAT synergizes with GATA4 to activate fetal gene program [137, 209]. In the present study, the importance of NFAT in the reactivation of ANP and BNP was further confirmed. Neutralization of this transcription factor *in vitro* by means of "naked" hpNFAT decoy ODNs, as well as AAV expressing hpNFAT RNA decoy ODNs led to a significant downregulation of the fetal gene program on mRNA and protein level in HL-1 cells stimulated with ET-1. Remarkably, the results could be reproduced *in vivo* in TAC-induced heart hypertrophy model.

Additionally, hypertrophic response includes the myosin heavy chain switch, which involves the β-MHC isoform reexpression and downregulation of α-MHC [123]. Transgenic mice expressing only β-MHC under basal levels presented a more pronounced hypertrophy under isoproterenol stimulation than wild type controls, showing the importance of this isoform in the disease progression [108]. The myosin switch was shown in various models of pathologic hypertrophy but not by physiological stimuli, such as exercise [179], [123] and is induced by pressure-overload [123]. The increase in the protein levels of β isoform of MHC was proven to influence heart function through reduced ATPase activity of this isoform and decreased contractility of expressing myocytes [109]. This can be an adaptive response to stress stimuli and has the role of increasing the metabolic efficiency.

The results of immunofluorescence experiments presented in this study show a significant increase in β-MHC protein level in ET-1 stimulated HL-1 cells. Similarly, it was noted a clear re-expression of the β isoform following TAC in the mouse myocardium. Taking into account that the myosin switch is a reversible process and β-MHC expression is downregulated after removal of the pathological stimuli [79], the effect of hpNFAT RNA decoy ODNs was further analysed. In a similar manner as the ANP and BNP expression levels, hpNFAT decoy ODNs reduced β-MHC protein level both *in vitro* and *in vivo*, in myocardium cryosections. This finding confirms the protective effect of the designed vector on heart hypertrophy.

Myocardium growth is accompanied by myocyte hypertrophy, while cardiomyocyte division is almost non-existent [154]. This process involves the elevation of protein translation rate [83], by a significant increase in the level of protein synthesis as compared to proteolysis. Pro-hypertrophic stimuli, such as ET-1, isoproterenol or AngII regulate the ribosome number in myocytes, as well as translational capacity [18].

The investigation of the exact mechanism through which NFAT inhibition leads to decreased protein translation level, as proven in this study, was not one of our purposes. However, UBF (Upstream binding factor), which is critical for increasing translation

efficiency in the context of heart hypertrophy [17], was shown to have an NFAT binding site in the promoter region [46]. Additionally, NFAT regulates RCAN1-4 which in turn upregulates eIF4E (Eukaryotic initiation factor 4E) [114], another key player of global protein synthesis [204].
Protein translation level was measured as well in the context of TAC-induced heart hypertrophy. The results are in consistence with previous studies [143], [142], proving a significant TAC-induced increase in protein synthesis in PBS-treated mice, as well as in the animals injected with AAV9 expressing hpNFAT mut RNA decoy ODNs. Importantly, treatment with AAV9 expressing hpNFAT cons RNA decoy ODNs led to a decrease in the level of global protein translation, proving reduced hypertrophic growth in cardiomyocytes.

6.2.4 Cardiomyocyte architecture in heart failure

Heart failure is accompanied by structural changes observed in cardiomyocytes. More speciffically, cell hypertrophy is complemented by an increase in sarcomerogenesis [50] and decrease in the regularity of T-tubules [126].
In the present study, cardiomyocyte size in tissue sections was quantified using two different validated approaches, specifically WGA and H&E staining. The evaluation of the measurements reveals that NFAT neutralization by RNA decoy ODNs leads to decreased TAC-induced myocyte dimensions, suggesting decreased hypertrophy. In line with these data, a decreased HW/TL ratio was observed in AAV9 treated mice.
In addition to increased myocardium weight, left ventricular dysfunction leads to notable lung remodelling [30]. TAC induces lung edema, fibrosis and inflammatory cell infiltration. Therefore, LW/TL ratio is a reliable parameter to assess the severity of heart failure [206]. In mice treated with hpNFAT RNA cons decoy ODNs - generating AAV9 prior to TAC, it was noted a decrease in LW/TL measurements. These results further confirm the preventive effect of decreased NFAT activity not only on heart hypertrophy, but also on heart failure.
Transverse tubules are membranes invaginations found in muscle cells which play a critical role in excitation-coupling. Structural changes in T-tubules arrangement has been described in models of heart failure [74]. The T-tubule disorganization was observed in a pressure-overload model starting from the incipient phase of left ventricular dysfunction and more rapidly during the transition of hypertrophy to heart failure. The degree of remodelling was correlated to the severity of the disease [215]. In addition, loss of T-tubule regularity was observed in failing human and rat cardiomyocytes [126]. The analysis of T-tubules arrangement in myocardium of mice subjected to TAC shows a

more regular pattern in the hpNFAT cons RNA decoy ODNs, while in the control animals presented detubulation of parts of cardiomyocytes. This observation can account for the severe heart function in the control group and for the progression of the disease into heart failure. More experiments have to be performed to address if NFAT is a direct factor of T-tubule disarrangement in the myocardium of mice subjected to TAC.

6.2.5 Remodeling of extracelular matrix in heart failure

Pressure overload or hypertension induces severe remodelling in the myocardium, associated with pro-inflammatory cells infiltration and extracellular matrix deposition. The amount of excess fibrotic tissue was shown to be correlated with the heart failure stage [178], proving the major role of this process in the development of the disease. Interstitial fibrosis is a beneficial event in the early stages of myocardium hypertrophy, being an adaptation to increased cardiomyocyte size. However, excessive collagen deposition due to chronic stress increases myocardium stiffness and decreases the contractility [39].
Previous studies on this topic show the emerging role of TGF-β in the progression of cardiac fibrosis. Transgenic mice overexpressing TGF-β show heart hypertrophy characterized by increased cardiomyocyte dimensions, as well as elevated fibrosis and abnormalities in heart function [171]. TGF-β inhibition ameliorates heart disease in a model of pressure overload and hypertension [113, 87]. Interestingly, TGF-β-mediated production of collagen 1 and fibronectin was proven to be NFAT-regulated in fibroblasts [238].
In the current study, the effect of hpNFAT RNA decoy ODNs on TAC-induced fibrosis was examined. As previously described [230], stenosis of the transverse aorta caused increased collagen deposition both in the interstitial and perivascular areas, as shown by Masson's Trichrome staining. However, the injection of the active AAV9 expressing hpNFAT cons RNA decoy ODNs decreased the fibrotic area. These results were confirmed on the mRNA level by a significant decrease in collagen 3, TGF-β and CTGF gene expression. The reduced fibrosis noted in AAV9 treated mice could account for the improvement in the cardiac performance.
In consistence to these results, NFAT inhibition through injection of FTY-720, a compound used in treatment for multiple sclerosis, was shown to reverse cardiac fibrosis in TAC-subjected mice [121]. Reduction in periostin protein level was proven to be responsible for this beneficial effect. This protein is an extracellular matrix component which is present in low amount in the myocardium on basal conditions, but its expression is remarkably increased in failing hearts [151]. Moreover, NFAT activity was shown to

be significantly higher in idiopathic pulmonary fibrosis, leading to intense lung remodelling and fibroblast proliferation [198].

6.2.6 NFAT transcription factors involved in heart hypertrophy

The designed decoy ODNs used in the present study are highly specific for NFAT1, NFAT2, NFAT3 and NFAT4. The four members are dephosphorylated by calcineurin and lead to the activation of the fetal gene program and initiation of hypertrophy [137]. The expression of all four proteins was detected in the myocardium [16]. NFAT1 deficiency ameliorated heart hypertrophy in a pressure-overload model, showing the importance of this transcription factor in the development of the disease [16]. NFAT3 associates with GATA4, GATA5 and GATA6 transcription factors to drive BNP expression [137]. NFAT4 deficient mice develop a low grade of calcineurin transgene-induced hypertrophy. However, the effect was incomplete, proving that other transcription are necessary for disease development [221].
The specificity of the decoy ODNs was shown by analysing NFAT5 activity *in vitro* after ODNs treatment. In contrast to NFAT1-4 transcription factors, which contain similar sequence identity, NFAT5 relates to the other members of the NFAT family only through the Rel-like DNA-binding domain and lacks the calcineurin-binding domain [124]. NFAT5 is involved in the response to osmotic stress by controlling transporter molecules and enzymes that replace electrolytes with uncharged organic compounds [32]. Homozygoous mice lacking NFAT5 showed embryonic lethality, impaired cardiomyocyte function, with reduced spontanous beating activity and decreased myocyte density [127]. Therefore, the assessment of NFAT5 activation in hpNFAT decoy ODNs treated cardiomyocytes was critical. The experiments demonstrated that neither the ”naked” hpNFAT decoy ODNs, nor AAV6 expressing the shRNA decoy ODNs affects NFAT5 nuclear translocation in osmotically challenged HL-1 cardiomyocytes. Moreover, there was no difference in the expression of genes involved in adaptation to osmotic stress. Taken together, these findings suggest that hpNFAT decoy ODNs treatment does not influence NFAT5 function.

6.2.7 Limitations and perspectives

The present study demonstrates an approach of preventing heart hypertrophy and its transition into heart failure, by RNA decoy ODNs which neutralize the activity of NFAT. The *in vivo* experimental model consisted of AAV9 injection two weeks prior to TAC, in order to allow the generation of the active RNA decoy ODNs in the myocardium.

Nevertheless, in the case of heart failure patients, a prophylactic AAV administration is not possible. Therefore, another set of experiments is required, which show the effect of the designed AAV9 after hypertrophy is established and ventricular dysfunction is noted.

Although AAV9 has tropism for muscle cells and the transduction efficiency of cardiomyocytes is high, this virus serotype was shown to transduce other organs and cell types [95]. The transduction efficiency of cardiomyocytes with AAV9, presented in this study, is consistent with previous published results [95, 152] which show an almost 100 % transduction efficiency of cardiomyocytes after tail-vein systemic delivery of AAV9. However, liver, skeletal muscle and lung transduction was also observed in mice, although the infection efficiency in these organs was proven to be much reduced as compared to the myocardium [61]. In addition, AAV9 was shown to be able to pass the brain blood barrier and transduce with high efficiency neuronal cells [61]. Nevertheless, for further successful and safe translation into a clinical approach, an AAV serotype with more specificity for the heart should be used. An AAV9 with targeted capsid to cardiomyocytes, selected from a random library, has been developed and was shown to target the heart [231]. Moreover, the AAV2 harbouring the cardiac myosin light chain promoter fused with CMV immediate-early enhancer [136] increased cardiomyocytes transduction efficiency following systemic injection, as compared to AAV2 containing CMV promoter. Moreover, the addition of a targeting capsid peptide to this new transcriptionally targeted AAV2 further improved vector specificity [136].

The mouse model of transverse aortic constriction is already a well-characterized heart hypertrophy system and allows the analysis of the molecular mechanisms of transition of hypertrophy into heart failure. The procedure mimics human aortic stenosis, making it a clinically relevant model to study the disease [44]. The main advantage of this model is the possibility to quantify the degree of stenosis by measuring the pressure gradient through the constriction site by means of echocardiography. TAC induces rapid cardiac dysfunction, as well as fibrosis [12] and depending on the needle size used to produce the banding, heart failure. One limitation of this model is the rapid onset of the stenosis, which cannot be correlated to the patient situation. TAC surgery is normally performed in young mice, which is also a difference to the clinical situation. Other approach for investigation of *in vivo* mechanisms of heart failure consist of genetically engineered mouse models, which do not entirely mimick the patient situation. In addition, isoproterenol treatment was shown to induce heart hypertrophy in mice, but a clear heart failure phenotype can be developed only with using high dosage of the catecholamine, which was shown to have high mortality rate in this model [71]. Therefore,

the effect of the described AAV9 vector on heart function could be studied in different animal models in which heart failure has different aetiology, such as hypertensive heart failure [173], neurohormonal stress models [102] or genetic models. This could expand the therapeutic application of the hpNFAT RNA decoy ODNs. Moreover, through this method, the role of NFAT in the progression of other types of heart disease could be investigated.
In addition, the use of a large animal model is a prerequisite for clinical translation. There are significant differences between the cardiovascular system of humans and mice in respect to oxygen consumption, heart rate and contractile protein expression [81], [49], making large animals experiments a critical step towards clinical application.
Moreover, the present study only proved the stable transduction of cardiomyocytes and hpNFAT decoy ODNs expression following AAV9 injection on a limited time span. However, before clinical translation, a long-term study should be performed to show the stability of the transgene in the cardiac tissue.

6.3 Conclusions

The recent advances in the discovery of molecular mechanisms of diseases made it possible to advance new therapeutic strategies targeting dysfunctional protein expression. The selective neutralization of transcription factor activity through decoy ODNs is one of the possibilities of altering gene expression. In this study, we proved successful RNA decoy ODNs generation through AAV transduction. This method allows the continuous downregulation of specific genes in target cells and can be applied to a variety of disorders with abnormal transcription factor activity. Moreover, the amount of hp decoy ODNs produced in transduced cells was proven to be sufficient to downregulate genes regulated by the transcription factor and to show a therapeutic effect.
The efficiency of this approach was demonstrated in two disease models, namely Marfan syndrome and heart hypertrophy in which blocking the activity of AP-1 and NFAT was aimed, respectively.
In the context of Marfan syndrome, the data presented show the possibility of delivering RNA decoy ODNs that neutralize AP-1 in aortic SMCs by means of an AAV construct. This allowed the transduction of the target cells, as well as endothelial cells, which afterwards expressed the active decoy ODNs in high amounts. Through this treatment, a significant reduction in the activity of the transcription factor was demonstrated, as shown by decreased downstream genes expression, as well as decreased number of elastin breaks in mgR/mgR grafts. The method proposed here could be further translated

into a new therapeutic approach to improve the characteristic elastin fibers remodelling observed in this Marfan syndrome model.

In the present study, the focus is limited on the development of a method to inhibit aortic aneurysm formation and dissection in the context of Marfan disease. However, the beneficial effects of AP-1 inhibition by hpAP-1 RNA decoy ODNs expressed through AAV9SLR transduction could be translated and explored in other vascular diseases with activated AP-1 activity or with inflammatory component. For example, abnormalities in SMCs function were observed in non-hereditary thoracic aneurysms, abdominal aneurysms [2] and aging-induced vascular calcification and hyperplasia [197]. Therefore, a similar method of transcription factor targeting could be evaluated in other disease models.

Reducing NFAT activity through the same concept by means of AAV9-mediated expression of hpNFAT decoy ODNs in cardiomyocytes was evaluated in an experimental model of pressure overload hypertrophy. AAV9-mediated hpNFAT RNA decoy ODNs generation into the myocardium decreased hypertrophic and fibrotic markers, and treated mice presented a significant improvement in heart function in comparison to controls. Additionally, heart failure marker LW/TL ration was dramatically reduced and the T tubule system structure was shown to be more regular than in control myocytes. In conclusion, AAV9 expressing hpNFAT decoy ODNs can prevent heart hypertrophy and inhibit its transition into heart failure. This approach shows, once again, the importance of inhibiting myocardium hypertrophy in order to prevent the transition into the decompensated phase of chronic heart failure.

7

Acknowledgements

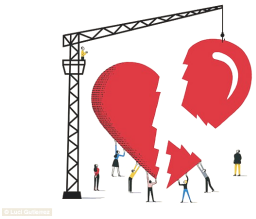

”It won’t be easy, but it will be worth it”

they say... And so it was. Everyone knows that PhD years are a demanding journey. You have to grow, you have to learn and become the person worthy of it. In a world aiming for instant gratification, you have to never lose focus, never give up and appreciate those who support you.

First of all, I would like to thank Prof. Hecker for the chance of working in the lab on two projects I loved and in which I invested inexhaustible passion, for his expert guidance and support. I am grateful to have worked with Andreas and Nina, the best supervisors anyone could ever hope for. I am happy to have met wonderful colleagues and friends in the Institute of Physiology and Pathophysiology, who were there for me when I needed advice, and especially Franzi, Nadine and Manu for technical support. Moreover, I must thank Gerd for all his help and patience with grant applications.

I have to express my gratitude to Prof. Kirsch and the whole Institute for Anatomy and Cell Biology, for the friendly working environment and for knowledgeable suggestions during progress reports. I am tremendously thankful to Prof. Oliver Müller and his lab for all their help and wonderful discussions, as well as to Prof. Klaus Kallenbach, Rawa and Max for their support with the surgeries, and to the liebe Antje, for all her assistence during these years.

Special thanks go to Markus, for always being there for me and supporting my much-needed coffee addiction, and to my lovely twin sister, my soul mate. I am indebted to my mom, for encouraging me and shaping who I am today. I will be forever thankful to have met my friends Herr Sachindra and Herr Elias, for being my two other musketeers, and to my SFB-friends, especially Laura, my ”partner in crime” for everything.

I couldn’t have done it alone... thank you, for helping me grow, learn and hopefully become the person worth it.

8

References

[1] Ágg B, Benke K, Szilveszter B, Pólos M, Daróczi L, Odler B, Nagy ZB, Tarr F, Merkely B, Szabolcs Z (2014) Possible extracardiac predictors of aortic dissection in Marfan syndrome. BMC Cardiovascular Disorders 14: 47

[2] Airhart N, Brownstein BH, Cobb JP, Schierding W, Arif B, Ennis TL, Thompson RW, Curci JA (2017) Smooth muscle cells from abdominal aortic aneurysms are unique and can independently and synergistically degrade insoluble elastin. Journal of Vascular Surgery 60: 1033–1042

[3] Akazawa H, Komuro I (2003) Roles of cardiac transcription factors in cardiac hypertrophy. Circulation Research 92: 1079–1088

[4] Arif R, Zaradzki M, Remes A, Seppelt P, Kunze R, Schröder H, Schwill S, Ensminger SM, Robinson PN, Karck M, Müller OJ, Hecker M, Wagner AH, Kallenbach K (2017) AP-1 oligodeoxynucleotides reduce aortic elastolysis in a murine model of Marfan syndrome. Molecular Therapy: Nucleic Acids 9: 69–79

[5] Atchison RW, Casto BC, Hammon WM (1965) Adenovirus-associated defective virus particles. Science 149: 754–755

[6] Bartlett JS, Wilcher R, Samulski RJ (2000) Infectious entry pathway of adeno-associated virus and adeno-associated virus vectors. J Virol 74: 2777–2785

[7] Bass GT, Ryall KA, Katikapalli A, Taylor BE, Dang ST, Acton ST, Saucerman JJ (2012) Automated image analysis identifies signaling pathways regulating distinct signatures of cardiac myocyte hypertrophy. Journal of Molecular and Cellular Cardiology 52: 923–930

[8] Bene A, Kurten RC, Chambers TC (2004) Subcellular localization as a limiting factor for utilization of decoy oligonucleotides. Nucleic Acids Res 32: e142–e142

[9] Benke K, Ágg B, Szilveszter B, Tarr F, Nagy ZB, Plos M, Darczi L, Merkely B, Szabolcs Z (2013) The role of transforming growth factor-β in Marfan syndrome. Cardiology Journal 3: 227–234

[10] Bera A, Sen D (2017) Promise of adeno-associated virus as a gene therapy vector for cardiovascular diseases. Heart Failure Reviews

[11] Bergman N MR, Cheng S, Honbo N, Piacentini L, Karliner JS, Lovett DH (2003) A functional AP-1 site regulates matrix metalloproteinase 2 transcription by cardiac cells through interactions with JunB-Fra1 and JunB-FosB heterodimers. Biochemical Journal 369: 485–496

[12] Bernardo BC, Nguyen SS, Gao XM, Tham YK, Ooi JYY, Patterson NL, Kiriazis H, Su Y, Thomas CJ, Lin RCY, Du XJ, McMullen JR (2016) Inhibition of miR-154 protects against cardiac dysfunction and fibrosis in a mouse model of pressure overload. Scientific Reports 6: 22442–22450

[13] Bernardo BC, Weeks KL, Pretorius L, McMullen JR (2010) Molecular distinction between physiological and pathological cardiac hypertrophy: Experimental findings and therapeutic strategies. Pharmacology & Therapeutics 128: 191 – 227

[14] Bickelhaupt S, Erbel C, Timke C, Wirkner U, Dadrich M, Flechsig P, Tietz A, Pfhler J, Gross W, Peschke P, Hoeltgen L, Katus HA, Grne HJ, Nicolay NH, Saffrich R, Debus J, Sternlicht MD, Seeley TW, Lipson KE, Huber PE (2017) Effects of CTGF blockade on attenuation and reversal of radiation-induced pulmonary fibrosis. JNCI: Journal of the National Cancer Institute 109: djw339

[15] Bostick B, Shin JH, Yue Y, Wasala NB, Lai Y, Duan D (2012) AAV microdystrophin gene therapy alleviates stress-induced cardiac death but not myocardial fibrosis in 21-m-old mdx mice, an end-stage model of Duchenne muscular dystrophy cardiomyopathy. Journal of Molecular and Cellular Cardiology 53: 217–222

[16] Bourajjaj M, Armand AS, da Costa Martins PA, Weijts B, van der Nagel R, Heeneman S, Wehrens XH, De Windt LJ (2008) NFATc2 is a necessary mediator of calcineurin-dependent cardiac hypertrophy and heart failure. Journal of Biological Chemistry 283: 22295–22303

[17] Brandenburger Y, Arthur JF, Woodcock EA, Du XJ, Gao Xm, Autelitano DJ, Rothblum LI, Hannan RD (2003) Cardiac hypertrophy *in vivo* is associated with increased expression of the ribosomal gene transcription factor UBF. FEBS Letters 548: 79–84

[18] Brandenburger Y, Jenkins A, Autelitano DJ, Hannan RD (2001) Increased expression of UBF is a critical determinant for rrna synthesis and hypertrophic growth of cardiac myocytes. The FASEB Journal 2051–2053

[19] Bridges AB, Gray JR, McLaren M, Tamei H, Belch JJF (1993) Endothelial cell and platelet function in Marfan's syndrome. Endothelium 1: 203–206

[20] Buchwald AB, Wagner AH, Webel C, Hecker M (2002) Decoy oligodeoxynucleotide against activator protein-1 reduces neointimal proliferation after coronary angioplasty in hypercholesterolemic minipigs. Journal of the American College of Cardiology 39: 732 – 738

[21] Bunton TE, Biery NJ, Myers L, Gayraud B, Ramirez F, Dietz HC (2001) Phenotypic alteration of vascular smooth muscle cells precedes elastolysis in a mouse model of Marfan syndrome. Circulation Research 88: 37–43

[22] Burchfield JS, Xie M, Hill JA (2013) Pathological ventricular remodeling. Circulation 128: 388–400

[23] Byrne M, Power J, Preovolos A, Mariani J, Hajjar R, Kaye D (2008) Recirculating cardiac delivery of AAV2/1SERCA2a improves myocardial function in an experimental model of heart failure in large animals. Gene Therapy 15: 1550–1557

[24] Cahill TJ, Ashrafian H, Watkins H (2013) Genetic cardiomyopathies causing heart failure. Circulation Research 113: 660–675

[25] Cameron VA, Aitken GD, Ellmers LJ, Kennedy MA, Espiner EA (1996) The sites of gene expression of atrial, brain, and C-type natriuretic peptides in mouse fetal development: temporal changes in embryos and placenta. Endocrinology 137: 817–824

[26] Campistol JM, Iigo P, Larios S, Bescos M, Oppenheimer F (2001) Role of TGF-β1 in the progression of chronic allograft nephropathy. Nephrology Dialysis Transplantation 16: 114–116

[27] Cao M, Khan JA, Kang BY, Mehta JL, Hermonat PL (2012) Dual AAV/IL-10 plus STAT3 anti-inflammatory gene delivery lowers atherosclerosis in LDLR KO mice, but without increased benefit. Int J Vasc Med 2012: 524235–52442

[28] Cao M, Theus SA, Straub KD, Figueroa JA, Mirandola L, Chiriva-Internati M, Hermonat PL (2015) AAV2/8-human FOXP3 gene therapy shows robust anti-atherosclerosis efficacy in ldlr-ko mice on high cholesterol diet. J Transl Med 13: 235–243

[29] Carta L, Smaldone S, Zilberberg L, Loch D, Dietz HC, Rifkin DB, Ramirez F (2009) p38 MAPK is an early determinant of promiscuous Smad2/3 signaling in the aortas of fibrillin-1-null mice. Journal of Biological Chemistry 284: 5630–5636

[30] Chen Y, Guo H, Xu D, Xu X, Wang H, Hu X, Lu Z, Kwak D, Xu Y, Gunther R, Huo Y, Weir EK (2012) Left ventricular failure produces profound lung remodel-

ing and pulmonary hypertension in mice: heart failure causes severe lung disease. Hypertension 59: 1170–1178

[31] Chen Y, McMicken HW (2003) Intracellular production of DNA enzyme by a novel single-stranded dna expression vector. Gene Ther 10: 1776–1780

[32] Cheung CY, Ko BC (2013) NFAT5 in cellular adaptation to hypertonic stress – regulations and functional significance. Journal of Molecular Signaling 8: 5–12

[33] Christelle L, Ali TH, Fanny B, Valeri M, An C, Florence C, Alexei B, Remi F (2007) Cell death in NFκB-dependent tumour cell lines as a result of NFκB trapping by linker-modified hairpin decoy oligonucleotide. FEBS Letters 581: 1143–1150

[34] Chung AW, Au Yeung K, Sandor GG, Judge DP, Dietz HC, van Breemen C (2007) Loss of elastic fiber integrity and reduction of vascular smooth muscle contraction resulting from the upregulated activities of matrix metalloproteinase-2 and -9 in the thoracic aortic aneurysm in Marfan syndrome. Circulation Research 101: 512–522

[35] Chung AW, Yang HHC, Radomski MW, van Breemen C (2008) Long-term doxycycline is more effective than atenolol to prevent thoracic aortic aneurysm in Marfan syndrome through the inhibition of matrix metalloproteinase-2 and -9. Circulation Research 102: 73–85

[36] Claycomb WC, Lanson NA, Stallworth BS, Egeland DB, Delcarpio JB, Bahinski A, Izzo NJ (1998) HL-1 cells: A cardiac muscle cell line that contracts and retains phenotypic characteristics of the adult cardiomyocyte. Proceedings of the National Academy of Sciences 95: 2979–2984

[37] Cohn RD, van Erp C, Habashi JP, Soleimani AA, Klein EC, Lisi MT, Gamradt M, ap Rhys CM, Holm TM, Loeys BL, Ramirez F, Judge DP, Ward CW, Dietz HC (2007) Angiotensin II type 1 receptor blockade attenuates TGF-β-induced failure of muscle regeneration in multiple myopathic states. Nat Med 13: 204–210

[38] Coselli JS, Volguina IV, LeMaire SA, Sundt TM, Connolly HM, Stephens EH, Schaff HV, Milewicz DM, Vricella LA, Dietz HC, Minard CG, Miller DC (2014) Early and 1-year outcomes of aortic root surgery in patients with Marfan syndrome: A prospective, multicenter, comparative study. The Journal of Thoracic and Cardiovascular Surgery 147: 1758–1767

[39] Creemers EE, Pinto YM (2011) Molecular mechanisms that control interstitial fibrosis in the pressure-overloaded heart. Cardiovascular Research 89: 265–272

[40] Crosas-Molist E, Meirelles T, López-Luque J, Serra-Peinado C, Selva J, Caja L, Gorbenko del Blanco D, Uriarte JJ, Bertran E, Mendizábal Y, Hernández V,

García-Calero C, Busnadiego O, Condom E, Toral D, Castellà M, Forteza A, Navajas D, Sarri E, Rodríguez-Pascual F, Dietz HC, Fabregat I, Egea G (2015) Vascular smooth muscle cell phenotypic changes in patients with Marfan syndrome. Arteriosclerosis, Thrombosis, and Vascular Biology 35: 960–972

[41] Dagenais GR, Yusuf S, Bourassa MG, Yi Q, Bosch J, Lonn EM, Kouz S, Grover J (2001) Effects of ramipril on coronary events in high-risk persons. Circulation 104: 522–526

[42] Davis E (1994) Immunolocalization of microfibril and microfibril-associated proteins in the subendothelial matrix of the developing mouse aorta. Journal of Cell Science 107: 727–736

[43] Daya S, Berns KI (2008) Gene therapy using adeno-associated virus vectors. Clin Microbiol Rev 21: 583–593

[44] deAlmeida AC, van Oort RJ, Wehrens XH (2010) Transverse aortic constriction in mice. J Vis Exp 1729–1736

[45] Dearth CL, Goh Q, Marino JS, Cicinelli PA, Torres-Palsa MJ, Pierre P, Worth RG, Pizza FX (2013) Skeletal muscle cells express ICAM-1 after muscle overload and ICAM-1 contributes to the ensuing hypertrophic response. PLOS ONE 8: 1–13

[46] Dhr S, Torres-Montaner A, Astola A, Garca-Cozar FJ, Pendn C, Bolvar J, Valdivia MM (2001) Short communication: Molecular analysis of the 5 region of human ribosomal transcription factor UBF. DNA Sequence 12: 267–272

[47] Dichtl W, Dulak J, Frick M, Alber HF, Schwarzacher SP, Ares MP, Nilsson J, Pachinger O, Weidinger F (2003) HMG-CoA reductase inhibitors regulate inflammatory transcription factors in human endothelial and vascular smooth muscle cells. Arteriosclerosis, Thrombosis, and Vascular Biology 23: 58–63

[48] Diwan A, Dorn GW (2007) Decompensation of cardiac hypertrophy: Cellular mechanisms and novel therapeutic targets. Physiology 22: 56–64

[49] Dixon JA, Spinale FG (2009) Large animal models of heart failure. Circulation: Heart Failure 2: 262–271

[50] Dorn GW, Robbins J, Sugden PH (2003) Phenotyping hypertrophy. Circulation Research 92: 1171–1175

[51] Drawnel FM, Archer CR, Roderick HL (2013) The role of the paracrine/autocrine mediator endothelin-1 in regulation of cardiac contractility and growth. British Journal of Pharmacology 168: 296–317

[52] Duan DD (2010) A leakage leads to failure. Hypertension 55: 849–851

[53] Dufour A, Sampson NS, Li J, Kuscu C, Rizzo RC, DeLeon JL, Zhi J, Jaber N, Liu E, Zucker S, Cao J (2011) Small-molecule anticancer compounds selectively

target the hemopexin domain of matrix metalloproteinase-9. Cancer Research 71: 4977–4988

[54] Eaton SL, Roche SL, Llavero Hurtado M, Oldknow KJ, Farquharson C, Gillingwater TH, Wishart TM (2013) Total protein analysis as a reliable loading control for quantitative fluorescent western blotting. PLOS ONE 8: 1–9

[55] Eduardo Carreño J, Apablaza F, Ocaranza MP, Jalil JE (2006) Cardiac hypertrophy: Molecular and cellular events. Revista Española de Cardiología (English Edition) 59: 473–486

[56] Ehlermann J, Pfisterer P, Schorle H (2003) Dynamic expression of Krppel-like factor 4 (Klf4), a target of transcription factor AP-2α during murine mid-embryogenesis. The Anatomical Record Part A: Discoveries in Molecular, Cellular, and Evolutionary Biology 273A: 677–680

[57] Ejiri J, Inoue N, Tsukube T, Munezane T, Hino Y, Kobayashi S, Hirata Ki, Kawashima S, Imajoh-Ohmi S, Hayashi Y, Yokozaki H, Okita Y, Yokoyama M (2003) Oxidative stress in the pathogenesis of thoracic aortic aneurysm. Protective role of statin and angiotensin II type 1 receptor blocker. Cardiovascular Research 59: 988–996

[58] Esposito G, Rapacciuolo A, Naga Prasad SV, Takaoka H, Thomas SA, Koch WJ, Rockman HA (2002) Genetic alterations that inhibit in vivo pressure-overload hypertrophy prevent cardiac dysfunction despite increased wall stress. Circulation 105: 85–92

[59] Finkbohner R, Johnston D, Crawford ES, Coselli J, Milewicz DM (1995) Marfan syndrome. Circulation 91: 728–733

[60] Flanagan WM, Corthesy B, Bram RJ, Crabtree GR (1991) Nuclear association of a T-cell transcription factor blocked by FK-506 and cyclosporin A. Nature 352: 803–807

[61] Foust KD, Nurre E, Montgomery CL, Hernandez A, Chan CM, Kaspar BK (2009) Intravascular AAV9 preferentially targets neonatal neurons and adult astrocytes. Nat Biotech 27: 59–65

[62] Frank K, Kranias EG (2000) Phospholamban and cardiac contractility. Annals of Medicine 32: 572–578

[63] Franken R, den Hartog A, Radonic T, Micha D, Maugeri A, van Dijk FS, Meijers-Heijboer HE, Timmermans J, Scholte AJ, van den Berg MP, Groenink M, Mulder BJ, Zwinderman AH, de Waard V, Pals G (2015) Beneficial outcome of losartan therapy depends on type of FBN1 mutation in Marfan syndrome. Circulation: Cardiovascular Genetics 8: 383–388

[64] Frey N, Katus HA, Olson EN, Hill JA (2004) Hypertrophy of the heart. Circulation 109: 1580–1589

[65] Frisk M, Koivumäki JT, Norseng PA, Maleckar MM, Sejersted OM, Louch WE (2014) Variable T-tubule organization and calcium homeostasis across the atria. American Journal of Physiology - Heart and Circulatory Physiology 307: H609–H620

[66] Fujiwara Y, Wada K, Kabuta T (2017) Lysosomal degradation of intracellular nucleic acidsmultiple autophagic pathways. The Journal of Biochemistry 161: 145–154

[67] Gao L, Mao Q, Wen D, Zhang L, Zhou X, Hui R (2011) The effect of beta-blocker therapy on progressive aortic dilatation in children and adolescents with Marfans syndrome: a meta-analysis. Acta Paediatrica 100: 101–105

[68] Garcia-Chaumont C, Seksek O, Grzybowska J, Borowski E, Bolard J (2000) Delivery systems for antisense oligonucleotides. Pharmacology & Therapeutics 87: 255–277

[69] Garcia-Menendez L, Karamanlidis G, Kolwicz S, Tian R (2013) Substrain specific response to cardiac pressure overload in C57BL/6 mice. Am J Physiol Heart Circ Physiol 305: H397–H402

[70] Gersony DR, McClaughlin MA, Jin Z, Gersony WM (2006) The effect of beta-blocker therapy on clinical outcome in patients with Marfan's syndrome: A meta-analysis. International Journal of Cardiology 114: 303–308

[71] Gomes AC, Falcão-Pires I, Pires AL, Brás-Silva C, Leite-Moreira AF (2013) Rodent models of heart failure: an updated review. Heart Failure Reviews 2: 219–249

[72] Granata A, Serrano F, Bernard WG, McNamara M, Low L, Sastry P, Sinha S (2017) An iPSC-derived vascular model of Marfan syndrome identifies key mediators of smooth muscle cell death. Nat Genet 49: 97–109

[73] Grimm D, Kay MA, Kleinschmidt JA (2003) Helper virus-free, optically controllable, and two-plasmid-based production of adeno-associated virus vectors of serotypes 1 to 6. Molecular Therapy 7: 839–850

[74] Guo A, Zhang C, Wei S, Chen B, Song LS (2013) Emerging mechanisms of T-tubule remodelling in heart failure. Cardiovascular Research 98: 204–215

[75] Guo G, Booms P, Halushka M, Dietz HC, Ney A, Stricker S, Hecht J, Mundlos S, Robinson PN (2006) Induction of macrophage chemotaxis by aortic extracts of the mgr Marfan mouse model and a GxxPG-containing fibrillin-1 fragment. Circulation 114: 1855–1862

[76] Guo G, Gehle P, Doelken S, Martin-Ventura JL, von Kodolitsch Y, Hetzer R, Robinson PN (2011) Induction of macrophage chemotaxis by aortic extracts from patients with Marfan syndrome is related to elastin binding protein. PLoS One 6: 1855–62

[77] Guo G, Muoz-Garca B, Ott CE, Grnhagen J, Mousa SA, Pletschacher A, von Kodolitsch Y, Knaus P, Robinson PN (2013) Antagonism of GxxPG fragments ameliorates manifestations of aortic disease in Marfan syndrome mice. Human Molecular Genetics 22: 433–443

[78] Guo G, Ott CE, Grnhagen J, Muoz-Garca B, Pletschacher A, Kallenbach K, von Kodolitsch Y, Robinson P (2013) Indomethacin prevents the progression of thoracic aortic aneurysm in Marfan syndrome mice. Aorta 1: 5–12

[79] Gupta M, Zak R (1992) Reversibility of load-induced changes in myosin heavy chain gene expression. American Journal of Physiology - Regulatory, Integrative and Comparative Physiology 262: 346–349

[80] Habashi JP, Judge DP, Holm TM, Cohn RD, Loeys BL, Cooper TK, Myers L, Klein EC, Liu G, Calvi C, Podowski M, Neptune ER, Halushka MK, Bedja D, Gabrielson K, Rifkin DB, Carta L, Ramirez F, Huso DL, Dietz HC (2006) Losartan, an AT1 antagonist, prevents aortic aneurysm in a mouse model of Marfan syndrome. Science 312: 117–121

[81] Haghighi K, Kolokathis F, Pater L, Lynch RA, Asahi M, Gramolini AO, Fan GC, Tsiapras D, Hahn HS, Adamopoulos S, Liggett SB, II GWD, MacLennan DH, Kremastinos DT, Kranias EG (2003) Human phospholamban null results in lethal dilated cardiomyopathy revealing a critical difference between mouse and human. The Journal of Clinical Investigation 111: 869–876

[82] Han P, Li W, Lin CH, Yang J, Shang C, Nurnberg ST, Jin KK, Xu W, Lin CY, Lin CJ, Xiong Y, Chien HC, Zhou B, Ashley E, Bernstein D, Chen PS, Chen HSV, Quertermous T, Chang CP (2014) A long noncoding RNA protects the heart from pathological hypertrophy. Nature 514: 102–106

[83] Hannan R, Jenkins A, Jenkins A, Brandenburger Y (2003) Cardiac hypertrophy: A matter of translation. Clinical and Experimental Pharmacology and Physiology 30: 517–527

[84] Harding SE (2005) The failing cardiomyocyte. Heart Failure Clinics 1: 171–181

[85] Hecker M, Wagner AH (2017) Transcription factor decoy technology: A therapeutic update. Biochemical Pharmacology 144: 29 – 34

[86] Hecker M, Wagner S, Henning SH, Wagner AH (2008) Therapeutic Oligonucleotides, chap. Decoy oligodeoxynucleotides to treat inflammatory diseases,

Chapter 8, 163188. The name of the publisher, Royal Society of Chemistry

[87] Hocher B, Godes M, Olivier J, Weil J, Eschenhagen T, Slowinski T, Neumayer HH, Bauer C, Paul M, Pinto Y (2002) Inhibition of left ventricular fibrosis by tranilast in rats with renovascular hypertension. Journal of hypertension 20: 745–51

[88] Holm TM, Habashi JP, Doyle JJ, Bedja D, Chen Y, van Erp C, Lindsay ME, Kim D, Schoenhoff F, Cohn RD, Loeys BL, Thomas CJ, Patnaik S, Marugan JJ, Judge DP, Dietz HC (2011) Noncanonical TGF-β signaling contributes to aortic aneurysm progression in Marfan syndrome mice. Science 332: 358–361

[89] Hong HM, Song EJ, Oh E, Kabir MH, Lee C, Yoo YS (2011) Endothelin-1- and isoproterenol-induced differential protein expression and signaling pathway in HL-1 cardiomyocytes. Proteomics 11: 283–297

[90] Horbelt D, Guo G, Robinson PN, Knaus P (2010) Quantitative analysis of TGFβR2 mutations in Marfan-syndrome-related disorders suggests a correlation between phenotypic severity and Smad signaling activity. Journal of Cell Science 123: 4340–4350

[91] Hulot JS, Ishikawa K, Hajjar RJ (2016) Gene therapy for the treatment of heart failure: promise postponed. European Heart Journal 37: 1651–1658

[92] Ijaz T, Tilton RG, Brasier AR (2016) Cytokine amplification and macrophage effector functions in aortic inflammation and abdominal aortic aneurysm formation. Journal of Thoracic Disease 8: 746–754

[93] Ikonomidis JS, Barbour JR, Amani Z, Stroud RE, Herron AR, McClister DM, Camens SE, Lindsey ML, Mukherjee R, Spinale FG (2005) Effects of deletion of the Matrix Metalloproteinase 9 gene on development of murine thoracic aortic aneurysms. Circulation 112: 242–248

[94] Ikonomidis JS, Jones JA, Barbour JR, Stroud RE, Clark LL, Kaplan BS, Zeeshan A, Bavaria JE, Gorman JH, Spinale FG, Gorman RC (2006) Expression of matrix metalloproteinases and endogenous inhibitors within ascending aortic aneurysms of patients with Marfan syndrome. Circulation 114: 365–370

[95] Inagaki K, Fuess S, Storm TA, Gibson GA, Mctiernan CF, Kay MA, Nakai H (2006) Robust systemic transduction with AAV9 vectors in mice: Efficient global cardiac gene transfer superior to that of AAV8. Mol Ther 14: 45–53

[96] Jensen EC (2013) Quantitative analysis of histological staining and fluorescence using ImageJ. The Anatomical Record 296: 378–381

[97] Jiang J, Wakimoto H, Seidman JG, Seidman CE (2013) Allele-specific silencing of mutant MYH6 transcripts in mice suppresses hypertrophic cardiomyopathy.

Science 342: 111–114

[98] Jo N, Ogata N, Aoki M, Otsuji T, Morishita R, Kaneda Y, Matsumura M (2002) Effective transfection of a cis element decoy of the nuclear factor-κB binding site into the experimental choroidal neovascularization. Current Eye Research 24: 465–473

[99] Kaartinen V, Warburton D (2003) Fibrillin controls TGF-β activation. Nat Genet 33: 331–332

[100] Kawamura T, Ono K, Morimoto T, Akao M, Iwai-Kanai E, Wada H, Sowa N, Kita T, Hasegawa K (2004) Endothelin-1 dependent Nuclear Factor of Activated T Lymphocyte signaling associates with transcriptional coactivator p300 in the activation of the B cell leukemia-2 promoter in cardiac myocytes. Circulation Research 94: 1492–1499

[101] Keane MG, Pyeritz RE (2008) Medical management of Marfan syndrome. Circulation 117: 2802–2813

[102] Kim JB, Porreca GJ, Song L, Greenway SC, Gorham JM, Church GM, Seidman CE, Seidman JG (2007) Polony multiplex analysis of gene expression (PMAGE) in mouse hypertrophic cardiomyopathy. Science 316: 1481–1484

[103] Kimura B, Mohuczy D, Tang X, Phillips MI (2001) Attenuation of hypertension and heart hypertrophy by adeno-associated virus delivering angiotensinogen antisense. Hypertension 37: 376–380

[104] Koglin J, Pehlivanli S, Schwaiblmair M, Vogeser M, Cremer P, von Scheidt W (2001) Role of brain natriuretic peptide in risk stratification of patients with congestive heart failure. Journal of the American College of Cardiology 38: 1934 – 1941

[105] Kohli S, Ahuja S, Rani V (2011) Transcription factors in heart: Promising therapeutic targets in cardiac hypertrophy. Curr Cardiol Rev 7: 262–271

[106] Koitabashi N, Kass DA (2012) Reverse remodeling in heart failure - mechanisms and therapeutic opportunities. Nat Rev Cardiol 9: 147–157

[107] Kotterman MA, Schaffer DV (2014) Engineering adeno-associated viruses for clinical gene therapy. Nat Rev Genet 15: 445–451

[108] Krenz M, Robbins J (2004) Impact of β-myosin heavy chain expression on cardiac function during stress. Journal of the American College of Cardiology 44: 2390 – 2397

[109] Krenz M, Sanbe A, Bouyer-Dalloz F, Gulick J, Klevitsky R, Hewett TE, Osinska HE, Lorenz JN, Brosseau C, Federico A, Alpert NR, Warshaw DM, Perryman

MB, Helmke SM, Robbins J (2003) Analysis of myosin heavy chain functionality in the heart. Journal of Biological Chemistry 278: 17466–17474

[110] Krum H, Abraham WT (2005) Heart failure. The Lancet 373: 941–955

[111] Kumar P, Shen Q, Pivetti CD, Lee ES, Wu MH, Yuan SY (2009) Molecular mechanisms of endothelial hyperpermeability: implications in inflammation. Expert Reviews in Molecular Medicine 11

[112] Kuriyama M, Matsushita M, Tateishi A, Moriwaki A, Tomizawa K, Ishino K, Sano S, Matsui H (2006) A cell-permeable NFAT inhibitor peptide prevents pressure-overload cardiac hypertrophy. Chemical Biology and Drug Design 67: 238–243

[113] Kuwahara F, Kai H, Tokuda K, Kai M, Takeshita A, Egashira K, Imaizumi T (2002) Transforming growth factor-β function blocking prevents myocardial fibrosis and diastolic dysfunction in pressure-overloaded rats. Circulation 106: 130–135

[114] Lee HJ, Kim YS, Sato Y, Cho YJ (2009) RCAN1-4 knockdown attenuates cell growth through the inhibition of Ras signaling. FEBS Letters 583: 2557–2564

[115] Lehmann LH, Rostosky JS, Buss SJ, Kreusser MM, Krebs J, Mier W, Enseleit F, Spiger K, Hardt SE, Wieland T, Haass M, Lscher TF, Schneider MD, Parlato R, Grne HJ, Haberkorn U, Yanagisawa M, Katus HA, Backs J (2014) Essential role of sympathetic endothelin A receptors for adverse cardiac remodeling. Proceedings of the National Academy of Sciences 111: 13499–13504

[116] Levy D, Garrison RJ, Savage DD, Kannel WB, Castelli WP (1990) Prognostic implications of echocardiographically determined left ventricular mass in the Framingham heart study. New England Journal of Medicine 322: 1561–1566

[117] Li M, Abdollahi A, Gröne HJ, Lipson KE, Belka C, Huber PE (2009) Late treatment with imatinib mesylate ameliorates radiation-induced lung fibrosis in a mouse model. Radiation Oncology 4: 66–75

[118] Li YT, He B, Wang YZ, Wang J (2009) Effects of intratracheal administration of NFκB decoy oligodeoxynucleotides on long-term cigarette smoke-induced lung inflammation and pathology in mice. Respiratory Research 10: 79–93

[119] Lim DS, Lutucuta S, Bachireddy P, Youker K, Evans A, Entman M, Roberts R, Marian AJ (2001) Angiotensin II blockade reverses myocardial fibrosis in a transgenic mouse model of human hypertrophic cardiomyopathy. Circulation 103: 789–791

[120] Lin JC, Lin SC, Chen WY, Yen YT, Lai CW, Tao MH, Lin YL, Miaw SC, Wu-Hsieh BA (2014) Dengue viral protease interaction with NFκB inhibitor results

in endothelial cell apoptosis and hemorrhage development. The Journal of Immunology 193: 1258–1267

[121] Liu W, Zi M, Tsui H, Chowdhury SK, Zeef L, Meng QJ, Travis M, Prehar S, Berry A, Hanley NA, Neyses L, Xiao RP, Oceandy D, Ke Y, Solaro RJ, Cartwright EJ, Lei M, Wang X (2013) A novel immunomodulator, FTY-720 reverses existing cardiac hypertrophy and fibrosis from pressure overload by targeting NFAT signaling and periostin: Clinical perspective. Circulation: Heart Failure 6: 833–844

[122] Liu Y, Sinha S, McDonald OG, Shang Y, Hoofnagle MH, Owens GK (2005) Kruppel-like factor 4 abrogates myocardin-induced activation of smooth muscle gene expression. Journal of Biological Chemistry 280: 9719–9727

[123] López JE, Myagmar BE, Swigart PM, Montgomery MD, Haynam S, Bigos M, Rodrigo MC, Simpson PC (2011) β-myosin heavy chain is induced by pressure overload in a minor subpopulation of smaller mouse cardiac myocytes. Novelty and significance. Circulation Research 109: 629–638

[124] Lopez-Rodrguez C, Aramburu J, Rakeman A, Rao A (1999) NFAT5, a constitutively nuclear NFAT protein that does not cooperate with Fos and Jun. Proceedings of the National Academy of Sciences of the United States of America 96: 7214–7219

[125] LR G (2010) Heart failure. Annals of Internal Medicine 152: ITC6–1

[126] Lyon AR, MacLeod KT, Zhang Y, Garcia E, Kanda GK, Lab MJ, Korchev YE, Harding SE, Gorelik J (2009) Loss of T-tubules and other changes to surface topography in ventricular myocytes from failing human and rat heart. Proceedings of the National Academy of Sciences 106: 6854–6859

[127] Mak MC, Lam KM, Chan PK, Lau YB, Tang WH, Yeung PKK, Ko BCB, Chung SMS, Chung SK (2011) Embryonic lethality in mice lacking the nuclear factor of activated T cells 5 protein due to impaired cardiac development and function. PLOS ONE 6: 1–8

[128] Manea A, Manea SA, Gafencu AV, Raicu M, Simionescu M (2008) AP-1 dependent transcriptional regulation of NADPH oxidase in human aortic smooth muscle cells. Arteriosclerosis, Thrombosis, and Vascular Biology 28: 878–885

[129] Mao N, Gu T, Shi E, Zhang G, Yu L, Wang C (2015) Phenotypic switching of vascular smooth muscle cells in animal model of rat thoracic aortic aneurysm. Interactive CardioVascular and Thoracic Surgery 21: 62–70

[130] Matt P, Schoenhoff F, Habashi J, Holm T, Van Erp C, Loch D, Carlson OD, Griswold BF, Fu Q, De Backer J, Loeys B, Huso DL, McDonnell NB, Van Eyk JE, Di-

etz HC (2009) Circulating Transforming Growth Factor-β in Marfan syndrome. Circulation 120: 526–532

[131] McCormick ML, Gavrila D, Weintraub NL (2007) Role of oxidative stress in the pathogenesis of abdominal aortic aneurysms. Arteriosclerosis, Thrombosis, and Vascular Biology 27: 461–469

[132] McLoughlin D, McGuinness J, Byrne J, Terzo E, Huuskonen V, McAllister H, Black A, Kearney S, Kay E, Hill AD, Dietz HC, Redmond JM (2011) Pravastatin reduces Marfan aortic dilation. Circulation 124: S168–S173

[133] Mietzsch M, Broecker F, Reinhardt A, Seeberger PH, Heilbronn R (2014) Differential adeno-associated virus serotype-specific interaction patterns with synthetic heparins and other glycans. Journal of Virology 88: 2991–3003

[134] Miyake T, Aoki M, Nakashima H, Kawasaki T, Oishi M, Kataoka K, Tanemoto K, Ogihara T, Kaneda Y, Morishita R (2006) Prevention of abdominal aortic aneurysms by simultaneous inhibition of NFκB and ets using chimeric decoy oligonucleotides in a rabbit model. Gene Ther 13: 695–704

[135] Miyake T, Aoki M, Osako MK, Shimamura M, Nakagami H, Morishita R (2010) Systemic administration of ribbon-type decoy oligodeoxynucleotide against NFκB prevents abdominal aortic aneurysm in rat model. Molecular Therapy 19: 181–187

[136] Mller OJ, Leuchs B, Pleger ST, Grimm D, Franz WM, Katus HA, Kleinschmidt JA (2006) Improved cardiac gene transfer by transcriptional and transductional targeting of adeno-associated viral vectors. Cardiovascular Research 70: 70–78

[137] Molkentin JD, Lu JR, Antos CL, Markham B, Richardson J, Robbins J, Grant SR, Olson EN (1998) A calcineurin-dependent transcriptional pathway for cardiac hypertrophy. Cell 93: 215–228

[138] Morihara H, Yamamoto T, Oiwa H, Tonegawa K, Tsuchiyama D, Kawakatsu I, Obana M, Maeda M, Mohri T, Obika S, Fujio Y, Nakayama H (2016) Phospholamban inhibition by a single dose of locked nucleic acid antisense oligonucleotide improves cardiac contractility in pressure overload-induced systolic dysfunction in mice. Journal of Cardiovascular Pharmacology and Therapeutics 22: 273–282

[139] Morishita R, Sugimoto T, Aoki M, Kida I, Tomita N, Moriguchi A, Maeda K, Sawa Y, Kaneda Y, Higaki J, Ogihara T (1997) In vivo transfection of cis element decoy against nuclear factor-κb binding site prevents myocardial infarction. Nat Med 3: 894–899

[140] Muller OJ, Kaul F, Weitzman MD, Pasqualini R, Arap W, Kleinschmidt JA, Trepel M (2003) Random peptide libraries displayed on adeno-associated virus to select for targeted gene therapy vectors. Nat Biotech 21: 1040–1046

[141] Murdoch JL, Walker BA, Halpern BL, Kuzma JW, McKusick VA (1972) Life expectancy and causes of death in the Marfan syndrome. New England Journal of Medicine 286: 804–808

[142] Nagai R, Low RB, Stirewalt WS, Alpert NR, Litten RZ (1988) Efficiency and capacity of protein synthesis are increased in pressure overload cardiac hypertrophy. American Journal of Physiology - Heart and Circulatory Physiology 255: 325–328

[143] Nagatomo Y, Carabello BA, Hamawaki M, Nemoto S, Matsuo T, McDermott PJ (1999) Translational mechanisms accelerate the rate of protein synthesis during canine pressure-overload hypertrophy. American Journal of Physiology - Heart and Circulatory Physiology 277: 2176–2184

[144] Nakamura H, Aoki M, Tamai K, Oishi M, Ogihara T, Kaneda Y, Morishita R (2002) Prevention and regression of atopic dermatitis by ointment containing NFκB decoy oligodeoxynucleotides in NC/Nga atopic mice model. Journal of Allergy and Clinical Immunology 109: S86–S87

[145] Naso MF, Tomkowicz B, Perry WL, Strohl WR (2017) Adeno-associated virus (AAV) as a vector for gene therapy. BioDrugs 31: 317–334

[146] Nataatmadja M, West M, West J, Summers K, Walker P, Nagata M, Watanabe T (2003) Abnormal extracellular matrix protein transport associated with increased apoptosis of vascular smooth muscle cells in Marfan syndrome and bicuspid aortic valve thoracic aortic aneurysm. Circulation 108: 329—334

[147] Nathwani AC, Tuddenham EG, Rangarajan S, Rosales C, McIntosh J, Linch DC, Chowdary P, Riddell A, Pie AJ, Harrington C, O'Beirne J, Smith K, Pasi J, Glader B, Rustagi P, Ng CY, Kay MA, Zhou J, Spence Y, Morton CL, Allay J, Coleman J, Sleep S, Cunningham JM, Srivastava D, Basner-Tschakarjan E, Mingozzi F, High KA, Gray JT, Reiss UM, Nienhuis AW, Davidoff AM (2011) Adenovirus-associated virus vector mediated gene transfer in Hemophilia B. New England Journal of Medicine 365: 2357–2365

[148] Naud P, Guasch E, Nattel S (2010) Physiological versus pathological cardiac electrical remodelling: potential basis and relevance to clinical management. J Physiol 588: 4855–4856

[149] Neptune ER, Frischmeyer PA, Arking DE, Myers L, Bunton TE, Gayraud B, Ramirez F, Sakai LY, Dietz HC (2003) Dysregulation of TGF-β activation con-

tributes to pathogenesis in Marfan syndrome. Nat Genet 33: 407–411

[150] Ng CM, Cheng A, Myers LA, Martinez-Murillo F, Jie C, Bedja D, Gabrielson KL, Hausladen JM, Mecham RP, Judge DP, Dietz HC (2004) TGF-βdependent pathogenesis of mitral valve prolapse in a mouse model of Marfan syndrome. The Journal of Clinical Investigation 114: 1586–1592

[151] Oka T, Xu J, Kaiser RA, Melendez J, Hambleton M, Sargent MA, Lorts A, Brunskill EW, Dorn GW, Conway SJ, Aronow BJ, Robbins J, Molkentin JD (2007) Genetic manipulation of periostin expression reveals a role in cardiac hypertrophy and ventricular remodeling. Circulation Research 101: 313–321

[152] Pacak CA, Mah CS, Thattaliyath BD, Conlon TJ, Lewis MA, Cloutier DE, Zolotukhin I, Tarantal AF, Byrne BJ (2006) Recombinant AAV9 leads to preferential cardiac transduction in vivo. Circulation Research 99: 3–9

[153] Pachori AS, Melo LG, Zhang L, Loda M, Pratt RE, Dzau VJ (2004) Potential for germ line transmission after intramyocardial gene delivery by adeno-associated virus. Biochemical and Biophysical Research Communications 3: 528–533

[154] Pasumarthi KB, Field LJ (2002) Cardiomyocyte cell cycle regulation. Circulation Research 90: 1044–1054

[155] Pazos-López P, Peteiro-Vázquez J, Carcía-Campos A, García-Bueno L, de Torres JPA, Castro-Beiras A (2011) The causes, consequences, and treatment of left or right heart failure. Vasc Health Risk Manag 7: 237–254

[156] Pereira L, Lee SY, Gayraud B, Andrikopoulos K, Shapiro SD, Bunton T, Biery NJ, Dietz HC, Sakai LY, Ramirez F (1999) Pathogenetic sequence for aneurysm revealed in mice underexpressing fibrillin-1. Proceedings of the National Academy of Sciences 96: 3819–3823

[157] Peter AK, Bjerke MA, Leinwand LA (2016) Biology of the cardiac myocyte in heart disease. Molecular Biology of the Cell 27: 2149–2160

[158] Pfaff MW (2001) A new mathematical model for relative quantification in real-time RT PCR. Nucleic Acids Res 29: 2003–2007

[159] Pikkarainen S, Kerkelä R, Pöntinen J, Majalahti-Palviainen T, Tokola H, Eskelinen S, Vuolteenaho O, Ruskoaho H (2002) Decoy oligonucleotide characterization of GATA-4 transcription factor in hypertrophic agonist induced responses of cardiac myocytes. Journal of Molecular Medicine 80: 51–60

[160] Pillay S, Meyer NL, Puschnik AS, Davulcu O, Diep J, Ishikawa Y, Jae LT, Wosen JE, Nagamine CM, Chapman MS, Carette JE (2016) An essential receptor for adeno-associated virus infection. Nature 530: 108–112

[161] Piva R, Gambari R (2002) Transcription factor decoy (TFD) in breast cancer research and treatment. Technology in Cancer Research & Treatment 1: 405–416

[162] Raake PW, Schlegel P, Ksienzyk J, Reinkober J, Barthelmes J, Schinkel S, Pleger S, Mier W, Haberkorn U, Koch WJ, Katus HA, Most P, Mller OJ (2013) AAV6 βARKct cardiac gene therapy ameliorates cardiac function and normalizes the catecholaminergic axis in a clinically relevant large animal heart failure model. European Heart Journal 34: 1437–1447

[163] Rad SMAH, Bamdad T, Sadeghizadeh M, Arefian E, Lotfinia M, Ghanipour M (2015) Transcription factor decoy against stem cells master regulators, Nanog and Oct-4: a possible approach for differentiation therapy. Tumor Biology 36: 2621–2629

[164] Radonic T, de Witte P, Groenink M, de Waard V, Lutter R, van Eijk M, Jansen M, Timmermans J, Kempers M, Scholte AJ, Hilhorst-Hofstee Y, van den Berg MP, van Tintelen JP, Pals G, Baars MJH, Mulder BJM, Zwinderman AH (2012) Inflammation aggravates disease severity in Marfan syndrome patients. PLOS ONE 7: 1–9

[165] Rao RK, Basuroy S, Rao VU, Karnaky Jr KJ, Gupta A (2002) Tyrosine phosphorylation and dissociation of occludin-ZO-1 and E-cadherin-β-catenin complexes from the cytoskeleton by oxidative stress. Biochem J 368: 471–481

[166] Reinkober J, Tscheschner H, Pleger ST, Most P, Katus HA, Koch WJ, Raake PWJ (2012) Targeting GRK2 by gene therapy for heart failure: benefits above β-blockade. Gene Ther 19: 686–693

[167] Reiser PJ, Portman MA, Ning XH, Moravec CS (2001) Human cardiac myosin heavy chain isoforms in fetal and failing adult atria and ventricles. American Journal of Physiology - Heart and Circulatory Physiology 280: H1814–H1820

[168] Rincon MY, VandenDriessche T, Chuah MK (2015) Gene therapy for cardiovascular disease: advances in vector development, targeting, and delivery for clinical translation. Cardiovascular Research 108: 4–20

[169] Robinson PN, Godfrey M (2000) The molecular genetics of Marfan syndrome and related microfibrillopathies. Journal of Medical Genetics 37: 9–25

[170] Romaniello F, Mazzaglia D, Pellegrino A, Grego S, Fiorito R, Ferlosio A, Chiariello L, Orlandi A (2014) Aortopathy in Marfan syndrome: an update. Cardiovascular Pathology 23: 261–266

[171] Rosenkranz S, Flesch M, Amann K, Haeuseler C, Kilter H, Seeland U, Schlüter KD, Böhm M (2002) Alterations of β-adrenergic signaling and cardiac hypertro-

phy in transgenic mice overexpressing TGF-β. American Journal of Physiology - Heart and Circulatory Physiology 283: H1253–H1262

[172] Ruiz-Ortega M, Lorenzo Ó, Rupérez M, Blanco J, Egido J (2001) Systemic infusion of angiotensin II into normal rats activates nuclear factor- and AP-1 in the kidney. The American Journal of Pathology 158: 1743–1756

[173] Rysä J, Leskinen H, Ilves M, Ruskoaho H (2005) Distinct upregulation of extracellular matrix genes in transition from hypertrophy to hypertensive heart failure. Hypertension 45: 927–933

[174] Sakai S, Kimura T, Wang Z, Shimojo N, Maruyama H, Homma S, Kuga K, Yamaguchi I, Aonuma K, Miyauchi T (2012) Endothelin-1induced cardiomyocyte hypertrophy is partly regulated by transcription factor II-F interacting C-terminal domain phosphatase of rna polymerase II. Life Sciences 91: 572 – 577

[175] Salmon M, Johnston WF, Woo A, Pope NH, Su G, Upchurch GR, Owens GK, Ailawadi G (2013) KLF4 regulates abdominal aortic aneurysm morphology and deletion attenuates aneurysm formation. Circulation 128: 163–174

[176] Sano M, Fukuda K, Kodama H, Pan J, Saito M, Matsuzaki J, Takahashi T, Makino S, Kato T, Ogawa S (2000) Interleukin-6 family of cytokines mediate angiotensin II-induced cardiac hypertrophy in rodent cardiomyocytes. Journal of Biological Chemistry 275: 29717–29723

[177] Satriano JA, Shuldiner M, Hora K, Xing Y, Shan Z, Schlondorff D (1993) Oxygen radicals as second messengers for expression of the monocyte chemoattractant protein, MCP-1, and the monocyte colony-stimulating factor, CSF-1, in response to tumor necrosis factor-alpha and immunoglobulin G. evidence for involvement of reduced nicotinamide adenine dinucleotide phosphate NADPH-dependent oxidase. The Journal of Clinical Investigation 92: 1564–1571

[178] Schelbert EB, Piehler KM, Zareba KM, Moon JC, Ugander M, Messroghli DR, Valeti US, Chang CCH, Shroff SG, Diez J, Miller CA, Schmitt M, Kellman P, Butler J, Gheorghiade M, Wong TC (2015) Myocardial fibrosis quantified by extracellular volume is associated with subsequent hospitalization for heart failure, death, or both across the spectrum of ejection fraction and heart failure stage. Journal of the American Heart Association 4

[179] Scheuer J, Malhotra A, Hirsch C, Capasso J, Schaible TF (1982) Physiologic cardiac hypertrophy corrects contractile protein abnormalities associated with pathologic hypertrophy in rats. J Clin Invest 70: 1300–1305

[180] Schiattarella GG, Hill JA (2015) Inhibition of hypertrophy is a good therapeutic strategy in ventricular pressure overload response to Schiattarella and Hill.

Circulation 131: 1435–1447

[181] Schmidt EK, Clavarino G, Ceppi M, Pierre P (2009) SUnSET, a nonradioactive method to monitor protein synthesis. Nature Methods 6: 275–277

[182] Schonthaler HB, Guinea-Viniegra J, Wagner EF (2011) Targeting inflammation by modulating the Jun/AP-1 pathway. Annals of the Rheumatic Diseases 70: 109–112

[183] Schwill S, Seppelt P, Grünhagen J, Ott CE, Jugold M, Ruhparwar A, Robinson PN, Karck M, Kallenbach K (2013) The fibrillin-1 hypomorphic mgr/mgr murine model of Marfan syndrome shows severe elastolysis in all segments of the aorta. Journal of Vascular Surgery 57: 1628–1636

[184] Seppelt PC, Schwill S, Weymann A, Arif R, Weber A, Zaradzki M, Richter K, Ensminger S, Robinson PN, Wagner AH, Karck M, Klaus K (2016) Loss of endothelial barrier in Marfan mice (mgr/mgr) results in severe inflammation after adenoviral gene therapy. PLoS ONE 11: 891–921

[185] Shah AS, White DC, Emani S, Kypson AP, Lilly RE, Wilson K, Glower DD, Lefkowitz RJ, Koch WJ (2001) In vivo ventricular gene delivery of a β-adrenergic receptor kinase inhibitor to the failing heart reverses cardiac dysfunction. Circulation 103: 1311–1316

[186] Shankman LS, Gomez D, Cherepanova OA, Salmon M, Alencar GF, Haskins RM, Swiatlowska P, Newman AAC, Greene ES, Straub AC, Isakson B, Randolph GJ, Owens GK (2015) KLF4-dependent phenotypic modulation of smooth muscle cells has a key role in atherosclerotic plaque pathogenesis. Nat Med 21: 628–637

[187] Song Y, Xie Y, Liu F, Zhao C, Yu R, Ban S, Ye Q, Wen J, Wan H, Li X, Ma R, Meng Z (2013) Expression of matrix metalloproteinase-12 in aortic dissection. BMC Cardiovascular Disorders 13: 34–45

[188] Stachler MD, Bartlett JS (2006) Mosaic vectors comprised of modified AAV1 capsid proteins for efficient vector purification and targeting to vascular endothelial cells. Gene Ther 13: 926–931

[189] Stadlbauer TH, Wagner AH, Hlschermann H, Fiedel S, Fingerhuth H, Tillmanns H, Bohle RM, Hecker M (2008) AP-1 and STAT-1 decoy oligodeoxynucleotides attenuate transplant vasculopathy in rat cardiac allografts. Cardiovascular Research 79: 698–705

[190] Sternlicht MD, Werb Z (2001) How matrix metalloproteinases regulate cell behaviour. Annu Rev Cell Dev Biol 17: 463–516

[191] Stojanovic T, Wagner AH, Schndube FA, Hecker M (2012) Cardiac Transplantation, vol. 20, chap. Pre-Transplant Therapy in Experimental Heart Transplantation, 143–156. InTech

[192] Stuart A, Williams A (2007) Marfan's syndrome and the heart. Arch Dis Child 92: 351–356

[193] Sturrock A, Cahill B, Norman K, Huecksteadt TP, Hill K, Sanders K, Karwande SV, Stringham JC, Bull DA, Gleich M, Kennedy TP, Hoidal JR (2006) Transforming growth factor-1 induces Nox4 NAD(P)H oxidase and reactive oxygen species-dependent proliferation in human pulmonary artery smooth muscle cells. American Journal of Physiology - Lung Cellular and Molecular Physiology 290: L661–L673

[194] Su H, Arakawa-Hoyt J, Kan YW (2002) Adeno-associated viral vector-mediated hypoxia response element-regulated gene expression in mouse ischemic heart model. Proceedings of the National Academy of Sciences 99: 9480–9485

[195] Suckau L, Fechner H, Chemaly E, Krohn S, Hadri L, Kockskämper J, Westermann D, Bisping E, Ly H, Wang X, Kawase Y, Chen J, Liang L, Sipo I, Vetter R, Weger S, Kurreck J, Erdmann V, Tschope C, Pieske B, Lebeche D, Schultheiss HP, Hajjar RJ, Poller WC (2009) Long-term cardiac-targeted RNA interference for the treatment of heart failure restores cardiac function and reduces pathological hypertrophy. Circulation 119: 1241–1252

[196] Summers KM, Raza S, van Nimwegen E, Freeman TC, Hume DA (2010) Co-expression of FBN1 with mesenchyme-specific genes in mouse cell lines: implications for phenotypic variability in Marfan syndrome. Eur J Hum Genet 18: 1209–1215

[197] Sun Z (2015) Aging, arterial stiffness and hypertension. Hypertension 65: 252–256

[198] Szema AM, Forsyth E, Ying B, Hamidi SA, Chen JJ, Hwang S, Li JC, Sabatini Dwyer D, Ramiro-Diaz JM, Giermakowska W, Gonzalez Bosc LV (2017) NFATc3 and VIP in idiopathic pulmonary fibrosis and chronic obstructive pulmonary disease. PLOS ONE 12: 1–18

[199] Tada Y, Yagi K, Kitazato KT, Tamura T, Kinouchi T, Shimada K, Matsushita N, Nakajima N, Satomi J, Kageji T, Nagahiro S (2010) Reduction of endothelial tight junction proteins is related to cerebral aneurysm formation in rats. Journal of Hypertension 28: 18831891

[200] Ten Dijke P, Arthur HM (2007) Extracellular control of TGF-β signalling in vascular development and disease. Nat Rev Mol Cell Biol 8: 857–869

[201] Thomas SP, Bircher-Lehmann L, Thomas SA, Zhuang J, Saffitz JE, Kléber AG (2000) Synthetic strands of neonatal mouse cardiac myocytes. Circulation Research 87: 467–473

[202] Tomita T, Takeuchi E, Tomita N, Morishita R, Kaneko M, Yamfamoto K, Nakase T, Seki H, Kato K, Kaneda Y, Ochi T (1999) Suppressed severity of collagen-induced arthritis by *in vivo* transfection of NFκB decoy oligodeoxynucleotides as a gene therapy. Arthritis and Rheumatism 42: 2532–2542

[203] Tsutamoto T, Wada A, Maeda K, Hisanaga T, Maeda Y, Fukai D, Ohnishi M, Sugimoto Y, Kinoshita M (1997) Attenuation of compensation of endogenous cardiac natriuretic peptide system in chronic heart failure. Circulation 96: 509–516

[204] Tuxworth WJ, Saghir AN, Spruill LS, Menick DR, McDermott PJ (2004) Regulation of protein synthesis by eIF4E phosphorylation in adult cardiocytes: the consequence of secondary structure in the 5'-untranslated region of mRNA. Biochem J 378: 73–82

[205] Umeyama K, Watanabe K, Watanabe M, Horiuchi K, Nakano K, Kitashiro M, Matsunari H, Kimura T, Arima Y, Sampetrean O, Nagaya M, Saito M, Saya H, Kosaki K, Nagashima H, Matsumoto M (2016) Generation of heterozygous fibrillin-1 mutant cloned pigs from genome-edited foetal fibroblasts. Scientific Reports 6: 24413–24423

[206] van Nierop BJ, van Assen HC, van Deel ED, Niesen LBP, Duncker DJ, Strijkers GJ, Nicolay K (2013) Phenotyping of left and right ventricular function in mouse models of compensated hypertrophy and heart failure with cardiac MRI. PLOS ONE 8: 1–9

[207] van Rooij E, Doevendans PA, de Theije CC, Babiker FA, Molkentin JD, De Windt LJ (2002) Requirement of NFAT in calcineurin-mediated cardiomyocyte hypertrophy. Journal of Biological Chemistry 277: 48617–48626

[208] Varadi K, Michelfelder S, Korff T, Hecker M, Trepel M, Katus H, Kleinschmidt J, Mller OJ (2012) Novel random peptide libraries displayed on AAV serotype 9 for selection of endothelial cell-directed gene transfer vectors. Gene Therapy 19: 800–809

[209] Vega RB, Bassel-Duby R, Olson EN (2003) Control of cardiac growth and function by calcineurin signaling. Journal of Biological Chemistry 278: 36981–36984

[210] Velagaleti RS, Pencina MJ, Murabito JM, Wang TJ, Parikh NI, D'Agostino RB, Levy D, Kannel WB, Vasan RS (2008) Long-term trends in the incidence of heart failure after myocardial infarction. Circulation 118: 2057–2062

[211] Verrecchia F, Vindevoghel L, Lechleider RJ, Uitto J, Roberts AB, Mauviel A (2001) Smad3/AP-1 interactions control transcriptional responses to TGF-β in a promoter-specific manner. Oncogene 20: 3332–3340

[212] Wagenseil JE, Mecham RP (2007) New insights into elastic fiber assembly. Birth Defects Research Part C: Embryo Today: Reviews 81: 229–240

[213] Wang Q, Zhou Y, Qi Y, Liu Hy, Ding GS, Yang L, Qiu B, Xu S, Guo Z (2011) Synthetic gelatinases inhibitor attenuates electromagnetic pulse-induced blood-brain barrier disruption by inhibiting gelatinases-mediated ZO-1 degradation in rats. Toxycology 285: 31–38

[214] Wang Z, Zhu T, Qiao C, Zhou L, Wang B, Zhang J, Chen C, Li J, Xiao X (2005) Adeno-associated virus serotype 8 efficiently delivers genes to muscle and heart. Nat Biotech 23: 321–328

[215] Wei S, Guo A, Chen B, Kutschke W, Xie YP, Zimmerman K, Weiss RM, Anderson ME, Cheng H, Song LS (2010) T-tubule remodeling during transition from hypertrophy to heart failure. Novelty and significance. Circulation Research 107: 520–531

[216] Whelan RS, Kaplinskiy V, Kitsis RN (2010) Cell death in the pathogenesis of heart disease: Mechanisms and significance. Annual Review of Physiology 72: 19–44

[217] White SJ, Nicklin SA, Büning H, Brosnan MJ, Leike K, Papadakis ED, Hallek M, Baker AH (2004) Targeted gene delivery to vascular tissue in vivo by tropism-modified adeno-associated virus vectors. Circulation 109: 513–519

[218] Wierzbicki AS, Viljoen A (2013) Alipogene tiparvovec: gene therapy for lipoprotein lipase deficiency. Expert Opinion on Biological Therapy 13: 7–10

[219] Wile BM, Ban K, Yoon YS, Bao G (2014) Molecular beacon-enabled purification of living cells by targeting cell type-specific mRNAs. Nature Protocols 9: 2411–2424

[220] Wilkins BJ, Dai YS, Bueno OF, Parsons SA, Xu J, Plank DM, Jones F, Kimball TR, Molkentin JD (2004) Calcineurin/NFAT coupling participates in pathological, but not physiological cardiac hypertrophy. Circulation Research 94: 110–118

[221] Wilkins BJ, De Windt LJ, Bueno OF, Braz JC, Glascock BJ, Kimball TF, Molkentin JD (2002) Targeted disruption of NFATc3, but not NFATc4, reveals an intrinsic defect in calcineurin-mediated cardiac hypertrophic growth. Molecular and Cellular Biology 22: 7603–7613

[222] Williamson MR, Shuttleworth A, Canfield AE, Black RA, Kielty CM (2007) The role of endothelial cell attachment to elastic fibre molecules in the enhancement

of monolayer formation and retention, and the inhibition of smooth muscle cell recruitment. Biomaterials 28: 5307 – 5318

[223] Wise SG, Waterhouse A, Michael P, Ng MK (2012) Extracellular matrix molecules facilitating vascular biointegration. J Funct Biomater 3: 569–587

[224] Wu CH, Lin CS, Hung JS, Wu CJ, Lo PH, Jin G, Shyy YJ, Mao SJT, Chien S (2001) Inhibition of neointimal formation in porcine coronary artery by a Ras mutant. Journal of Surgical Research 99: 100–106

[225] Xia Y, Lee K, Li N, Corbett D, Mendoza L, Frangogiannis NG (2009) Characterization of the inflammatory and fibrotic response in a mouse model of cardiac pressure overload. Histochemistry and Cell Biology 131: 471–481

[226] Xiao X, Gang Y, Wang H, Wang J, Zhao L, Xu L, Liu Z (2015) Double-stranded RNA transcribed from vector-based oligodeoxynucleotide acts as transcription factor decoy. Biochemical and Biophysical Research Communications 457: 221 – 226

[227] Xie M, Burchfield JS, Hill JA (2013) Pathological ventricular remodeling. Circulation 128: 1021–1030

[228] Xiong W, Knispel RA, Dietz HC, Ramirez F, Baxter BT (2017) Doxycycline delays aneurysm rupture in a mouse model of Marfan syndrome. Journal of Vascular Surgery 47: 166–172

[229] Yamasaki K, Asai T, Shimizu M, Aoki M, Hashiya N, Sakonjo H, Makino H, Kaneda Y, Ogihara T, Morishita R (2003) Inhibition of NFκB activation using cis-element decoy of nfκb binding site reduces neointimal formation in porcine balloon-injured coronary artery model. Gene Ther 10: 356–364

[230] Yang J, Savvatis K, Kang JS, Fan P, Zhong H, Schwartz K, Barry V, Mikels-Vigdal A, Karpinski S, Kornyeyev D, Adamkewicz J, Feng X, Zhou Q, Shang C, Kumar P, Phan D, Kasner M, López B, Diez J, Wright KC, Kovacs RL, Chen PS, Quertermous T, Smith V, Yao L, Tschöpe C, Chang CP (2016) Targeting LOXL2 for cardiac interstitial fibrosis and heart failure treatment. Nature Communications 7: 13710–13728

[231] Ying Y, Muller OJ, Goehringer C, Leuchs B, Trepel M, Katus HA, Kleinschmidt JA (2010) Heart-targeted adeno-associated viral vectors selected by *in vivo* biopanning of a random viral display peptide library. Gene Ther 17: 980–990

[232] Yuan HF, Huang H, Li XY, Guo W, Xing W, Sun ZY, Liang HP, Yu J, Chen DF, Wang ZG, Hao J, Xu X (2013) A dual AP-1 and SMAD decoy ODN suppresses

tissue fibrosis and scarring in mice. Journal of Investigative Dermatology 133: 1080 – 1087

[233] Yusuf S, Pepine CJ, Garces C, Pouleur H, Rousseau M, Salem D, Kostis J, Benedict C, Bourassa M, Pitt B (1992) Effect of Enalapril on myocardial infarction and unstable angina in patients with low ejection fractions. The Lancet 340: 1173–1178

[234] Zacchigna S, Zentilin L, Giacca M (2014) Adeno-associated virus vectors as therapeutic and investigational tools in the cardiovascular system. Circulation Research 114: 1827–1846

[235] Zarain-Herzberg A, Fragoso-Medina J, Estrada-Avils R (2011) Calcium-regulated transcriptional pathways in the normal and pathologic heart. IUBMB Life 63: 847–855

[236] Zeyer KA, Reinhardt DP (2015) Fibrillin-containing microfibrils are key signal relay stations for cell function. J Cell Commun Signal 9: 351356

[237] Zhang P, Andrianakos R, Yang Y, Liu C, Lu W (2010) Kruppel-like factor 4 (Klf4) prevents embryonic stem cell differentiation by regulating Nanog gene expression. Journal of Biological Chemistry 285: 9180–9189

[238] Zimmerman KA, Graham LV, Pallero MA, Murphy-Ullrich JE (2013) Calreticulin regulates transforming growth factor-β-stimulated extracellular matrix production. Journal of Biological Chemistry 288: 14584–14598

[239] Zincarelli C, Soltys S, Rengo G, Rabinowitz JE (2008) Analysis of AAV serotypes 1-9 mediated gene expression and tropism in mice after systemic injection. Molecular Therapy 16: 1073–1080

[240] Zsebo K, Yaroshinsky A, Rudy JJ, Wagner K, Greenberg B, Jessup M, Hajjar RJ (2014) Long-term effects of AAV1/SERCA2a gene transfer in patients with severe heart failure. Novelty and significance. Circulation Research 114: 101–108